Physics l8OE

Plasma Physics Laboratory

INTRODUCTION TO EXPERIMENTAL PLASMA PHYSICS

Volume 1

Alfred Y. Wong
Physics Department
University of California at Los Angeles

 Spring, 1977

Plasma Physics Laboratory

Physics 180 E

CONTENTS:

Acknowledgments

In the course of writing this volume, I have drawn upon the experience of many of my former and present colleagues, in particular: Drs. W. Gekelman, W. Quon, K. MacKenzie, E. Ripin, and R. Stenzel. Many graduate students have made many useful suggestions and contributions to the text: W. DiVergilio contributed to the Appendix on ion beam-plasma interaction; K. Jones and D. Eggleston carefully proof-read the many chapters and assisted in bringing the volume to its present form; R. Schumacher assisted me in earlier drafts.

Symbols and Commonly Used Constants

Symbols

C_s= ion sound speed

$$\cong \sqrt{\frac{KT_e}{M}}$$

E = particle kinetic energy

E_b = beam energy

I_{es}, I_{is} = electron, ion saturation current

K = Boltzmann's constant

M, m_i = ionic mass

T_b = ion beam temperature equivalent

T_e, T_i = electron, ion temperature

V_d = discharge potential

V_g = grid potential

V_f = floating potential

V_s = plasma space potential

a_e = electron thermal speed

$$= \sqrt{\frac{KT_e}{m}}$$

a_i = ion thermal speed

$$= \sqrt{\frac{KT_e}{M}}$$

e = electronic charge

$f_b(v)$ = beam ion velocity distribution

$f_e(v)$, $f_i(v)$ = electron, ion velocity distribution functions

k = wavenumber

m, m_e= electronic mass

n, n_i = electron density, ion density

n_b = beam density

V_b = Bohm (Tonks-Langmuir) speed

$$= \sqrt{\frac{KT_e}{M}}$$

v_b = beam velocity

V_e = average magnitude of electron velocity (3 dim)

$$= \sqrt{\frac{8KT_e}{m}}$$

v_g = group velocity

v_p = phase velocity

z_o = axial plasma position

λ_D, λ_{De} = electron Debyelength

$$= \sqrt{\frac{\gamma KT_e}{4\pi ne^2}}$$

θ =ion/electron temperature ratio

$$= \frac{T_i}{T_e}$$

ω = frequency

ω_p, ω_{pe} = electron plasma frequency

$$= \sqrt{\frac{4\pi ne^2}{m}}$$

ω_{pi} = ion plasma frequency

$$= \sqrt{\frac{4\pi ne^2}{M}}$$

ω = normalized wave frequency

$$= \frac{\omega}{\omega_{pi}}$$

σ_c = charge exchange cross sections, e.g. $\sigma_{Ar+-Ar} \sim 5 \times 10^{-15}$ cm2

(velocity dependent)

Physical Constants (CGS)

Boltzmann's constant	$K = 1.3807 \_ 10^{-16}$ erg/° K
Elementary charge	$e = 4.8032 \_ 10^{-10}$ statcoulomb
Electronic mass	$m = 9.1095 \_ 10^{-28}$ gram
Hydrogen atom mass	$M_p = 1.6734 \_ 10^{-24}$ gram
Speed of light in vacuum	$c = 2.9979 \times 10^{10}$ cm/sec

Temperature associated with 1 eV = 1.1605×10^4 °K

Atomic Masses for Typical Plasma Gases

Gas	Mass (AMU)
He	4.0026
Ne	19.9924
Ar	39.9624
Kr	83.9115
Xe	130.905

__Chapter I: Plasma Production

A plasma source which possesses the desirable characteristics of quiescence and uniformity has been developed at the UCLA Plasma Physics Laboratory and is now being used in many parts of the world for basic plasma research. Because this source is economical to build and simple to operate, it is ideally suited to the undergraduate or graduate plasma laboratory. All the experiments to be described in this text can be performed in this one device.

1) The D.C. Discharge

Plasma can be produced by electron bombardment of a neutral gas in an otherwise evacuated vessel. In the D.C. discharge, a current is passed through a set of filaments (tantalum or thoriated tungsten wire) to heat them by joule heating. A significant number of electrons in the hot filament can have an energy greater than the work function and are emitted. These electrons, called primary electrons, are accelerated by an external D.C. electric field such that they have sufficient energy to ionize the neutral gas. The minimum energy required to remove the first valence electron from the neutral atom (the first ionization energy) is in the neighborhood of 20 eV for commonly used gases at room temperature. A discharge potential above this energy must be applied between the filaments (cathode) and the chamber wall (anode) to obtain a discharge. The removed valence electron is called a secondary electron and is scattered with less energy than the corresponding incident primary electron at any given time; most electrons in the plasma are secondaries._

The probability of an ionizing collision (ionization cross section) generally has a broad maximum for electrons with energy about 100 eV as seen in Figure I-l. The D.C. discharge is typically operated with a potential of 30 to 100 volts between the cathode and the anode wall. Doubly ionizing collisions can also occur when the primary electrons' energy exceeds the second ionization energy however, the ionization cross section for double ionization is usually much smaller than for single ionizations. The first and the second ionization energies of several commonly used gases are listed in Table I-l. Schematic diagram of the D.C. discharge system is shown in Figure I-2.

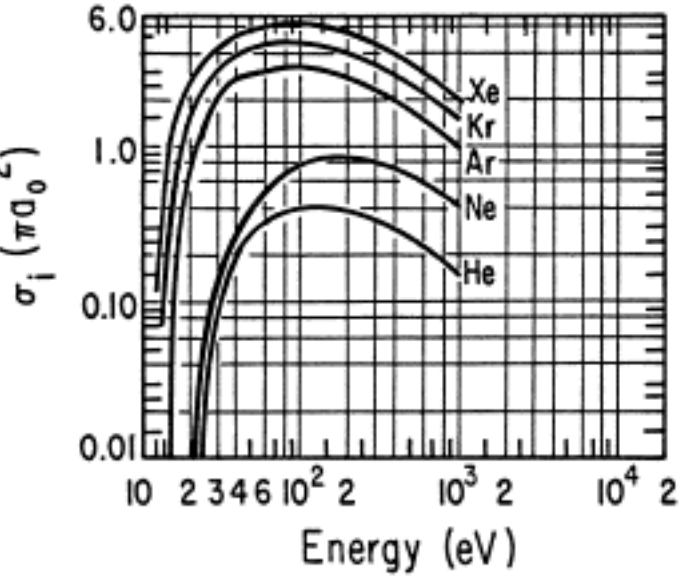

Figure I-1.

Ionization cross sections for Xe, Kr, A, Ne and He by electron impact.

πa_o^2 = cross section of H atom = 8.8×10^{-17} cm^2

a) Space charge limited emission: In the presence of an insignificant number of neutral atoms (as in a vacuum tube) only a small current can flow between the cathode and the anode. This current limiting is the result of space charge due to electrons that accumulate near the cathode and repel some of the newly emitted electrons. The space charge limited emission current is given by the Child-Langmuir law[1]:

$$J = 2.33 \times 10^{-6} x \bullet \left(\frac{(V_d)^{3/2}}{d^2} \right) A / cm^2$$

where V_d is the discharge potential in volts and d is the distance between anode and cathode in cm. For instance, for d = l5 cm, V_d = 40 V, J = 2.6 x 10 $^{-6}$ A/cm2.

b) Temperature limited emission: In a plasma device, the initially small space charge limited discharge current ionizes some neutrals. The ions produced partially neutralize the space charge allowing a larger discharge current which produces more plasma. Eventually a sheath is formed around the cathode making the plasma the effective anode. This reduces d to a few Debye lengths. For n = 10^{10} cm^3 and T_e = 3 eV, the Debye length is about 10^{-2} cm and the space charge limiting current density, J = 5.9 A/cm^2.

The total emission current is, however, limited by the filament temperature. The temperature limited emission current is given by the Richardson law: $J = AT^2e^{-W/KT}$ A/cm^2 where W and T are the work function and temperature respectively of the filament metal. The theoretical limit for A is 4 meK^2/h^3 = 120 $A/cm^2 – K^{o2}$. In actual practice, A varies from 30 - 200 A/cm^2 - K^{o2}. For tungsten, W ≈ 4.5 eV, A ≈ 60 A/cm^2 - K^{o2}, and the melting temperature is 3650° K. The Richardson law gives for tungsten at 2000° K, J= 1.1 x 10^{-3} A/cm^2.

Comparison of the temperature and space charge limiting processes shows that in the presence of the plasma, $J_{space\ charge} >> J_{temperature}$ discharge current, which is just the emission current, is, then, a sensitive function of the filament temperature.

One method of producing a high % ionization is to heat the filaments to a high temperature (white hot at 3000° K) by high current pulses (50 amps for a filament of .030" diameter, 3" length). In this manner, plasma densities exceeding 10^{l2} cm^3 can be achieved while preserving filament life span.

GAS	FIRST IONIZATION LEVEL (eV)	SECOND IONIZATION LEVEL (eV)
H	13.595	--------
He	24.481	54.403
Ne	21.559	41.07
Ar	15.755	27.62
Kr	13.9	26.4
Xe	12.127	21.2

Table 1-1

Source: CRC Handbook of Chemistry and Physics, 1967 Edition (Page E-56)

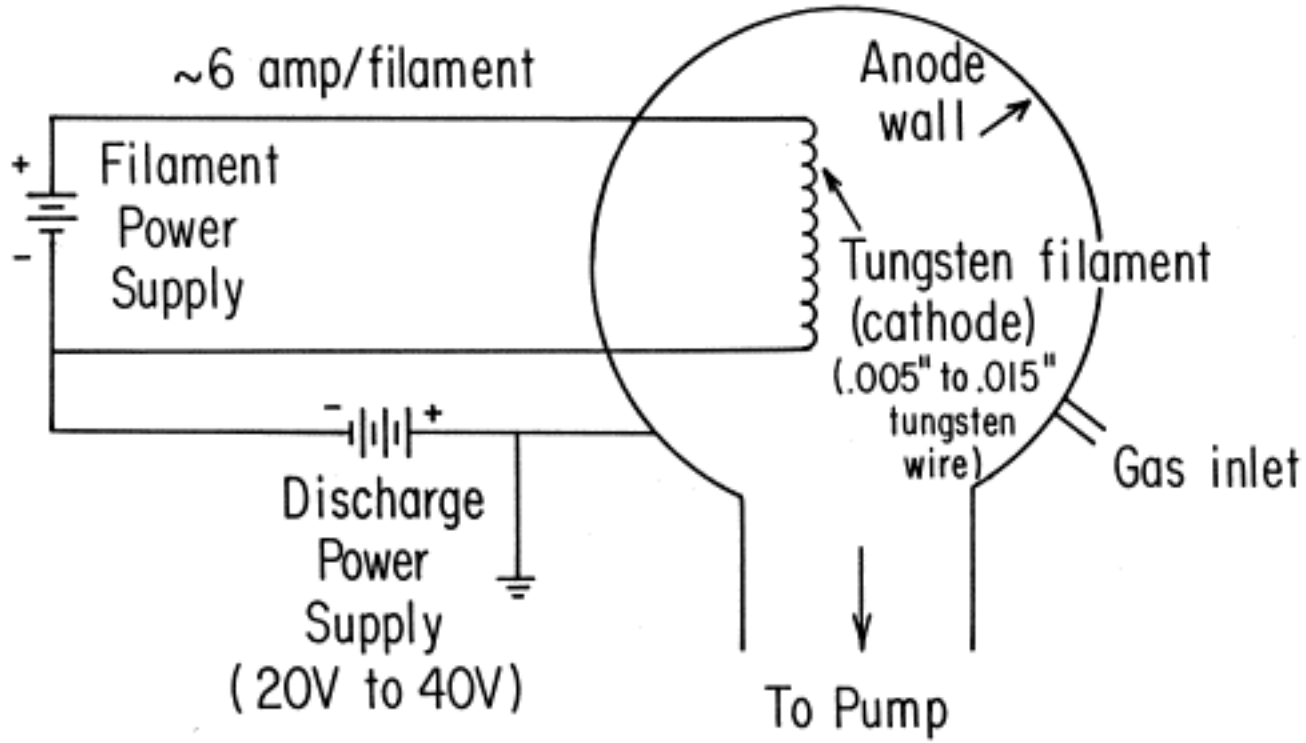

Figure I-2.

Discharge Diagram

c) Balance between production and losses: The plasma production and losses can be represented by the following rate equation:

$$\frac{\partial N}{\partial t} = \left(\frac{\partial N}{\partial t}\right)_{production} - \left(\frac{\partial N}{\partial t}\right)_{loss}$$

In the steady-state, we have:

$$\left(\frac{\partial N}{\partial t}\right)_{production} = \left(\frac{\partial N}{\partial t}\right)_{loss}$$

where N is the total number of plasma particles (electron-ion pair) in the system. Let σ represent the ionization cross-section of the neutral gas to be ionized by electrons of energy eV_d; n_O the density of neutrals; l_{eff} the average total distance a primary electron travels before it is lost from the plasma (effective path length) $n_e v_d$ the primary electron flux through a surface of area A enclosing the filaments and $\lambda = \frac{1}{n_o \sigma}$ the ionizing collision mean free path for primary electrons.
Then, in the D.C. discharge

(I-1)

$$\left(\frac{\partial N}{\partial t}\right)_{production} = n_o \sigma l_{err} (n_e v_d A) = n_o \sigma l_{eff} \frac{I_{discharge}}{e}$$

in the limit $\lambda >> l_{eff}$ .For simplicity, imagine a primary electron discharge surface of area A as

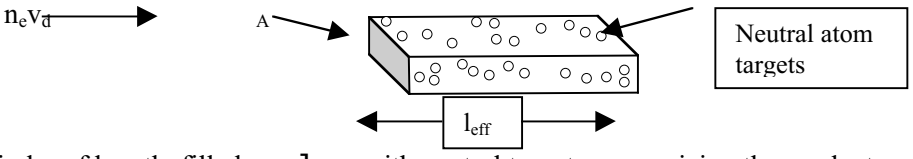

the end of a cylinder of length filled l_{eff} with neutral targets, recognizing the product $(n_e)(l_{eff} A)$ above as the number of primary electrons per unit volume times the total volume of neutral atom targets accessible to the primaries. We can now understand (I-l) by rearranging it as

$$\left(\frac{\partial N}{\partial t}\right)_{production} = (n_e l_{err} A)(n_o \sigma v_d),$$

and identify $n_e l_{err} A$ as the total number of ionizing primary electrons available within the plasma volume at any given instant of time and $n_o \sigma v_d$ as the rate of ionizing collisions by a single primary

electron. The limit $\lambda = \frac{1}{n_o \sigma} >> l_{eff}$ states that the ionization mean free path is sufficiently long such that the primary electrons are uniformly distributed inside the plasma volume. Under this condition of uniform probability of plasma production over the entire volume equation (I-l) is valid.

There are generally three types of major losses of plasma particles.

1. Loss to the chamber wall.
2. Volume recombination - secondary electrons engage in low velocity collisions with ions to produce neutrals.
3. Loss to probes, filament supports, any other obstacles, insulators or conductors which become plasma sinks through surface recombination. The total plasma loss can be expressed by:

$$\left(\frac{\partial N}{\partial t}\right)_{loss} \cong \frac{nV}{\tau}$$

where V is the volume of the system, n is the plasma density and τ is the plasma lifetime. In a system where ions can flow to the chamber wall freely, the plasma lifetime is $\tau = \frac{L}{v_i}$ where v_i is the flow velocity of ions and L is the scale length of the system. Using this expression, we obtain

$$\left(\frac{\partial N}{\partial t}\right)_{loss} \cong n v_i A$$

where A is the total plasma surface area.

2) Discharge in Magnetic Multipole Machines

To increase the efficiency of the plasma source, lines of permanent magnets (B ~ 1.8 KG at the surface) are installed on the surface of the chamber wall to form a multi-mirror surface field (multi-magnetic cusps), as shown in Figure I-3. Particles can be reflected from the magnetic field region into the center region of the system that is almost magnetic field free. The advantages of this magnetic multipole machine can be out-lined as follows.

a) Longer primary path length, l_{eff} : Because primaries can be bounced back and forth in the multipole system rather than flowing freely to the wall, their effective path can be much longer (up to two hundred times of the system length has been measured[2]). Thus the production rate could increase substantially.

b) Reduction of effective loss surface area A: The surface fields set up by the permanent magnets prevent the direct flight of plasma particles to the walls. Instead, escaping particles must either diffuse across the magnetic field (region 1 in Figure I-3) or be lost through the small cusp surface (region

2). The condition for reflection from a magnetic barrier is the variation of magnetic field in one cyclotron orbit be small as the particle approaches the surface. This condition is much more likely to be satisfied by electrons than ions. The dimensions of the loss area can be 10^2 - 10^3 times smaller than the total wall surface.

c) High percentage ionization: By increasing the efficiency of the primary electrons and reducing the loss, high fractional ionization rate can be achieved by a D.C. discharge in the multipole machine. A high density, highly ionized, uniform and quiescent plasma can be produced.

An improvement over the cusp confinement by permanent magnets has been found which uses two layers of internal surface conductors with oppositely directed currents,[3] as shown in Figure I-4. This configuration creates a surface magnetic layer of closed magnetic field lines. The spatial variation of magnetic fields can be made sufficiently gentler than that using permanent magnets such that ions can be reflected by the surface. Plasma particles are lost to the chamber wall and current carrying conductors only by diffusion across the magnetic barriers. The diffusion velocity can be two to three orders of magnitude smaller than the ion flow velocity in a system without the surface field.

3) Experimental Procedure

a) General familiarization: Leak in enough Argon to raise the neutral pressure to about 10^{-4} torr and turn the filament power supply to a minimum voltage with the switch off. Then the switch is turned on, and the filament voltage is carefully turned up until the cathode wires glow red hot. The discharge power supply is set to the desired value (about 40 V) and then the filament voltage is turned up until the desired discharge current (I_d) is obtained. Notice that as the filament voltage is turned up, the discharge current increases rapidly (emission limited current flow). Be very careful in the adjustment of the filament voltage, since when the filament is hot enough to emit electrons, it is on the verge of melting. The filament biased negatively with respect is slowly to the plasma destroyed by ion bombardment and must be replaced periodically. The filament's life span will be shortened if it is subjected to a large surge of current. Thus, always vary the filament voltage slowly will be shortened until the discharge current is obtained. The neutral gas pressure can be read off an ionization gauge. Pressure adjustments are made with a leak valve. Some typical operating conditions are listed in Appendix B.

b) Saturation electron current and ion current measurement: Locate the radially movable probe in the center of the chamber, connect the probe to a power supply and apply about +100 volts to clean the probe surface by electron bombardment. Use a resistor in series to limit the cleaning current to 200 mA.

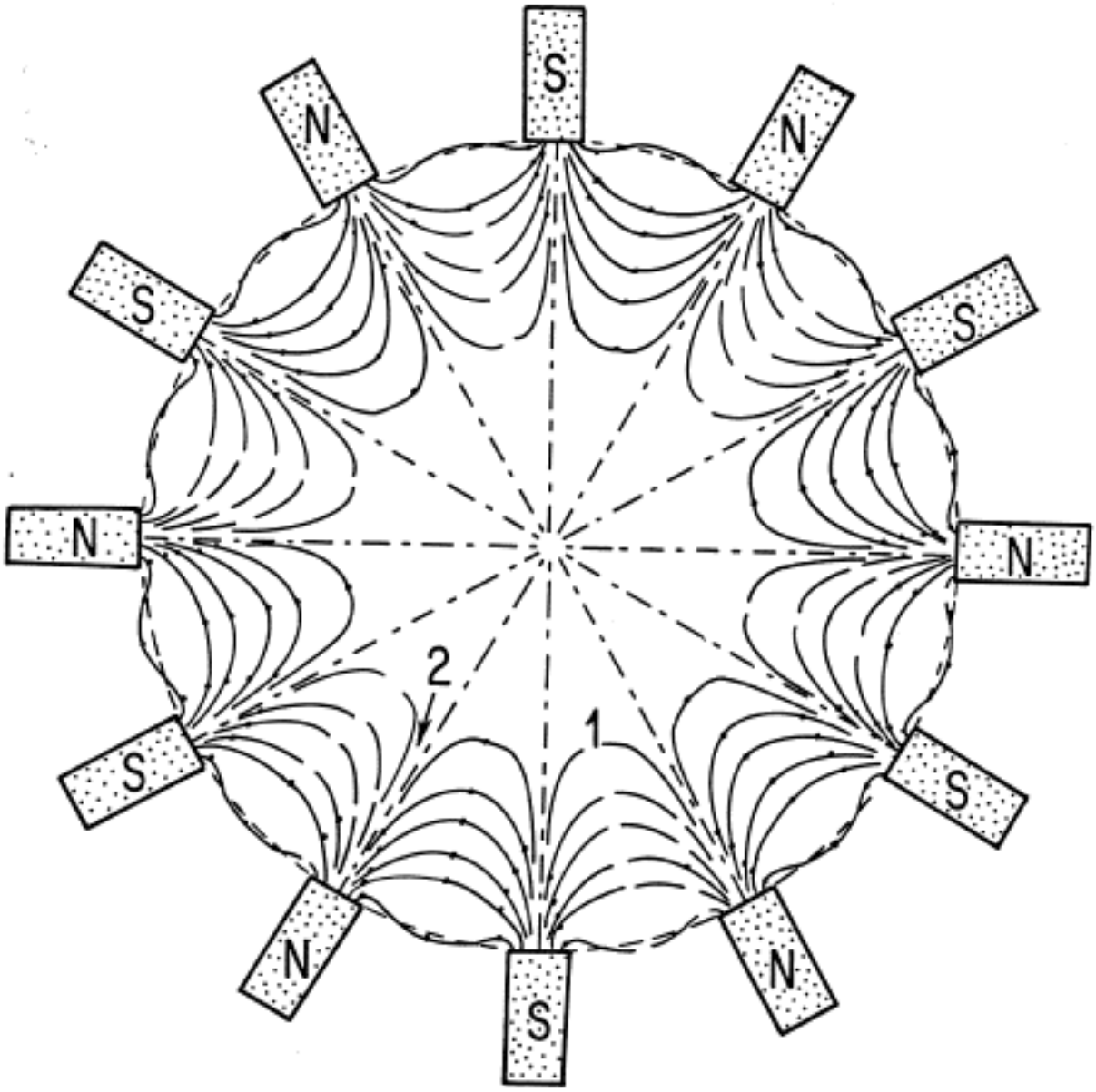

Figure I-3.

Surface magnetic cusps provided by rows of permanent magnets of alternating polarities.

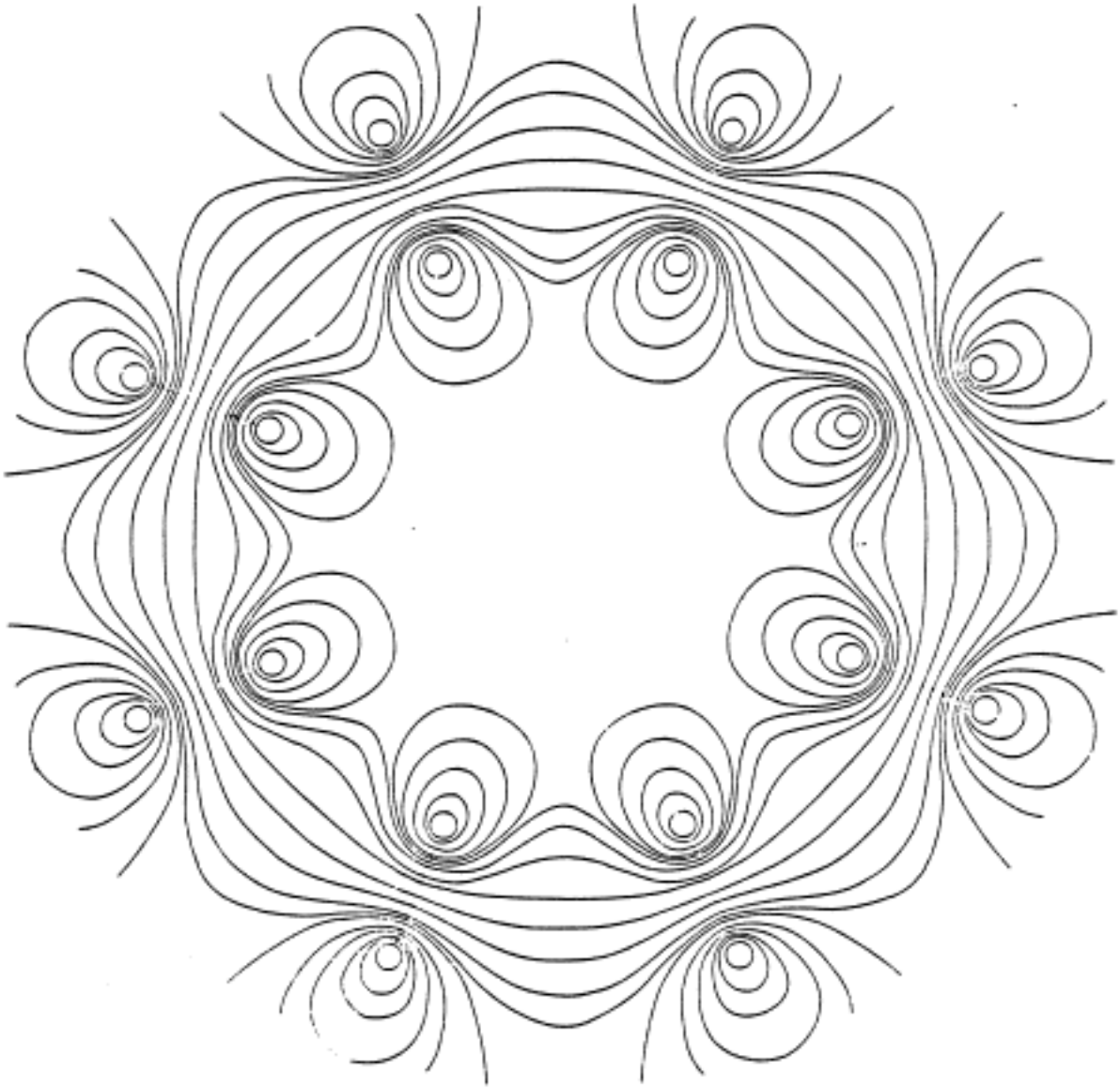

Figure I-4.

Surface magnetic fields created by two layers of internal surface conductors with oppositely directed currents.

The probe s disc surface should glow dull red. Set up the simple bias (+3 volts) circuit of Figure I-5 to draw electron saturation current $I_{es} = \frac{1}{4} ne \; v_e A$ * where n is the electron density, v_e is the average

velocity of the electrons collected by a planar probe, $v_e = \left(\frac{8^{KT_e}}{\pi m} \right)^{1/2}$, ,and A is the probe surface area. Make sure the value R of the termination resistor you choose satisfies $I_{es}R << V_{bias}$ yet produces a large enough voltage drop for oscilloscope or x-y recorder measurement. Calculate the electron density n by choosing $KT_e \cong 1$ eV, the typical electron temperature of the discharge.

Set up a negative bias (-45 volts) circuit to obtain the ion saturation current, I_{is}. Check to see that current is positive (if not, increase bias). Compute the ratio I_{es}/I_{is}. Does this ratio depend on the plasma density? How should this ratio depend on ion mass?

c) Dependence of plasma parameters on external parameters: Measure the electron saturation current as a function of:

1. Discharge voltage (with chosen neutral pressure and filament current).
2. Discharge current with chosen discharge voltage and neutral pressure). This is adjusted by varying the filament current. Be careful not to turn the filament current up too high and destroy the filaments.
3. Neutral pressure (10^{-5} - 10^{-3} torr, at fixed discharge and filament currents)

To make the results of these measurements more accurate, the electron saturation current and the electron temperature should be measured by displaying the full Langmuir probe trace on an oscilloscope. The student should look ahead to Chapter II, pages 43-49 for an explanation of the Langmuir probe method.

Determine the dependence of plasma density on the discharge voltage. How does this dependence relate to the variation of ionization cross section with electron energy (Figure I-l)? Compute the fractional ionization, nonneutral for at least three different pressure settings. Does the fractional ionization remain constant for a constant discharge current?

d) Plasma lifetime measurement: A flat stainless steel plate is placed in the magnetic field-free region and biased at -75 volts with respect to the anode. This induces additional ion loss such that in the

---

* The factor _ arises from the following:
_ - Due to plasma at edge of sheath surrounding probe being composed of particles with velocity $0 \rightarrow \infty$ toward probe face only.
to the probe plane.

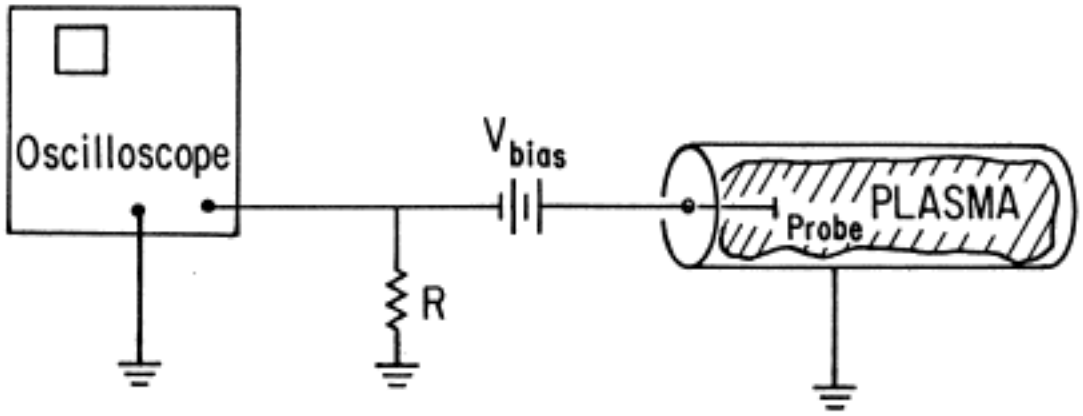

Figure I-5.

steady state, the balance equation becomes:

$$\left(\frac{\partial N}{\partial t}\right)_{\text{production}} = \frac{n_1 V}{\tau} + \frac{I_i}{e}$$

where n_i is the plasma density when there is an ion current I_i extracted by the plate. The plasma production rate may be expressed in terms of the discharge current I_d and the effective electron path length l_{eff} as:

$$\left(\frac{\partial N}{\partial t}\right)_{\text{production}} = \sigma(eV_d) n_o \; l_{\text{eff}} \; \frac{I_d}{e}$$

If we withdraw the plate from the plasma, the balance equation becomes:

$$\left(\frac{\partial N}{\partial t}\right)_{\text{production}} = \frac{n_2 V}{\tau}$$

If the production rate and the lifetime of the plasma does not change for the second case,[3] we obtain:

$$\frac{n_2 V}{\tau} = \frac{n_1 V}{\tau} - \frac{I_i}{e} \quad \text{or} \quad \tau = (n_2 - n_1) V \frac{e}{I_i}$$

i) Using the saturation electron current to obtain the plasma densities, and measuring the extracted ion current I, compute the lifetime.

ii) Estimate the effective path length of the primary electrons, $_{\text{eff}}$, and express it in terms of the system diameter.

iii) A more direct method of measuring consists in suddenly terminating the discharge and measuring the decay of the plasma density.

$$\frac{\partial(nV)}{\partial t} = - \; nvA \;\; \text{or} \;\; \tau = \frac{V}{vA}$$

Introduce different areas of loss surface A and check the dependence of τ on A.

Experimentally the discharge current is repetitively pulsed on and off by a simple transistor circuit as shown in Figure I-6. Plasma characteristics such as density and temperature can be sampled with a boxcar integrator or an intensity-modulated scope to be described in Chapter II.

e) Radial density profile: Obtain the radial plasma density profile by monitoring the electron saturation current as a function of radial position. Observe a uniform density in the center region and a steep density gradient in the magnetic field region near the wall. Calculate the density gradient length: $L = \left(\frac{1}{n} \frac{dn}{dx} \right)^{-1}$ .Can the steep density gradient be explained in terms of plasma production, particle reflection or plasma loss?

f) Quiescence: Monitor the density fluctuations by recording the fluctuations I about the mean electron saturation current I_o. This can be accomplished experimentally by displaying I_o on an oscilloscope and measuring the percentage signal fluctuation. This should be done with a 50 ohm terminating resistor. (Explain)

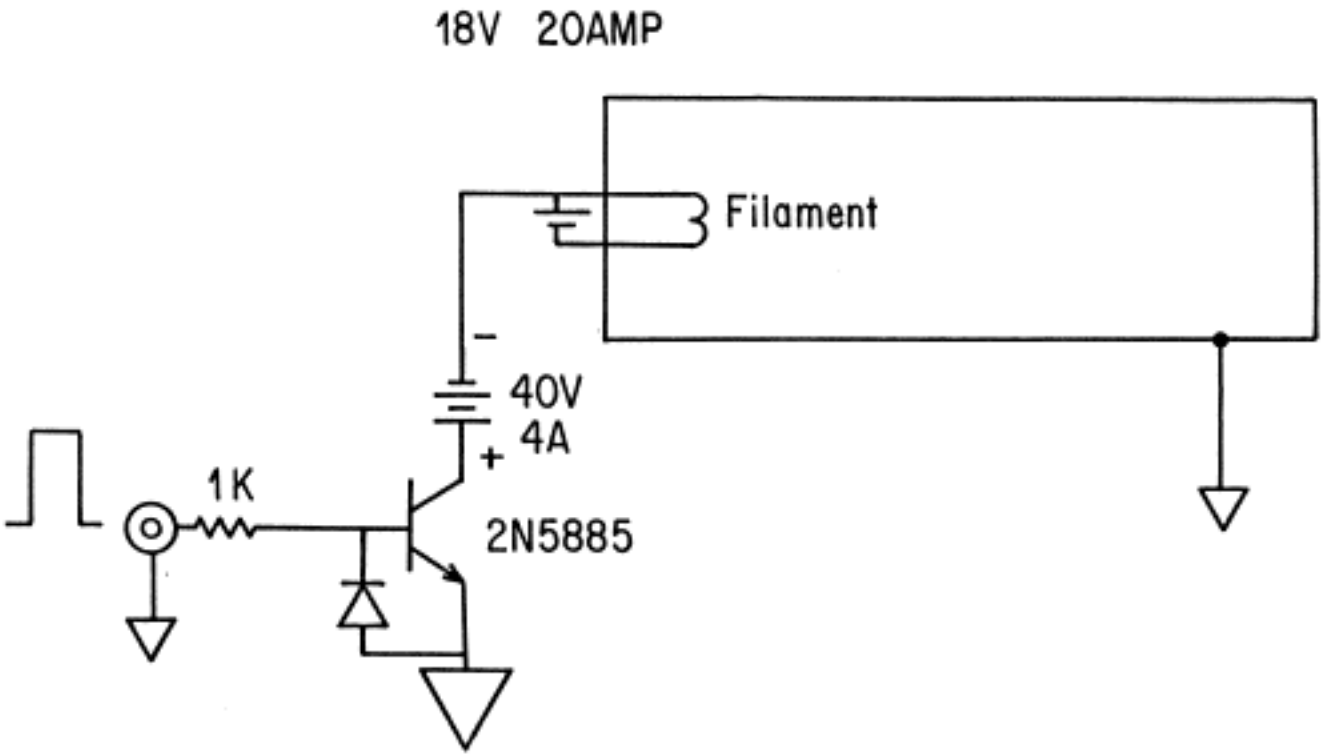

Figure I-6.

Transistor circuit for pulsing discharge current.

4) Appendix A: The Vacuum System[4,5]

All vacuum systems used in the plasma physics laboratory employ a water-cooled oil vapor diffusion pump backed by a rotary vacuum pump, as sketched in Figure I-7. In the normal mode of operation, valves 1 (high vacuum valve) and 2 (foreline valve) are open and valve 3 (roughing line valve) is closed. In this mode, the diffusion pump is pumping on the system and the rotary (or mechanical pump is pumping on the diffusion pump. The base pressure of the system may be as low as 10^{-6} torr (mm Hg) and the foreline pressure should be in the range 1 - 50 microns (1 micron =10^{-3} torr).

The oil diffusion pump cannot pump gases at pressures greater than a few hundred microns. Attempting to operate the pump at pressures greater than this will result in the cracking of the diffusion oil and possibly in the contamination of the system. Never expose a hot diffusion pump to pressures greater than a few hundred microns. If the system is at atmospheric pressure, it must be pumped down to less than 75 microns before the high vacuum valve is opened. This is accomplished by opening valve 3 (with valves 1 and 2 closed) and allowing the mechanical pump to pump the system through the roughing line. When the system pressure is below 75 microns, valve 3 is closed and valves 1 and 2 are opened.

Valves 4 and 5-control neutral gas pressure in the system. Valve 4 functions as on-off valve, while the leak valve controls the gas pressure. The two gases used most frequently in our laboratory are Argon and Helium, and typical operating pressures range from 2 x 10^{-5} torr to 2 x 10^{-3} torr.

Valve 6 is used to bring the system to atmospheric pressure when it is desired to open the plasma chamber.

Pressure Measurements

The wide range of pressures to be measured necessitates the use of two different types of pressure gauges. The Hastings gauge, a thermocouple type of gauge, can read pressures from about 1 micron to atmosphere. The Hastings gauge serves two purposes in our vacuum systems. When roughing out the system, the Hastings gauge determines when the pressure is low enough to open the high vacuum valve connecting the diffusion pump to the system. When the system is in the normal operating mode, the gauge is used to monitor the foreline pressure.

In the normal operating mode, the system pressure is too low to be read with a Hastings gauge, and an ionization gauge must be used. The ion gauge reads pressure accurately from about 10^{-3} to 10^{-8} torr. Operation of the gauge at pressures above a few microns for any length of time will severely shorten the tube life. Be sure to turn off the filament of the ion gauge tube whenever the possibility of its being exposed to higher than recommended pressures exists. AC power to the ion gauge, as well as to the Hastings gauge should be left on at all times.

The ion gauge operates by ionizing the gas in the tube and measuring the collected ion current.

Therefore, the sensitivity of the gauge depends on the ionization cross section of the gas. The gauge is calibrated for dry air and the correction chart for various gases appears in Table I-2.

Operating Procedures

When the system is in the normal operating mode only the gas control valves, 4 and 5, need be operated. Valve 4 is opened and the leak valve is adjusted to obtain the desired neutral pressure. Close valve 4 when the experiment is completed.

Except in the event of a major leak, or for maintenance purposes, the diffusion and mechanical pumps are never shut off. If the pumps must be shut off, steps 1 through 4 in the shut down procedure should be followed. To put the system back into operation, follow steps 1 through 5 in the turn on procedure.

The plasma chamber is left under high vacuum except when it is necessary to bring the chamber to atmosphere in order to replace filaments or make other changes. In this case, steps 1 and 2 in the shut down procedure are followed. To resume operation, follow steps 4 through 6 of the turn on procedure.

Turn On Procedure

1. Turn on water cooling for diffusion pump. Shut all valves.
2. Open valve 2 and turn on mechanical pump.
3. When foreline pressure reaches 50 microns or less, turn on diffusion pump. The diffusion pump will take about one half hour to reach operating temperature.
4. When the diffusion pump is hot, close valve 2 and open valve 3 to rough out system.
5. When the system pressure goes below 50 microns, shut valve 3 and open valve 2. Slowly open the high vacuum valve (1), while monitoring the foreline pressure. Do not allow the foreline pressure to go above a few hundred microns. If the foreline pressure does not drop below 1 hundred microns after a few minutes, there is probably a large leak in the system, and the high vacuum valve should be shut.
6. The ionization gauge filament may be turned on after the high vacuum valve has been open a few minutes.

Shut Down Procedure

1 Shut off ionization gauge filament and close high vacuum valve. (Valve 2) should be open and valve 3 closed.)
2. Open valve 6, bringing the plasma chamber to atmospheric pressure.
3. Shut off diffusion pump heater. Allow one half hour for the pump to cool.
4. When the diffusion pump is cool, the mechanical pump and the cooling water may be shut off.

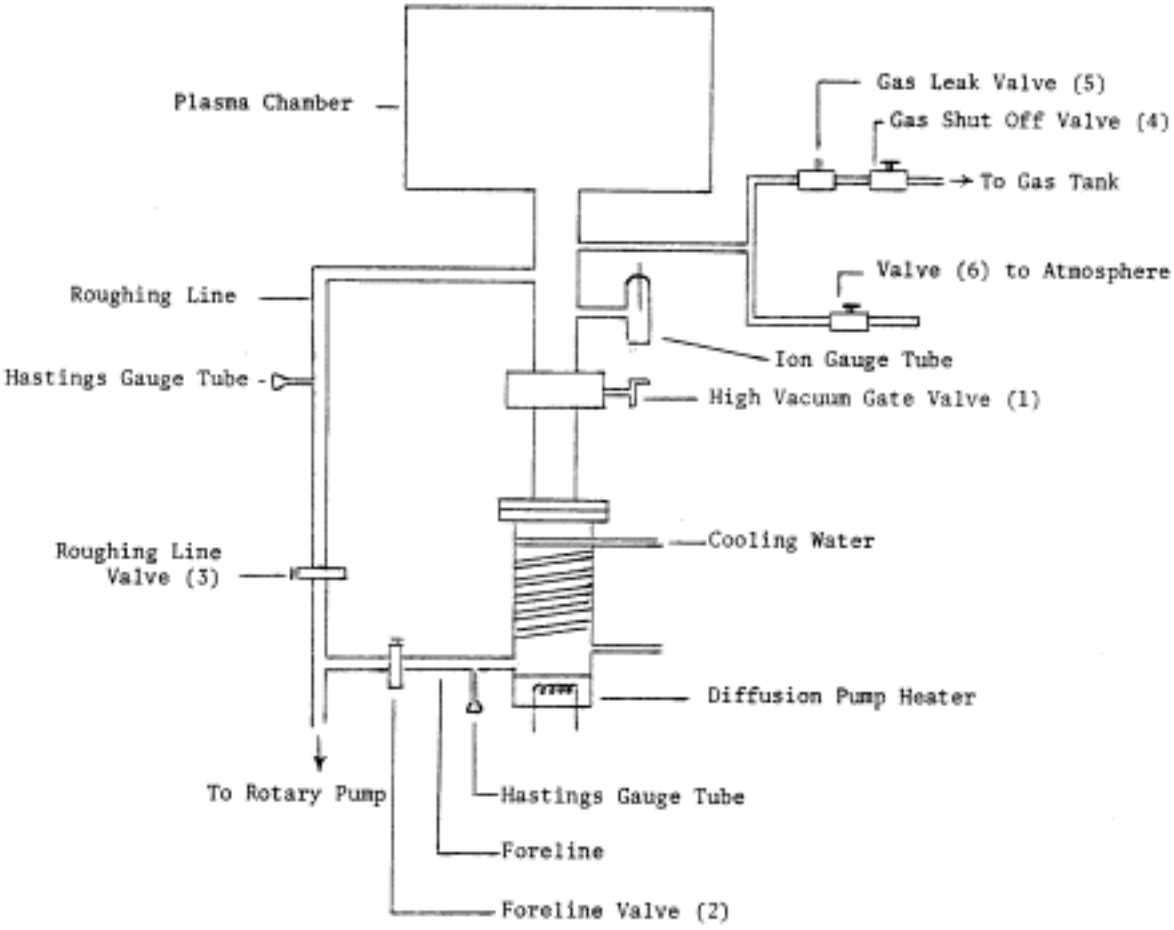

Figure I-7.
Typical Vacuum System

5) Appendix B: Construction of Plasma Sources

Two double plasma device[†] configurations will be described here. One uses permanent magnetic dipoles while the other does not. The choice of configuration depends upon the experimental requirements. The following table summarizes the advantages of each configuration.

TABLE I-3

Simple DP	DP with Surface Magnetic Confinement
1. T_e can be varied with the "Maxwell Demon".	1. High % ionization can be achieved using fewer filaments.
2. Spatial density inhomogeneity can be easily adjusted.	2. Lower neutral pressure needed to Achieve a given plasma density.
3. Plasma potential is controlled by the anode.	3. Little or no cooling required because of low filament dissipation power.
	4. Suitable for afterglow studies.

a) Simple DP device: As illustrated in Figures I-8 - I-10, a vacuum chamber and filament structure are the only components required to construct this device. The vacuum wall may serve as the discharge anode whenever the plasma source desired is only a single plasma, Figure I-11.

The concentric inner grid of Figures I-9 and I-10 becomes the plasma anode when the device operates as a double plasma source. In that case, the two plasmas are isolated from each other by a launching grid of fine meshed wire. The potential of each plasma can be controlled independently from the potential of the other.

[†] These sources are called Double Plasma or DP devices because two sources are usually used together in wave experiments.

b) DP device[3] with surface magnetic confinement:

i) The simple double plasma system described above can be converted into one with surface magnetic confinement by permanent magnets if the wall is made sufficiently thin. (The wall must be thick enough to withstand atmospheric pressure.) A non-magnetic stainless sheet (.090" thick) has been rolled into a 14" (35 cm) diameter chamber. Access ports are welted into the 10 cm diameter holes on the sides. Ferrite magnets (Crucible Magnetic Division 2.2 cm diameter by 2.5 cm long $B_{max} \approx 2$ kG) are held in place on the surface with stainless steel straps as shown in Figure I-11. The placement of permanent magnets on the outside surface prevents contamination of the vacuum system by impurities on surfaces of magnets. This arrangement has the added advantage that in confinement experiments students can check the effectiveness of surface magnetic confinement by removing the magnets. Optimization of the spacing between adjacent rows of magnets can be easily achieved without reopening the vacuum system.

ii) An economical method of producing this plasma with clean vacuum uses a non-magnetic stainless steel restaurant vessel. Figure I-12 shows a 24 liter thin walled (0.92 mm of 1/32") vessel with 30 cm diameter and 33 cm length. For conversion into a plasma device, the vessel is covered with an aluminum flange in which a groove is cut to vacuum seal the system by means of an 0-ring as shown in Figure I-l3. Filaments and probes are inserted through this end flange. Radial probes as well as glass windows are installed on the side of the vessel, using swageloks as illustrated in Figure I-14. By simply tightening the nut on the inner side of the vessel the 0-ring of the swagelok makes a good vacuum seal against a flattened portion of the cylindrical wall. Using a 2" NRC oil diffusion pump and an Edwards (ED-100) mechanical pump, an effective pumping speed of 285 liter/sec and a base pressure of 6×10^{-7} torr have been obtained.

The single vessel system with an external arrangement of magnets described above is easily joined with another similar size vessel to form a double vessel system. In this case, the rim of the first vessel is attached to the O-ring of flange A as seen in Figure I-16. The bottom of the second vessel is cut away and then placed inside a deep O-ring groove of flange B. The two flanges are then clamped together with another O-ring in between. Obviously a long multi-vessel system can be constructed by applying this technique.

iii) Typical operating parameters for three representative D.C. discharge devices suitable for introductory plasma experiments are summarized in Table I-4.

References

1. C. D. Child, Phys. Rev. 32, 492 (1911) I. Langmuir, Phys. Rev. 2, 450 (1913).
2. R. Limpaecher and K. R. MacKenzie, Rev. Sci. Instrum. 44, 726 (1973) UCLA PPG-114 (1972).
3. K. N. Leung, UCLA PPG-222 (1975).
4. S. Dushman, Scientific Foundations of Vacuum Techniques, 2nd Ed. (Wiley, New York) 1972.
5. G. Lewin, Fundamentals of Vacuum Science and Technology, (McGraw-Hill, New York) 1965.

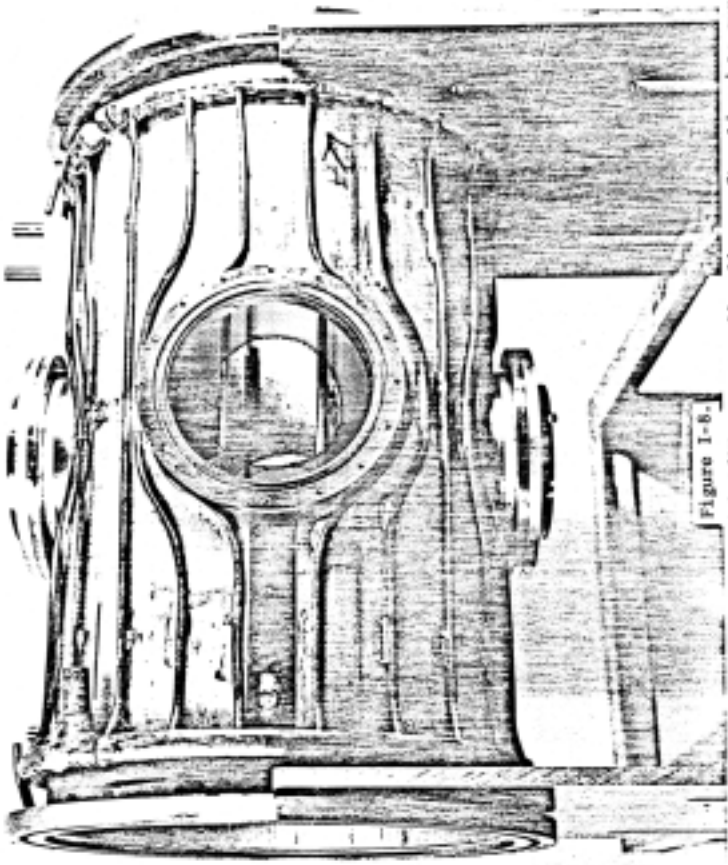

Figure I-8.

Picture of a stainless steel vacuum chamber with 1/2" copper cooling lines soft-soldered to surface. The 1" leads to the filament structure are visible in the upper right-hand corner. The diameter is 35 cm and the length is 70 cm. Wall thickness is 0.64 cm.

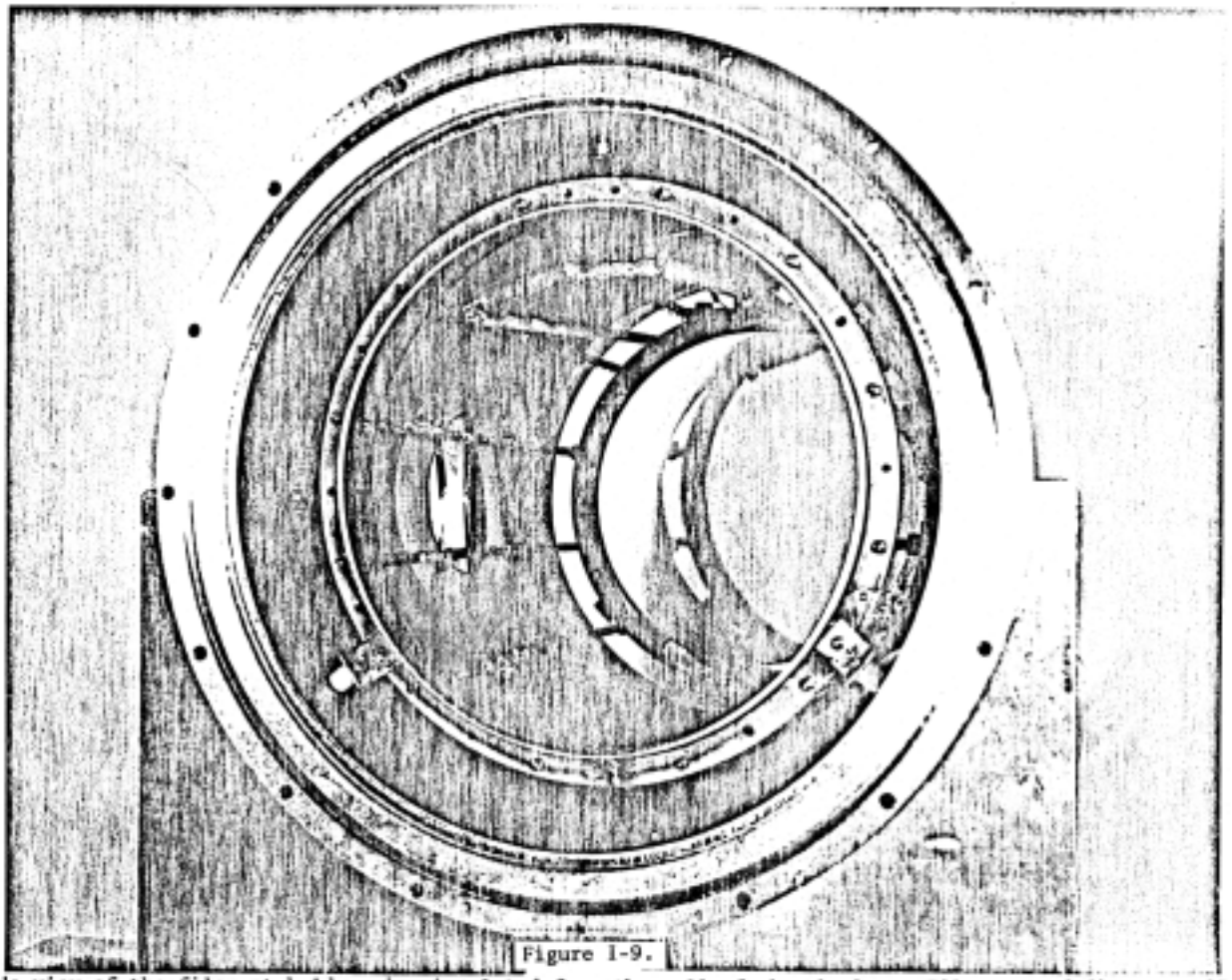

Figure 1-9.

Side view of the filament holder ring insulated from the wall of the chamber. Filaments of diameter .25 mm - .32 mm (or .01" - .015") are wound onto the connection posts. The voltage between adjacent axial rods is the applied filament voltage (typically 15 V). The screen grid behind serves as the anode which is insulated from the wall and the cylindrical filament structure.

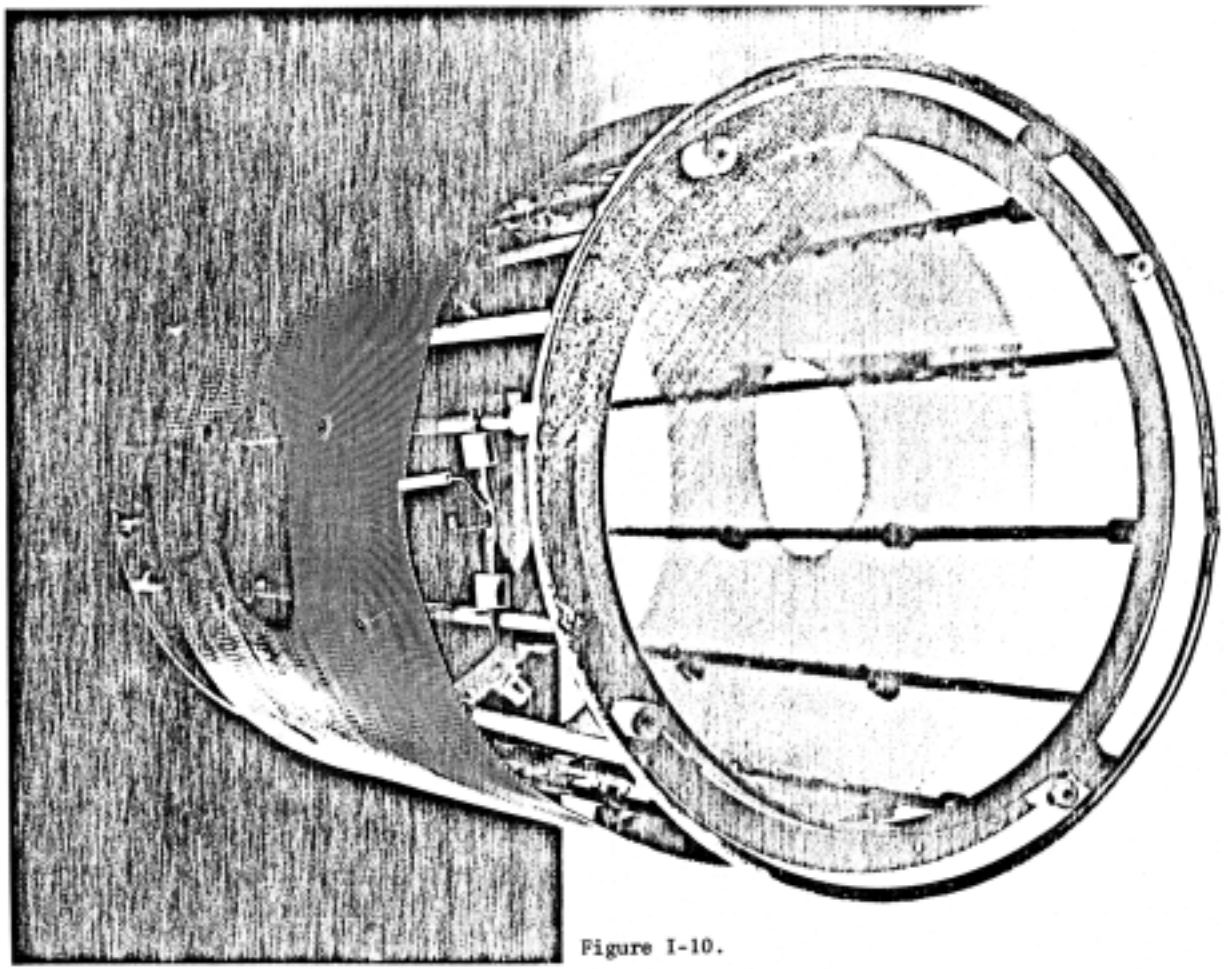

Figure I-10.

The filament structure together with the anode grid (20 lines/inch, tungsten). The fine grid (100 lines/inch, tungsten) in front is used to isolate one filament chamber from another when a double plasma configuration is desired. This grid is isolated from all other elements and its voltage can be separately controlled through an electrical connection outside the chamber.

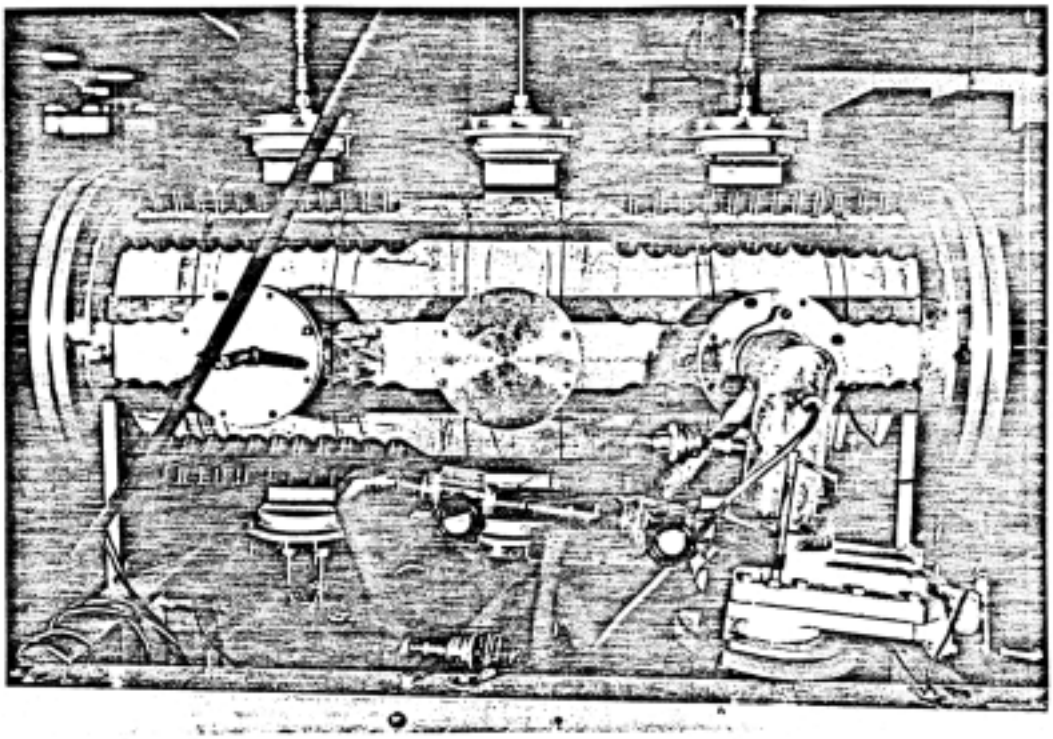

Figure I-11.

A useful single plasma source showing exterior permanent magnets, diagnostic ports and vacuum apparatus.

TABLE I-4

OPERATING CONDITIONS FOR THREE TYPICAL REGIMES (Reference 3)

Device Characteristics: 24 liter volume, 30 cm diameter, 33 cm length, .92 mm wall thickness

5 tungsten wire filaments, .013 cm diameter (3 mil), 10 cm length

Discharge voltage = 60 V, Argon neutral gas

Surface Magnetic Confinement	Plasma Density	Neutral Pressure	Total Discharge Current	Filament Heating Current (per filament)
None	2×10^{8} cm^{-3}	10-4 torr	1 amp	3 amp
Exterior surface Permanent magnets	6×10^{10} cm-3	10^{-4} torr	1 amp	3 amp
Exterior surface permanent magnets	1×10^{12} cm^{-3}	4×10^{-4} torr	10 amp	4 amp

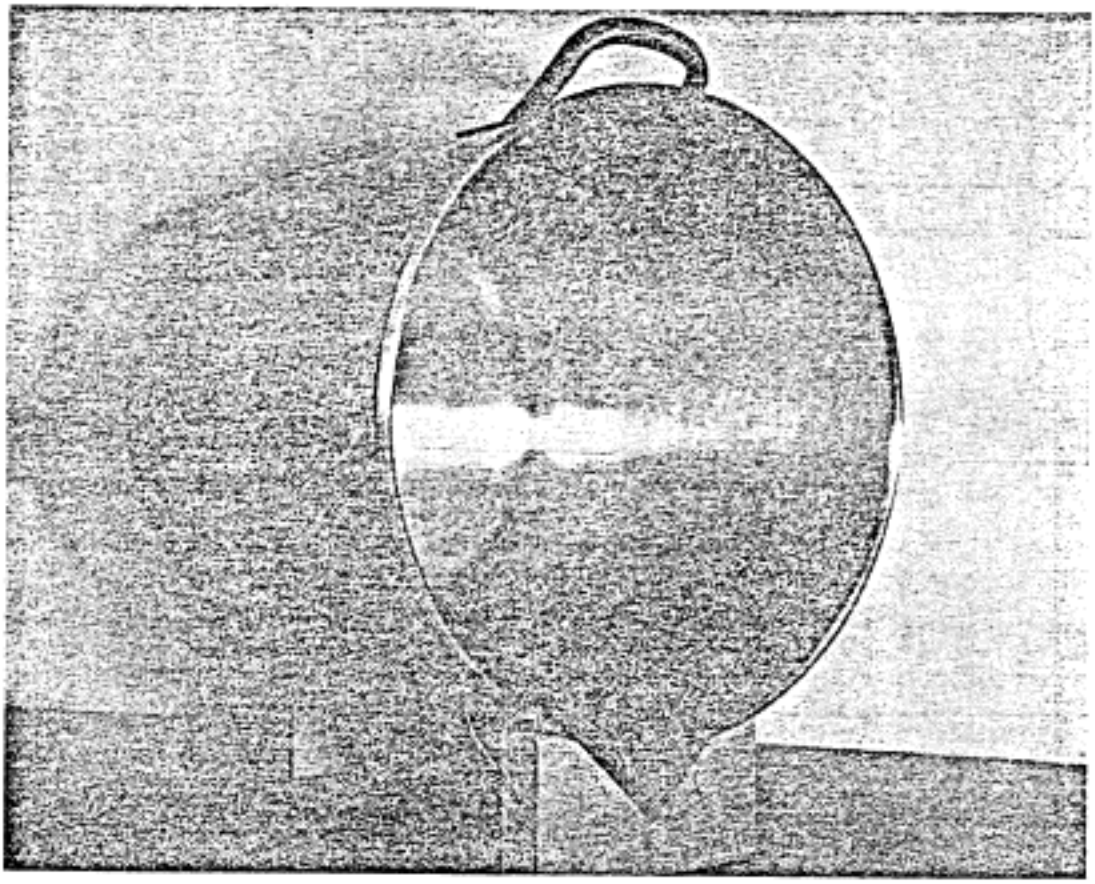

Figure I-12.

A stainless-steel cooking vessel, with $\frac{1}{4}$" thick wall, 35 cm diameter and 40 cm length. Used as a plasma container (after K. N. Leung).

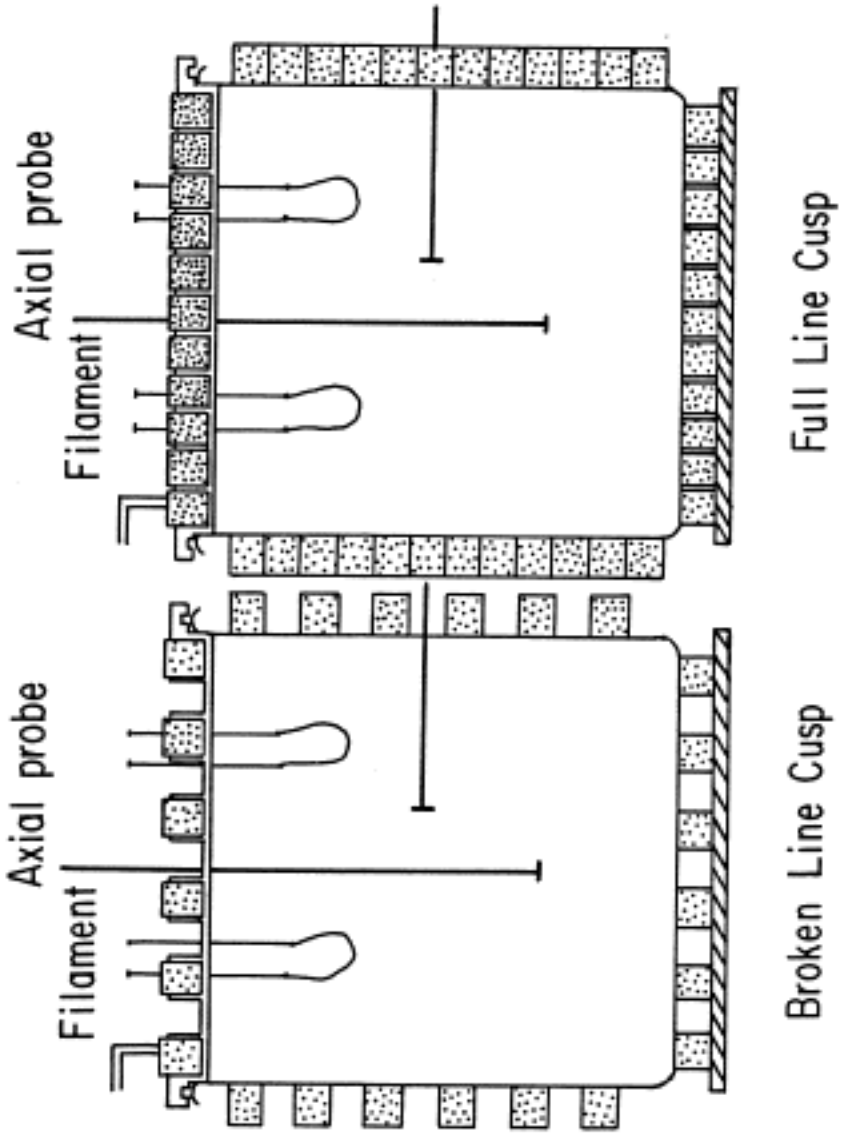

Figure I-13.

The Single Vessel System (after K. N. Leung)

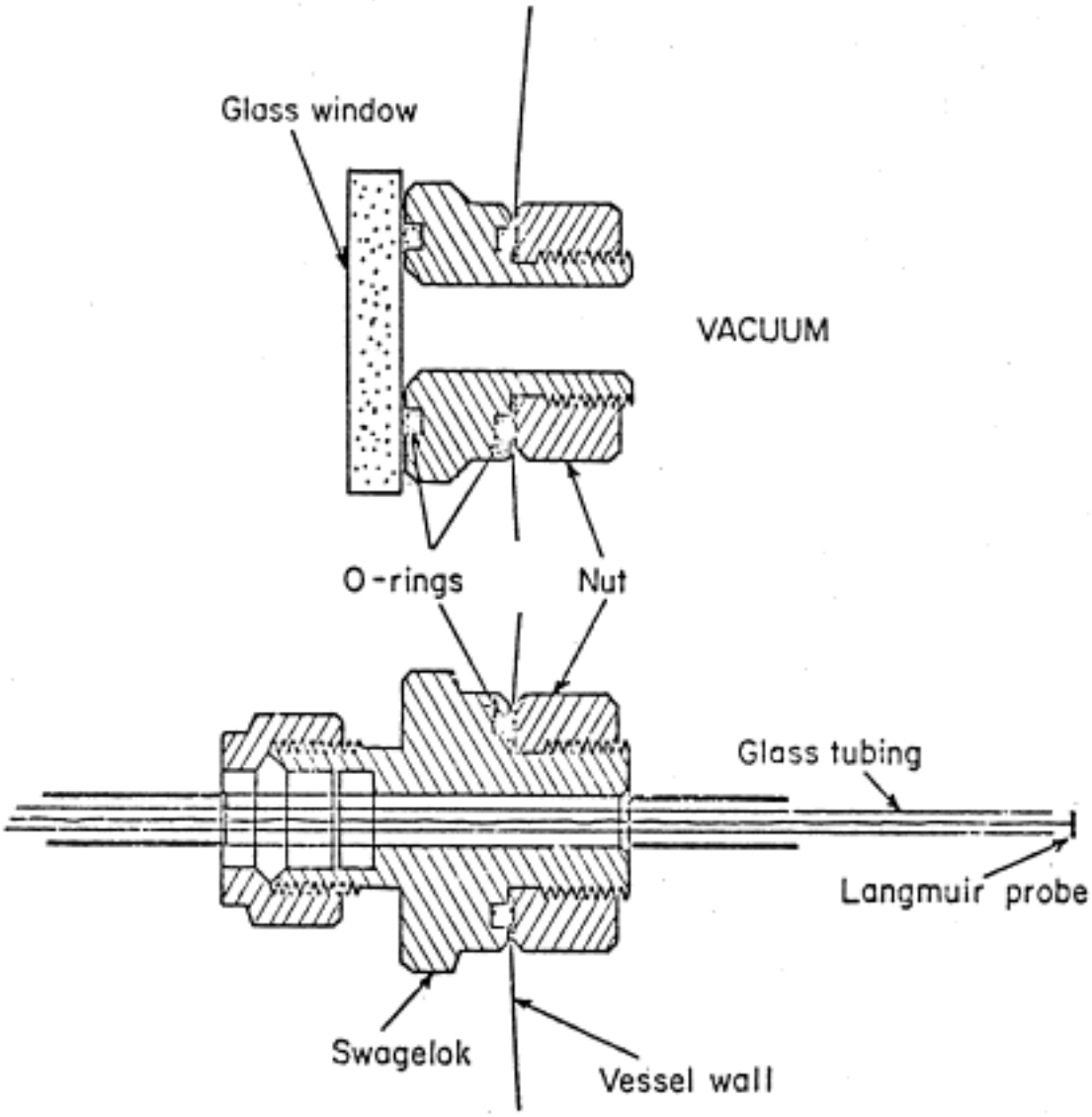

Figure I-14.

(after K. N. Leung)

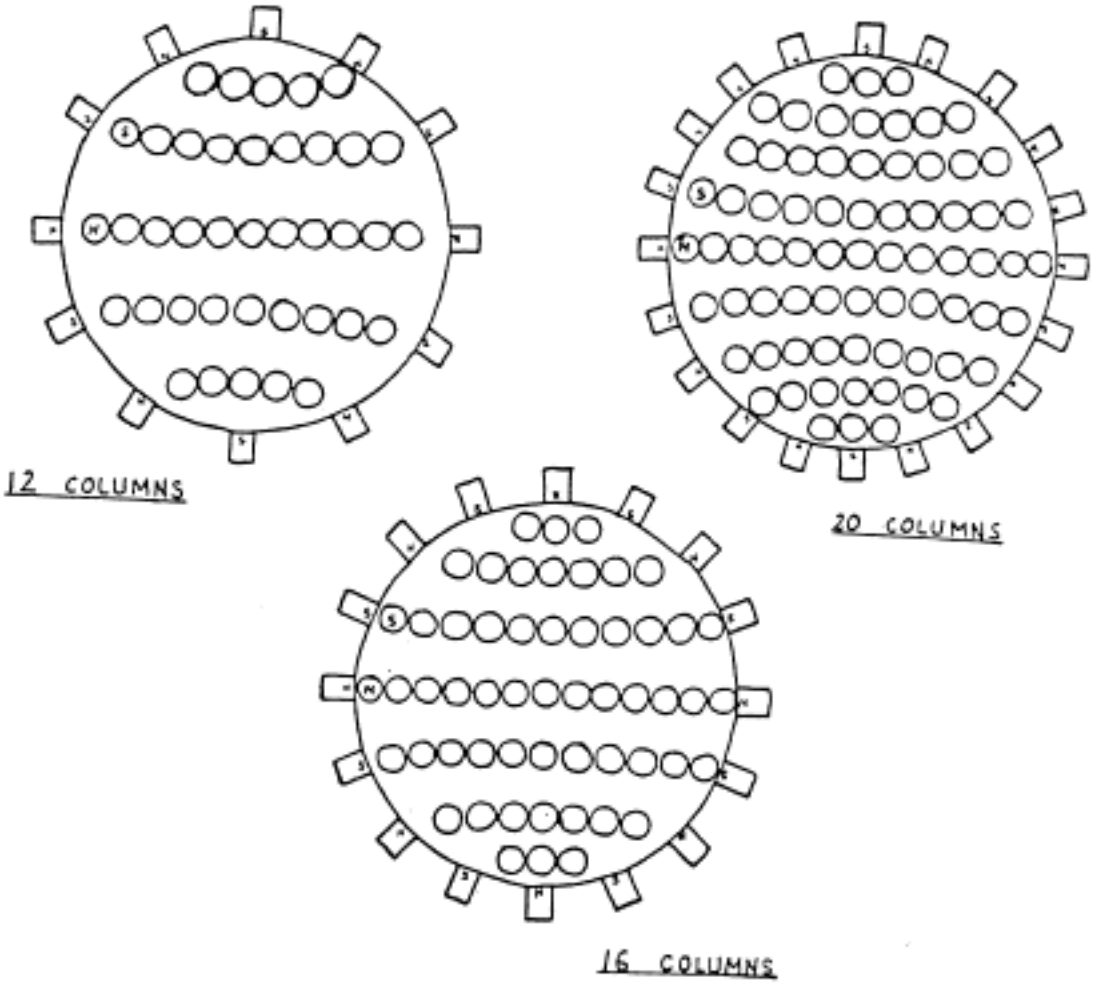

Figure I-15.

Magnet Arrangements on End Plate (after K. N. Leung)

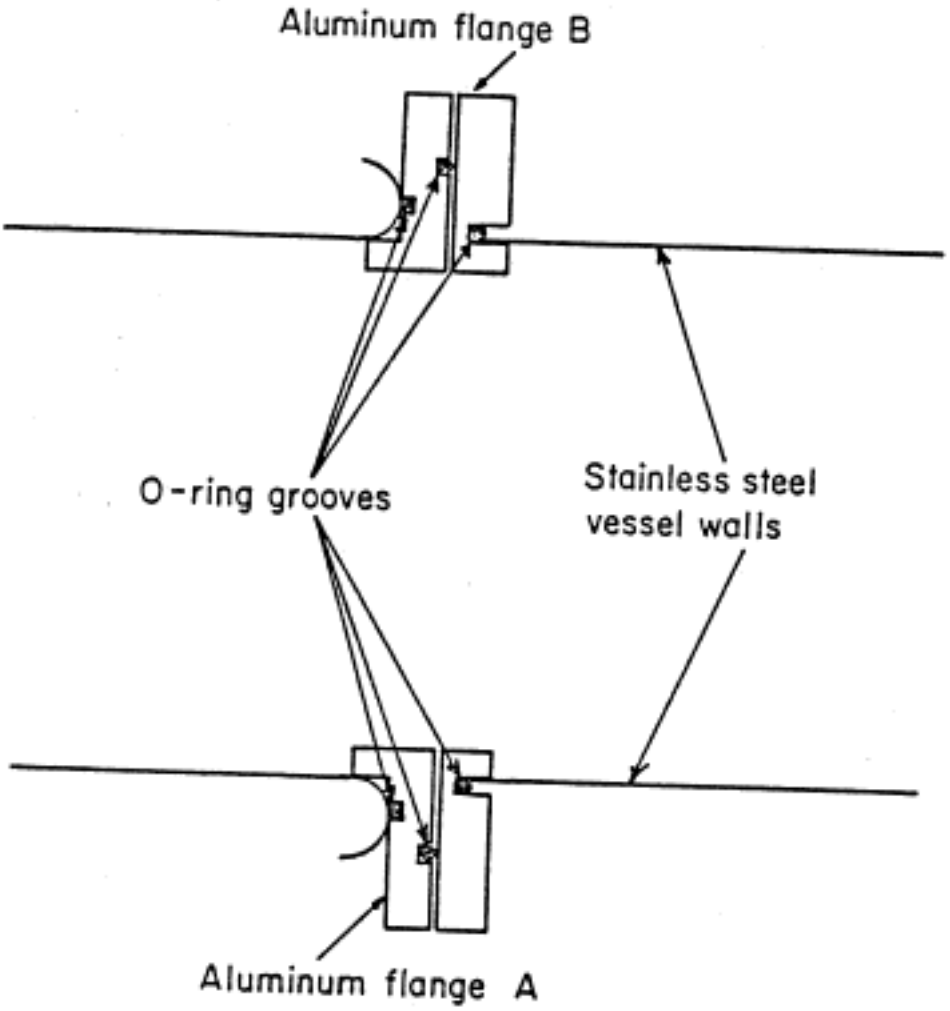

Figure I-16

(after K. N. Leung)

Chapter II. Basic Plasma Diagnostics

One of the most important and frequently used plasma diagnostic techniques is the Langmuir probe method. This method, which was first introduced by Langmuir[1] about fifty years ago, can be used to determine the values of the ion and electron densities, the electron temperature, and the electron distribution function. This method involves the measurement of electron and ion currents to a small metal electrode or probe as different voltages are applied to the probe. This yields a curve called the probe characteristic of the plasma.

Another important technique, using microwaves, is frequently employed to measure plasma parameters, especially in situations where it is difficult to insert probes into the medium. An interferometer method is used to determine the phase shift of the microwaves transmitted through the plasma and the average electron density is deduced from the amount of phase shift.

By combining the microwave or ratio frequency method with the probe technique, we can measure the density to better than 1% accuracy. Electromagnetic waves propagating along a density gradient with frequency ω_o excite electron plasma waves at the critical density layer z_o for which $\omega_o = \omega_p(z_o)$, where ω_p is the plasma frequency. Since the propagation of these electron plasma waves is a sensitive function of the density profile, a careful mapping of the electron plasma wave propagation characteristics will reveal the density along its propagation path. This more advanced method is described in Chapter V.

1) Langmuir Probe

The fundamental plasma parameters can be determined by placing a small conducting probe into the plasma and observing the current to the probe as a function of the difference between the probe and plasma space potentials. The plasma space potential is just the potential difference of the plasma volume with respect to the vessel wall (anode). It arises from an initial imbalance in electron and ion loss rates and depends in part upon anode surface conditions, and filament emission current.

Referring to the probe characteristic, Figure II-l, we see that in region A when the probe potential, V_p, is above the plasma space potential, V_s, the collected electron current reaches a saturated level and ions are repelled, while in region B just the opposite occurs. By evaluating the slope of the electron I-V characteristic in region B the electron temperature T_e is obtained, and by measuring the ion or electron saturation current and using the T_e measurement, the density can be computed.

The current collected by a probe is given by summing over all the contributions of the various plasma species:

$$I = A\sum_i n_i q_i \bar{v}_i \tag{1}$$

where A is the total collecting surface area of the probe; $\bar{v}_i$ = the average velocity of species I, and $\bar{v}_i = \frac{1}{n}\int v f_i(\vec{v}) d\vec{v}$ for unnormalized $f_i(\vec{v})$. It is well known in statistical mechanics that collisions among particles will result in an equilibrium velocity distribution f given by the Maxwellian function:

$$f_\alpha(\vec{v}) = n\left(\frac{2\pi KT_\alpha}{m_\alpha}\right)^{-3/2} Exp\left(\frac{-\frac{1}{2}m_\alpha|\vec{v}|^2}{KT_\alpha}\right) \tag{2}$$

This distribution function is used to evaluate the average velocity of each species.

We will first consider a small plane disc probe which is often used in our experiments. When it is placed in the xy plane, a particle will collide with the probe and give rise to a current only if it has some v_x component of velocity. Thus, the current to the probe does not depend on v_y or v_z. The current to the probe from each species is a function of V º V_p - V_s.

$$I(v) = nqA\int_{-\infty}^{\infty} dv_y\left(\frac{2\pi KT_\alpha}{m_\alpha}\right)^{1/2} Exp\left(\frac{\frac{1}{2}m_\alpha v_y^{\,2}}{KT_\alpha}\right)\int_{-\infty}^{\infty} dv_z\left(\frac{2\pi KT_\alpha}{m_\alpha}\right)^{1/2} Exp\left(\frac{\frac{1}{2}m_\alpha v_z^{\,2}}{KT_\alpha}\right)$$
$$\cdot\left(\int_{v_{min}}^{\infty} dv_x v_x\left(\frac{2\pi KT_\alpha}{m_\alpha}\right)^{1/2} Exp\left(\frac{\frac{1}{2}m_\alpha v_x^{\,2}}{KT_\alpha}\right)\right). \tag{3}$$

The lower limit of integration in the integral over v_x is v_{min} since particles with v_x component of velocity less than $v_{min} = \left(\frac{2qV}{m_\alpha}\right)^{1/2}$ are repelled, Figure II-2.

The integrals over v_y and v_z in (3) give unity so the current of each species is just

$$I(v) = nqA\int_{v_{min}}^{\infty} dv_x v_x\left(\frac{2\pi KT_\alpha}{m_\alpha}\right)^{-1/2} Exp\left(\frac{\frac{1}{2}m_\alpha v_x^{\,2}}{KT_\alpha}\right) \tag{4}$$

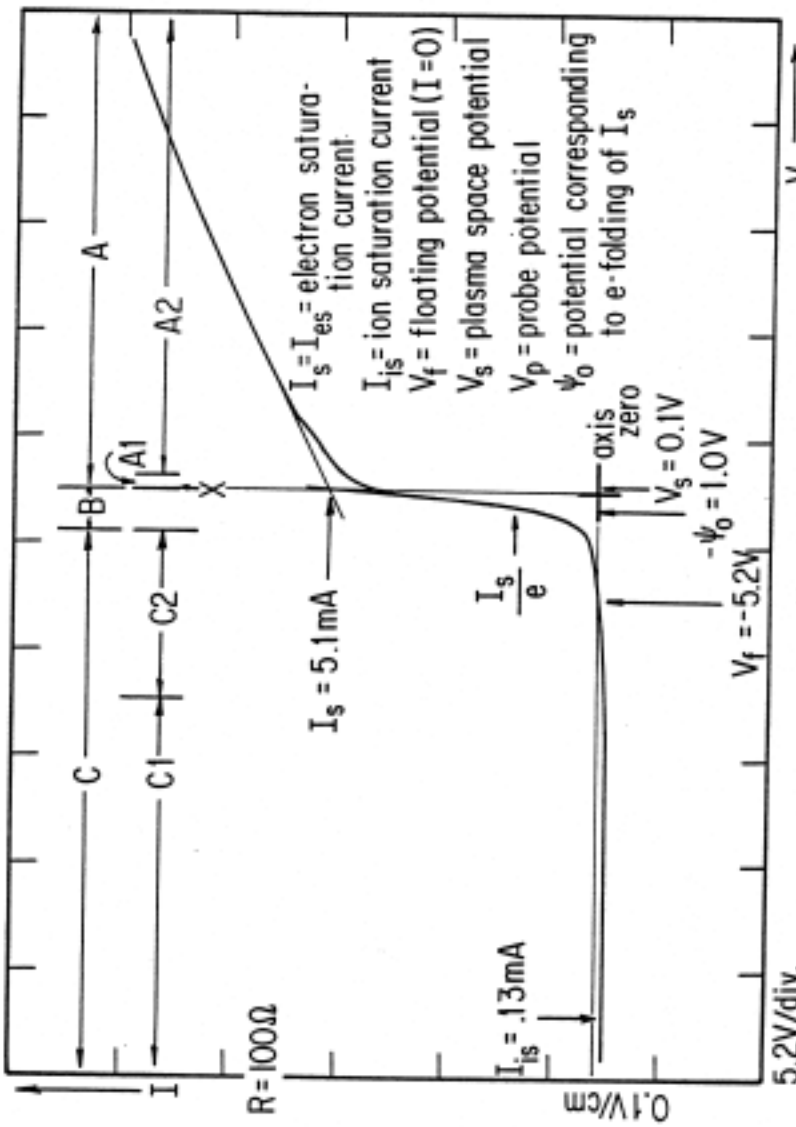

Figure II-1.
Sample Langmuir Probe Characteristic (Radial disc probe placed near center of single plasma): Region C1 - Ion saturation (electrons repelled); Region C2 - Ion saturation plus small primary electron current; Region B - Secondary electrons added to current of primaries and ions; X - Probe at space potential (zero electric probe field); Region A1 - Electron saturation with cooler ions being repelled; Region A2 - Electron saturation, no ion current. Note how ψ_o facilitates identification of secondary electron temperature, T_e (1.0 eV for this data).

a) The electron saturation current, I_{es}: In this region all electrons with v_x component toward probe are collected. We obtain the electron saturation current

$$I_{es} = -neA\int_0^\infty dv_x v_x \left(\frac{2\pi KT_e}{m_e}\right)^{-1/2} Exp\left(\frac{-\frac{1}{2}m_e v_x^{\,2}}{KT_e}\right) = -neA\left(\frac{KT_e}{2\pi m_e}\right)^{1/2} \tag{5}$$

Similarly, in region B and C where $V_p < V_s$ and electrons are repelled, the total current is

$$I(v) = I_{is} - neA\int_{v_{\min}}^\infty dv_x v_x \left(\frac{2\pi KT_e}{m_e}\right)^{-1/2} Exp\left(\frac{-\frac{1}{2}m_e v_x^{\,2}}{KT_e}\right). \tag{6}$$

Substituting $\frac{1}{2}m_e v_{\min}^{\,2} = -eV$, (6) becomes

$$I(v) = I_{is} - neA\left(\frac{KT_e}{2\pi m_e}\right)^{1/2} Exp\left(\frac{eV}{KT_e}\right) \tag{7}$$

since $V < 0$ in region B and C. Equation (7) shows that the electron current increases exponentially until the probe voltage is the same as the plasma space potential ($V = V_p - V_s = 0$).

b) The ion saturation current, I_{is}: The ion saturation current is not simply given by an expression similar to (5). In order to repel all the electrons and observer I_{is}, V_p must be negative and have a magnitude near KT_e/e as shown in Figure II-3. The sheath criterion[2] requires that ions arriving at the periphery of the probe sheath be accelerated toward the probe with an energy $\sim KT_e$, which is much larger than their thermal energy KT_i. The ion saturation current is then approximately given as

$$I_{is} = neA\left(\frac{2KT_e}{m_i}\right)^{1/2}. \tag{8}$$

Even though this flux density is larger than the incident flux density at the periphery of the collecting sheath, the total particle flux is still conserved because the area at the probe is smaller than the outer collecting area at the sheath boundary.[2-5]

c) Floating potential V_f: Next we consider the floating potential. When $V = V_f$, the ion and electron currents are equal and the net probe current is zero. Combining equations (7) and (8), and letting $I = 0$, we get

$$V_f = -\frac{KT_e}{e}\ln\left(\frac{m_i}{4\pi m_e}\right)^{1/2} \tag{9}$$

d) The electron temperature, T_e : Measurement of the electron temperature can be obtained from equation (7). For $I_{is} < I$ we have

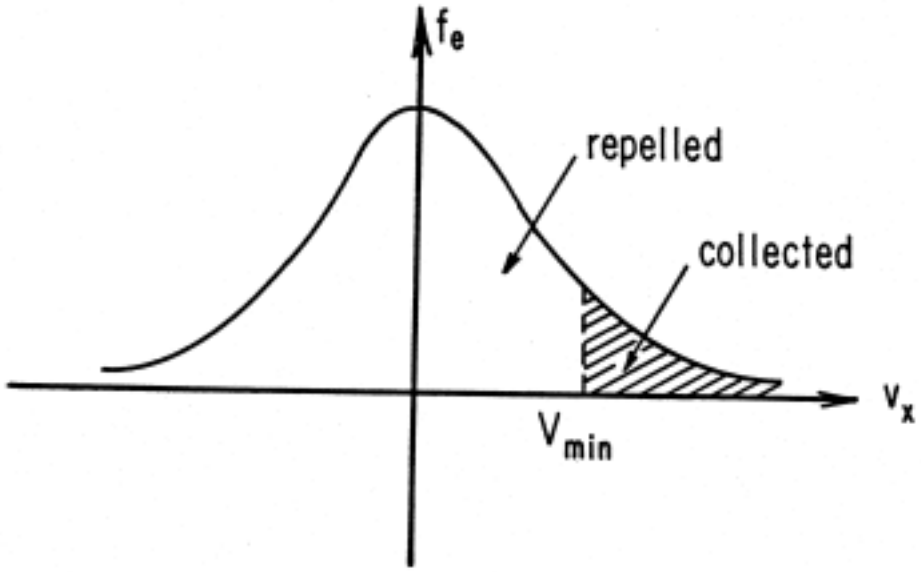

Figure II-2.

Electron Velocity Distribution
All electrons with energy $|eV|$ greater than $\frac{1}{2} m_e v_{min}^2$ are collected.

$$I(v) = -neA\left(\frac{KT_e}{2\pi m_e}\right)^{1/2} Exp\left(\frac{eV}{KT_e}\right) = I_{es}\ Exp\left(\frac{ev}{KT_e}\right)$$

(10)

$$\frac{d\ln|I|}{dV} = \frac{e}{KT_e}.$$

(11)

By differentiating the logarithm of the electron current with respect to the probe voltage V for V < 0, the electron temperature is obtained. We note that the slope of lnI vs. V is a straight line only if the distribution is a Maxwellian.

e) Measurement of the electron distribution function, $f_e(v_x)$: The electron current to a plane probe could be written in a more general expression as (again neglecting the ion current)

$$I = nqA\int_{v_{\min}}^{\infty} v_x f(v_x) dv_x = \frac{nqA}{m_e}\int_{qV}^{\infty} f(qV) d(qV)$$

(12)

$$\frac{dI}{d(qV)} \alpha\ f(qV)$$

where q = -e, the electron charge. This is a very simple way of obtaining the electron energy distribution function. If we measure $f(v_x)$ as a function of plasma position, we can obtain the phase space distribution $f(v_x,x)$. A further refinement is to observe the distribution at a given time t after a certain event using a sampling oscilloscope. This results in the complete description, f(v,x,t), of the electrons in a given system.

2) Double Probes[5-8]

A double probe consists of two electrodes of equal surface area, separated by a small distance and immersed in the plasma, Figure II-4. One probe draws current I_1 while the other is drawing current I_2. To find the electron temperature of the plasma, we consider quantitatively the current to the probe for various potential differences between the probes, Figure II-5. Since the probes are floating at V_f of the plasma, i.e., the double probe circuit has no plasma ground (anode) connection, the total current in the probe circuit must be zero. From (7) and (5), the current collected by probe #1 is

$$I_1 = I_1\ is - I_1\ es\ Exp\left(\frac{e(V_1 + V_f - V_s)}{KT_e}\right)$$

(13)

Using the definition of the floating potential with (7),

$$I_{es}\ Exp\left(\frac{e(V_f - V_s)}{KT_e}\right) = I_{is}$$

(14)

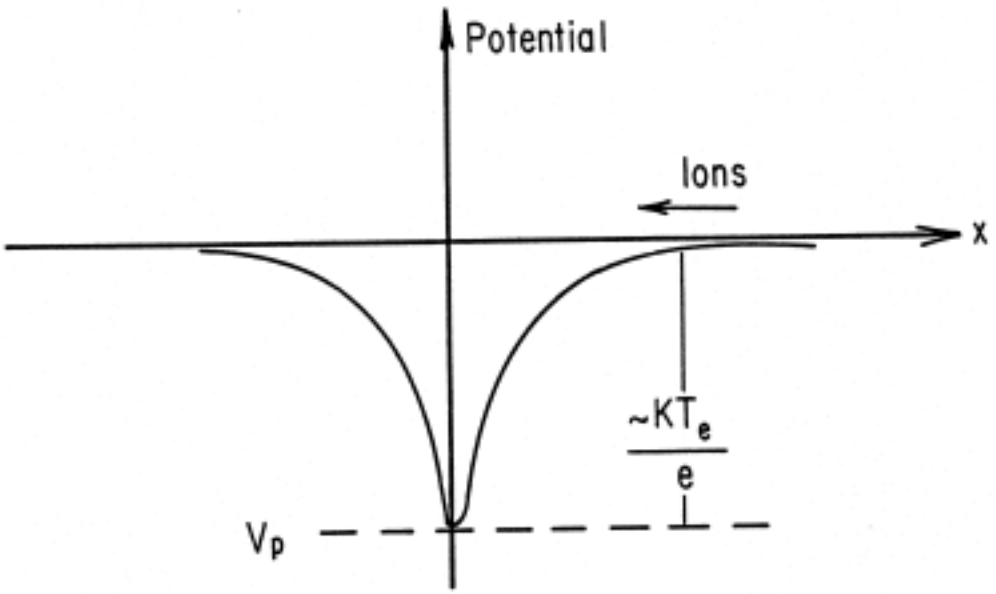

Figure II-3.

Sheath potential as function of distance x from infinite plane probe.

hence (13) becomes

$$I_1 = I_1\ is\left[1 - Exp\left(\frac{eV_1}{KT_e}\right)\right] \tag{15}$$

In the same manner we get

$$I_2 = I_2\ is\left[1 - Exp\left(\frac{eV_2}{KT_e}\right)\right] \tag{16}$$

If the probe areas are equal, then (8) implies

$$I_1\ is = I_2\ is = I_{is} \tag{17}$$

Zero net probe circuit current motivates the definition

$$I \equiv I_1 = -I_2$$

Combining this with equations (15), (16), and (17) yields

$$\frac{I - I_{is}}{-I - I_{is}} = Exp\left(\frac{e\psi}{KT_e}\right) \tag{18}$$

where the double probe potential is defined by $\psi \equiv V_1 - V_2$. Solving equation (18) for I

$$I = -I_{is}\tanh\left(\frac{e\psi}{2KT_e}\right) \tag{19}$$

Differentiating equation (19) with respect to ψ at ψ=0

$$\left.\frac{dI}{d\psi}\right|_{\psi=0} = -I_{is}\left.\sec h^2\frac{e\psi}{2KT_e}\right|_{\psi} = 0\left(\frac{e}{2KT_e}\right) \tag{20}$$

i.e., electron temperature is related to the slope of the double probe characteristic by

$$\frac{dI}{d\psi} = -I_{is}\left(\frac{e}{2KT_e}\right) \tag{21}$$

The double probe can collect a maximum current equal to the ion saturation current and does not disturb the plasma as much as the single probe with its anode connection. However, the small amount of detected current (microampere range) does warrant a much more sensitive detection circuit, as in Figure II-4.

The student is required to compare the electron temperatures and plasma densities obtained with the single and the double probes.

3) Microwave Interferometer[9,10]

The basic idea behind this diagnostic scheme is as follows. The plasma acts like a dielectric medium to electromagnetic radiation, and a wave propagating through the plasma will suffer a change in phase

$$\Delta\phi = \int_0^L \left(k_{vacuum} - k_{plasma}\right) dx \tag{22}$$

where L is the path length of the plasma, k_{vacuum} = w/c is the free space wave number of the electromagnetic waves, and k_{plasma} is the wave number of the wave propagating in the plasma, which is given by the dispersion relation

$$k_{plasma} = \frac{\left(\omega^2 - \omega_{pe}{}^2\right)^{1/2}}{c} \tag{23}$$

Here w is the wave frequency, $\omega_{pe} = \left(\frac{4\pi n e^2}{m}\right)^{1/2}$, the electron plasma frequency and c is the speed of light. If the plasma density is uniform over the distance L, we obtain from equation (23) for the phase shift

$$\Delta\phi = \frac{\omega}{c}\left(1 - \left(1 - \frac{\omega_{pe}{}^2}{\omega^2}\right)^{1/2}\right) L. \tag{24}$$

a) Density measurement by phase shift: When $w_{pe} << w$ (note this restriction) we obtain a relation between the phase shift and plasma density

$$\Delta\phi = \frac{\omega}{c}\left(\frac{1}{2}\frac{\omega_{pe}{}^2}{\omega^2}\right) L. \tag{25}$$

Defining the critical density by $\frac{4\pi n_c e^2}{m_e} \equiv \omega^2$ we can express equation (25) alternatively by

$$\frac{n}{n_c} = \frac{2\Delta\phi}{k_{vac} L}, \; where \; k_{vac} \equiv \frac{w}{c} \tag{26}$$

Since all laboratory plasmas have a certain degree of inhomogeneity, i.e., some density gradient, the phase shift Df is an integrated quantity as represented by equation (23). However, the density profile can be obtained by relative density measurement using movable probes. If we write $n(x)=n_0 f(x)$, where f(x) contains the spatial variation in the plasma density, a relation similar to equation (26) can be achieved using

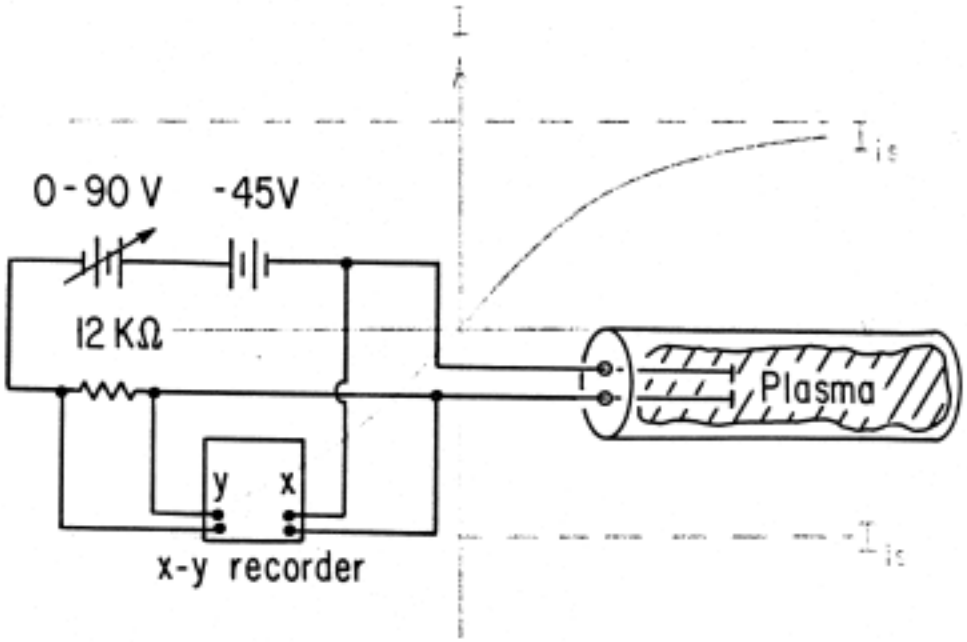

Figure II-4.

Typical Double Probe Manual Sweep Circuit. Note that there is no connection made to plasma ground in this diagnostic; it is independent of plasma potential.

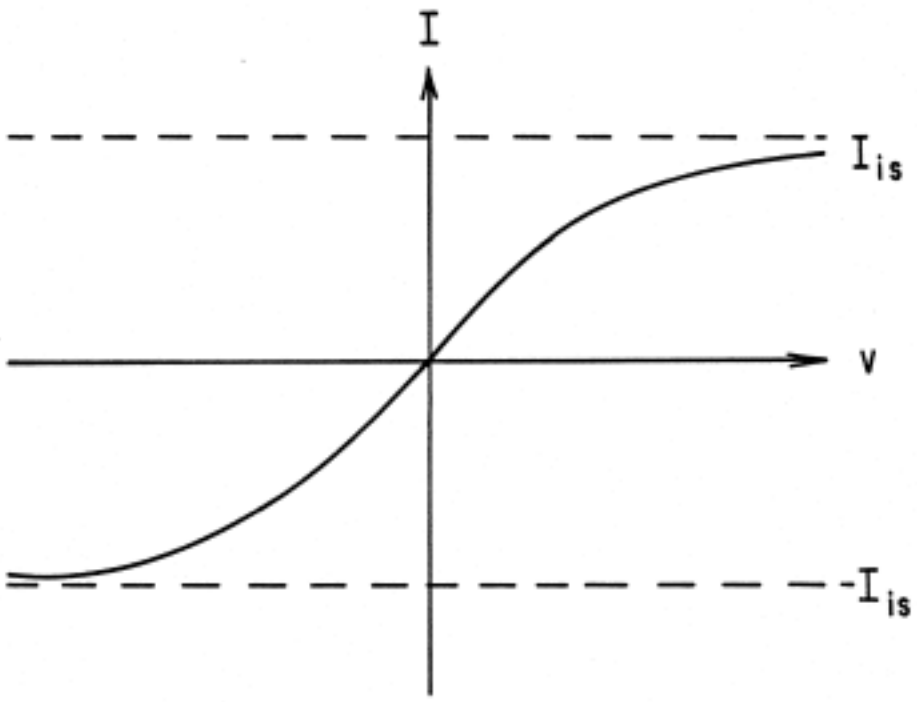

Figure II-5.

Current vs. voltage characteristic of a double probe.

$$n_0 = \frac{2n_c\Delta\phi}{k_{vac}\int_0^L f(x)dx} \tag{27}$$

Thus with the help of the radial probe measurement on the relative density profile, the microwave interferometer technique could be used to obtain the absolute density at any radial position.

b) Observation of cut-off: For $w = w_{pe}$ the relation given by equation (26) or (27) is no longer valid (why?). One must use equation (23) or (24) directly and the relation between Dy and n becomes quite complicated. However, when $w = w_{pe}$, the wave number becomes purely imaginary and no propagation is possible. By observing the cut-off, we can calculate the maximum density in the plasma, $n_{max} = n_c$, where n_c is the critical density defined above. The student is required to compare this microwave method with the Langmuir probe result.

4) Experimental Procedure

a) Follow the procedure as described in Chapter I to obtain a D.C. discharge. Clean up probes and set up a sweeper circuit as described in Appendix A. Observe a Langmuir characteristic curve by using the oscilloscope. For recording, the single sweep mode must be used with sweep rate of 1 to 2 seconds per cm, such that the mechanical movement of the recorder pin can follow the changes of the signal. The manual sweeping circuit of Figure II-7a is a possible substitute for oscilloscope and automatic sweeper when recording the Langmuir curve graphically.

b) Details of the probe characteristic: Take several single probe traces using the probe sweeper circuit and the x-y recorder. Replot each trace on semi-log paper and subtract out the ion saturation current to obtain the current contributed by the secondary electrons. At low neutral pressures the primary electron current will appear as a long, high temperature (gently sloping) tail with negative current in the ion saturation region of probe bias. In this case, subtract the primary electron current (as well as the ion saturation current) from the total probe current to obtain actual secondary electron current. (Primary electron current collected for a given probe bias can be estimated by extrapolating the straight-line primary tail.) Obtain the electron temperature from the slope of the curve and the density from both the ion and electron saturation currents. Experimentally determine how the ratio I_{es}/I_{is} depends on the mass ratio.

You will find that the primary electron current usually overshadows the ion current. However, the ratio of primary electron to ion current can be reduced significantly and the ion saturation current can be observed by simply raising the neutral pressure to about 10^{-3} torr (explain why).

c) Double probe: Set up the double probe manual sweeper circuit with the x-y recorder and obtain a double probe trace. Compute the density and electron temperature and compare the result

with n and T_e obtained from a single probe characteristic at the same time in the same region of the plasma.

d) Microwave interferometer: The X-band microwave interferometer set-up is shown in Figure II-6. Microwave signal generated by the oscillator is split into two paths, one propagating through the plasma, $V_1 \cos (wt + o_1)$, the other through a variable phase shifter to provide a reference signal, $V_2 \cos(wt + o_2)$. The signal propagating through the plasma is received by a pickup horn on the other side of the vacuum system, and then added to the reference signal by the magic tee: $V_{sum} = V_1 \cos (wt + 0_1) + V_2 \cos (wt + 0_2)$. This signal is then fed into a crystal detector, which produces a current signal I V^2_{sum}. By taking a time average of the current I from the crystal,

$$\langle I \rangle \propto \langle V_{sum}{}^2 \rangle = \tfrac{1}{2} V_1^2 + \tfrac{1}{2} V_2^2 + V_1 V_2 \cos(\phi_1 - \phi_2) \tag{28}$$

For a given plasma density, f_1 is fixed. Vary V_2 with the variable attenuator and f_2 with the phase shifter to obtain a null (f_1 $f_2 = p$). Be careful not to overattenuate the reference signal V_2 as this will result in a phase independent signal [$V_2 = 0$ in (28)].

The crystal diode output signal is so small that a high gain amplifier must be used. Furthermore, the microwave signal should be gated on and off (i.e., square wave modulated output) to avoid confusion over D.C. shifting of the output signal in the high gain amplifier.

Turn off the plasma (by turning off the discharge), find the null again and record Df. In finding the null, large errors can develop. To minimize these, plot $<V_{sum}^2>$ versus f_z for the case where the plasma is present and the case where it is turned off to obtain two cosine curves offset by phase Df. Although this procedure is tedious, it is recommended for improved accuracy.

Calculate the plasma density using equation (26) and compare the results with those obtained from the probe measurements. If the density is non-uniform, try to correct the result by measuring relative density profile using a movable Langmuir probe. Difficulties arise whenever the dimensions of the plasma container are comparable to the wavelength of the microwaves. In this case, the waveguide horn is not large enough to sharply define the microwave beam and unwanted cavity modes are excited in the vacuum chamber as a result. These modes have multiple paths through the plasma and can drastically alter the measurement of Df. Hence, steel wool has been placed near both the sending and receiving horns to attenuate these undesirable multiple path signals.

e) Density Measurement via Plasma Resonance: The most accurate local density measurement in an inhomogeneous plasma is achieved by exciting the local plasma resonance $_p(x)$. An oscillating electric field of frequency w_0 is externally excited in the plasma by a capacitor plate oriented to give an electric field along the density gradient as shown in Figure II-7. Where ever the

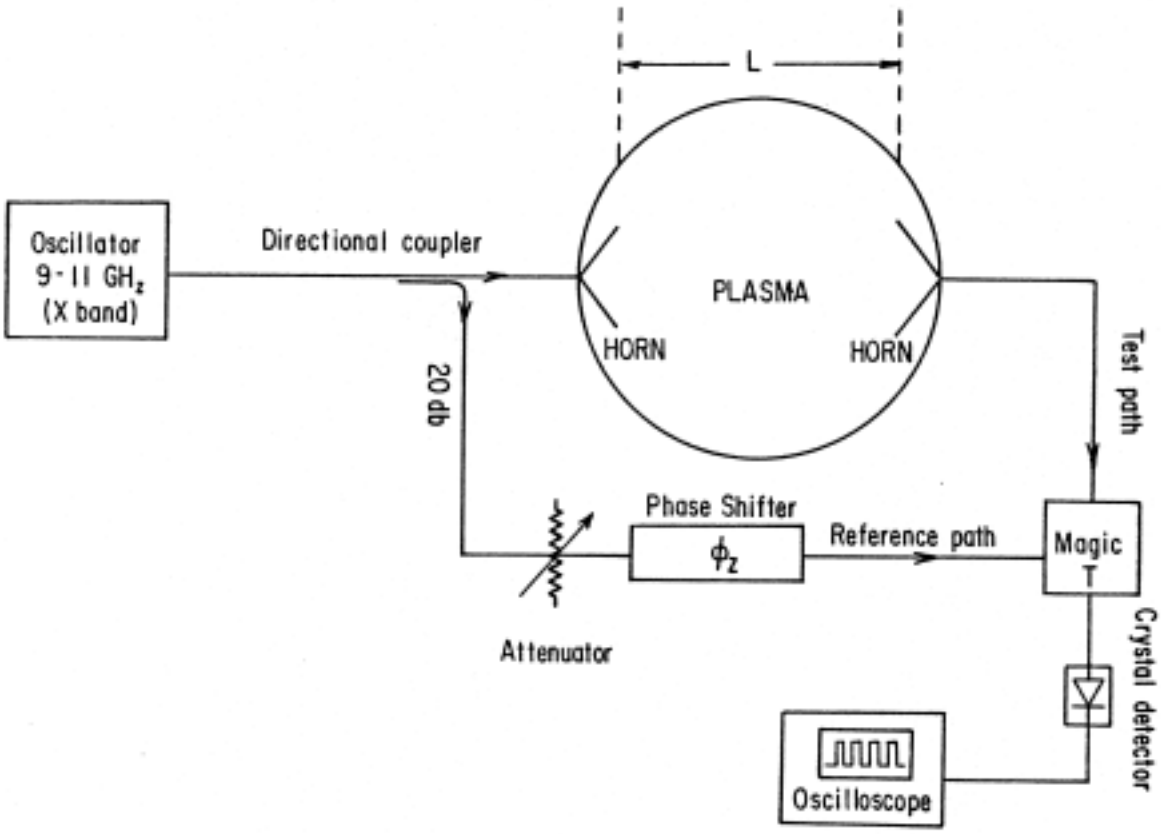

Figure II-6.

Interferometer Setup

external frequency matches the local plasma frequency $_0 = _p(x_0)$, the amplitude of the external electric field is found to be enhanced by an order of magnitude or more. This resonance is best detected by noting the deflection of an electron beam traversing the resonant location (Figure II-7) in a direction perpendicular to the density gradient. (A detailed description of this electron beam diagnostic is to be presented in Chapter V.) Since the external oscillating field frequency $_0$ can be precisely measured, the plasma density can be determined to better than 1%. A Langmuir probe can be calibrated using this technique.

Questions

1. Why does the ion saturation current depend on kT_e?
2 If there is an excess of primary electrons in the plasma, what kind of effect can one see by using (1) single probe, (2) double probe, and (3) microwave interferometer? Can you measure the density of the primary electrons?
3. For a plasma consisting of positive and negative ions of equal mass, draw the probe characteristics, carefully labeling the quantities I_{s+}, I_{s-}, V_f and V_s. How do you deduce T_+ and T_-?
4. What processes determine potential difference between the plasma and the anode?
5. When a fine conducting grid (called "plasma demon") is biased to some positive potential, it was found that the electron temperature increases by a factor up to 2-3. Can you explain this effect?

5) Appendix A: Description of Probe and Circuitry

a) Langmuir probe: A typical disc Langmuir probe in our laboratory experiment is spot welded onto a 0.010" diameter tungsten wire extending from the end of a glass insulating tube which is surrounded by a ceramic support sleeve, [c.f. Chapter I, Figure I-14]. A circuit diagram which is useful for plotting the current-voltage characteristics on an x-y recorder is given in Figure II- 4.

The probe voltage is obtained from a stabilized power supply (0 to 100 V), or better still a large battery, and can be varied in polarity and magnitude with a potentiometer. The probe voltage is also monitored on the x-axis of an x-y recorder which is easily calibrated with a voltmeter. As in Chapter I, the probe current is found from the voltage drop across a small resistor. The y axis is most conveniently calibrated by replacing the probe with a known resistor. More sophisticated circuits which electronically generate a voltage ramp may also be used to obtain probe I-V characteristics. One of these is shown in Figure II-8b.

The Langmuir characteristic is obtained by sweeping the probe voltage slowly between the negative and positive limits so as to include all the important regions of the curve.

c) Double probe: The double probe used in these experiments consists of two planar discs separated by a small distance. An alternative circuit to that of Figure II-4, suitable for measuring the double probe characteristic is the same as shown in Figure II-7, except that the ground (anode) is replaced by the second probe. No part of this circuit should be grounded. Each component probe of the double probe should be cleaned in the same manner as the Langmuir probe.

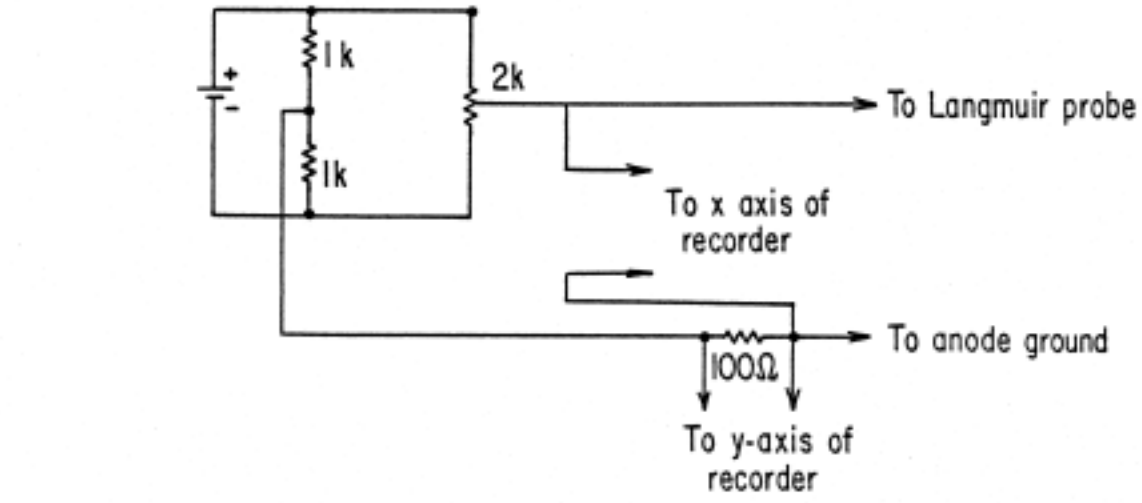

(a) Manual probe sweeper

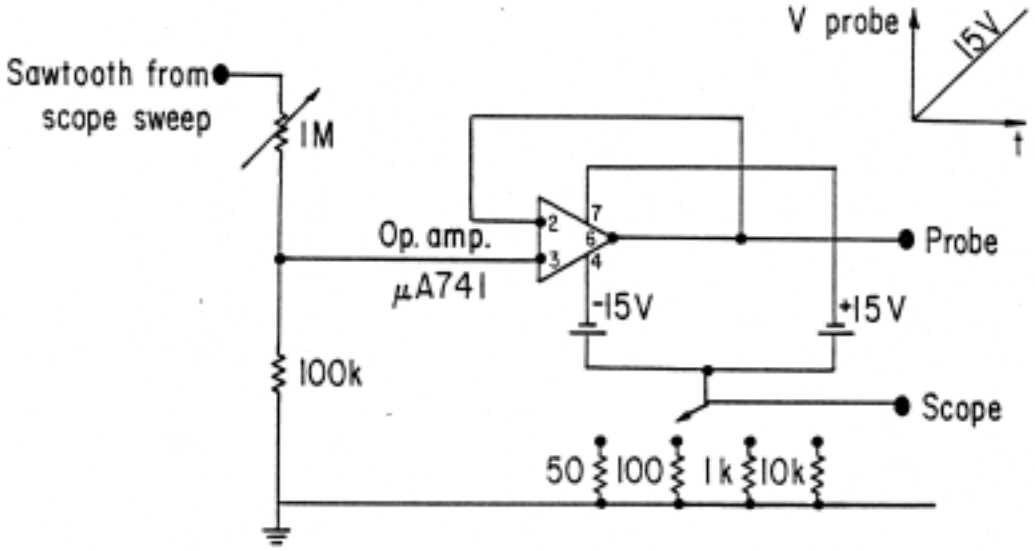

(b) Electronic probe sweeper

Figure II-8.

Probe Sweeper Circuits. For the electronic sweeper, a constant, positive bias is often applied in the form of a battery (0 - 9 volts) placed in series with the probe; this shifts the limits of the voltage ramp to sweep the desired features of the trace.

References

General Langmuir Probe

1. 0. Mawardi, Amer. J. Phys. 34, 112 (1966).
2. F. F. Chen, "Electric Probes," Plasma Diagnostic Techniques, Ed. by Huddlestone and Leonard (Academic Press, 1965).
3. F. F. Chen, C. Etievant and D. Mosher, Phys. Fluids 2, 811 (1968).
4. J. G. Laframboise, "Theory of Spherical and Cylindrical Langmuir Probes in a Collisionless, Maxwellian Plasma at Rest," UTIAS Report #100, Univ. Toronto (1966).
5. L. Schott, "Chapter 11," Plasma Diagnostics, Ed. by W. Lochte -Holtgreven (North Holland, 1968).

Double Probe

6. F. Johnson and L. Malter, Phys. Rev. 80, 59 (1950).
7. S. Ariga, J. Phys. Soc. Japan 31, 4, 1221 (1971).
8. P. Demchenko, L. Krupnik and N. Shulika, Sov. Phys. -Tec. Phys. 18, 8, 1054 (1974).

Microwave in Plasmas

9. C. Wharton, "Microwave Techniques," Plasma Diagnostic Techniques.
10. M. Heald and C. Wharton, Plasma Diagnostics with Microwaves (Wiley, 1965).

Chapter III Energy Analyzer

While a simple plane probe yields information on the electron density and temperature, an ion energy analyzer using additional electrodes to eliminate the electron contribution is required to measure the ion temperature. In this chapter we will discuss its design, practical applications as well as its limitations.

1) Energy Analyzer Design

One design of an ion energy analyzer as depicted in Figure III-l has been found to possess adequate resolution for the study of ion distribution functions. It consists of two mesh grids (Gl and G2) and a collector plate (P) located behind the grids.

The first grid is left at the plasma floating potential so that it repels electrons but allows most ions to pass through. The second grid[1], called the discriminator, is biased positively in order to retard those ions with energy per unit charge less than its potential ϕ, measured with respect to the plasma potential. The collector plate, which is biased very negatively (typically ~60 V), repels the residual high energy electrons which penetrate through the first grid and collects all the ion current. A schematic of the relative potentials of different electrodes is shown in Figure III-2. The placement of the analyzer and the physical connections to its various electrodes are depicted in Figure III-3. The sawtooth output of a scope is used to provide a ramp for a electronic sweeper which drives the discriminator. A display of the collector current vs the sweep voltage is shown in Figure III-4.

[1] Do not overbias the discriminator grid. The large electron current it collects can burn out the fine mesh.

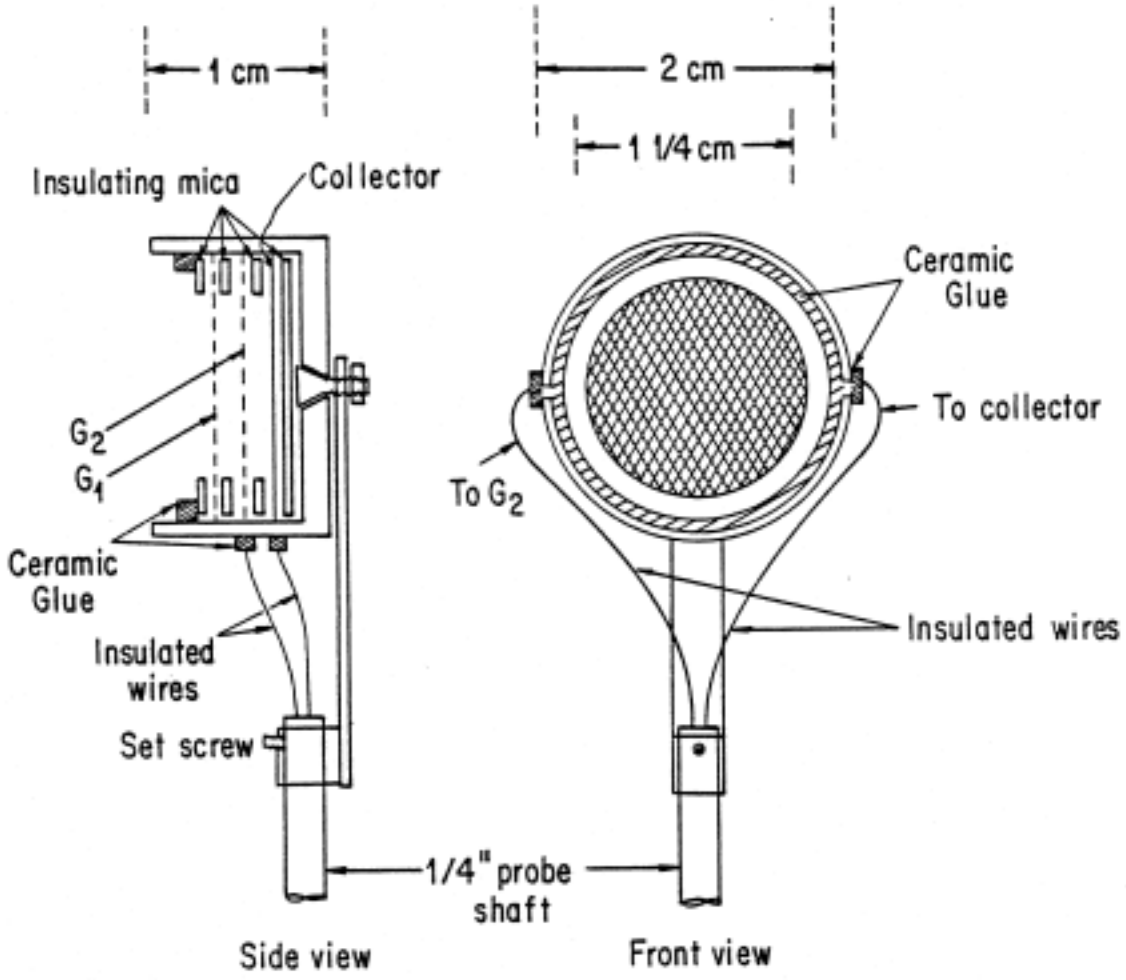

Figure III-1.

Ion energy analyzer.

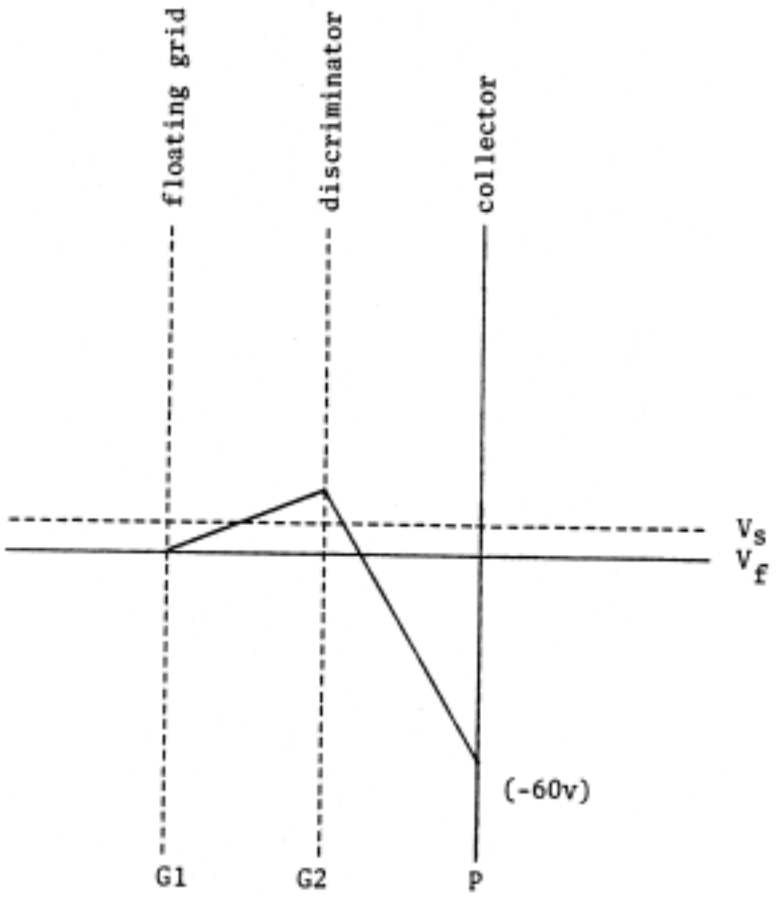

Figure III-2.

Potential distribution in the three-electrode analyzer for studying ion component of plasma current. G1 is left at the floating potential to retard electrons. This minimizes disturbance of the plasma by the analyzer. G2, the discriminator, is biased to repel ions with energy less than its potential ϕ (relative to V_s). P, the collector, is biased negatively to repel all the electrons and collect all the ions which pass the discriminator.

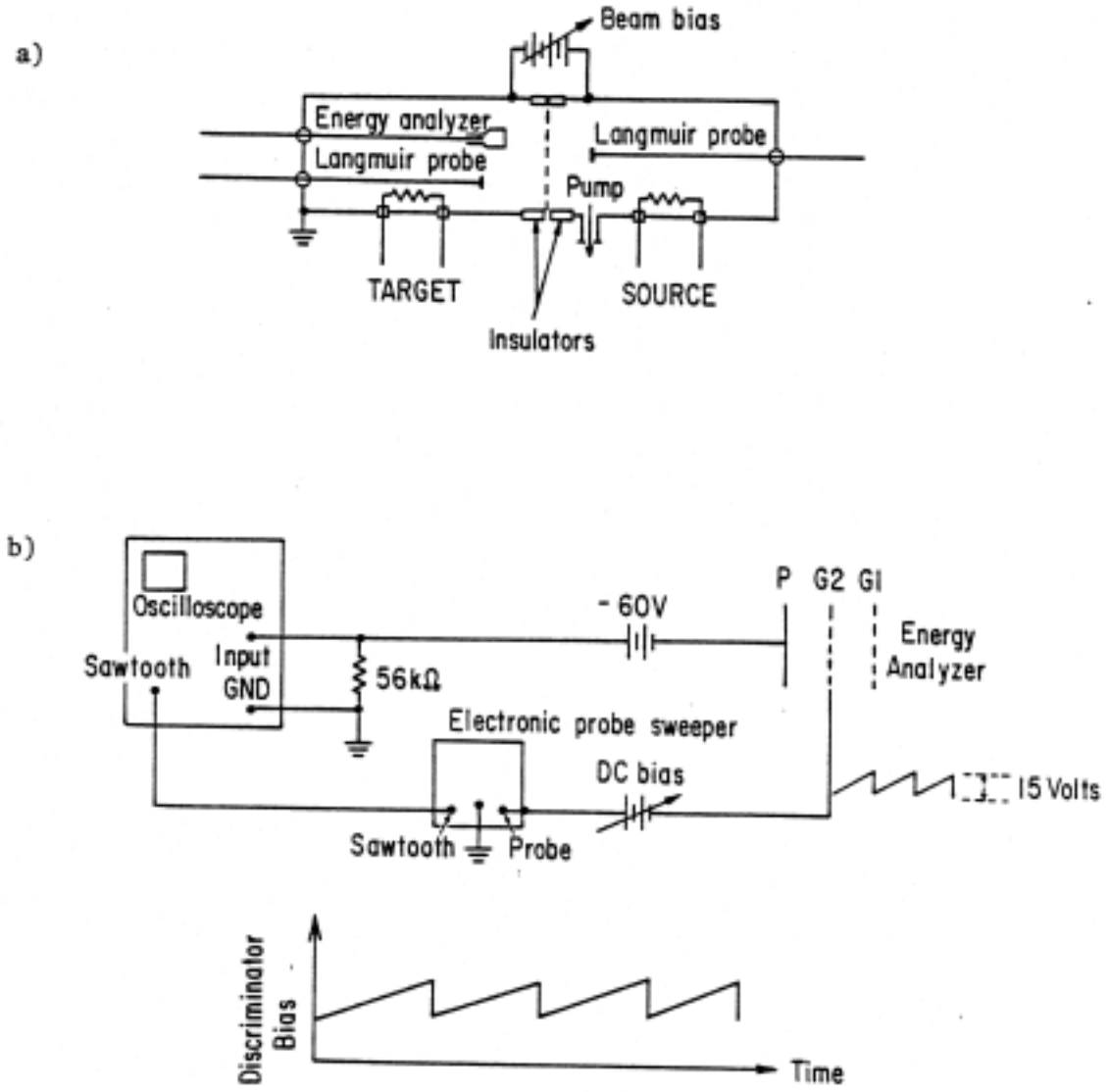

Figure III-3.

a) Placement of ion energy analyzer in double plasma machine.
b) Schematic diagram for the measurement of ion temperature.

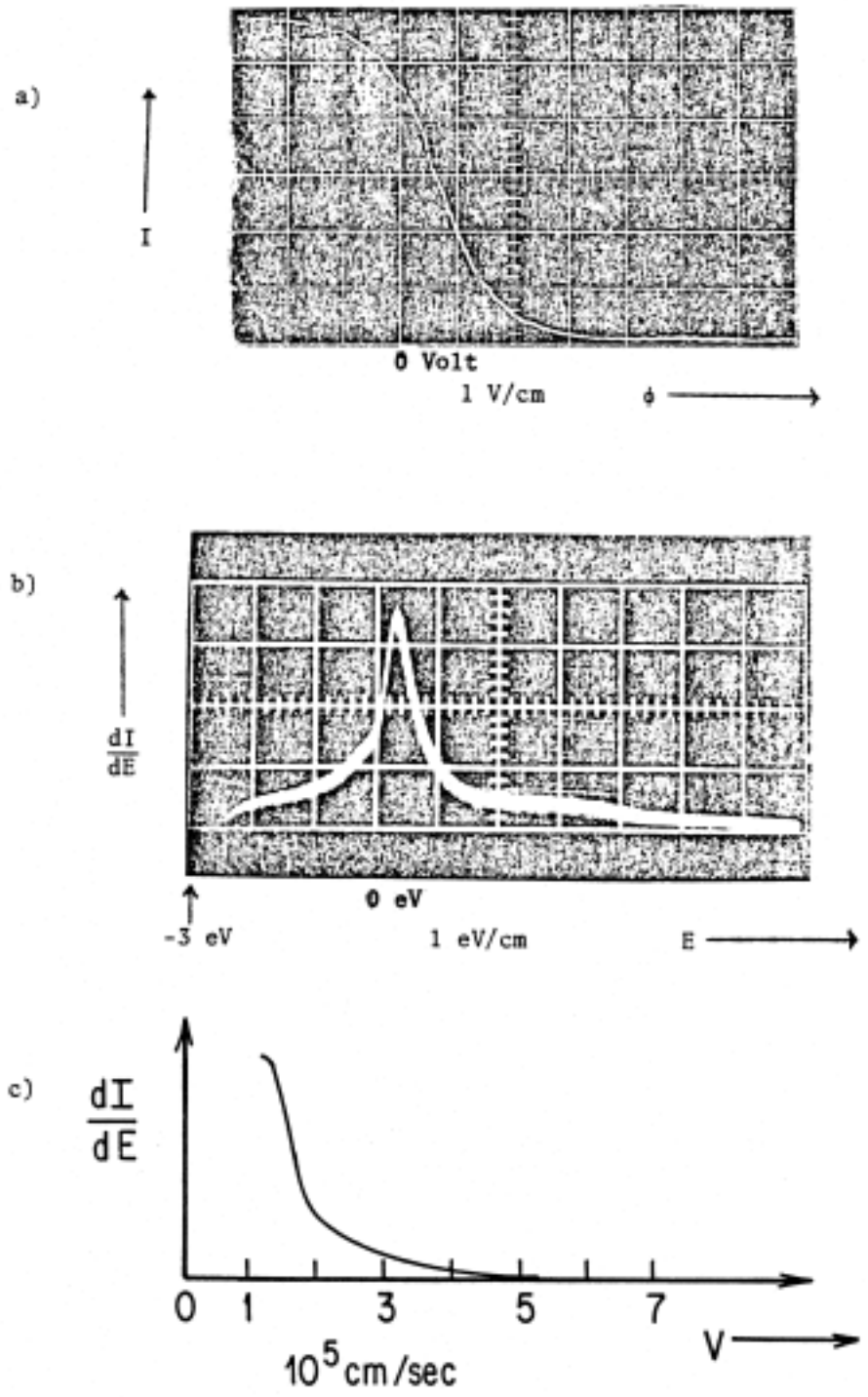

Figure III-4.

a) Typical current-voltage characteristic, I vs. ϕ. ($T_i \sim 0.7$ eV.) The exponential behavior of the curve for $\phi < 1/2$ Volt is a (spurious) probe effect.
b) Differentiated current-voltage characteristic, F(v) vs. E.
c) Ion velocity distribution function, F(v) vs. v, obtained from scaling the energy axis into its ion velocity equivalent.

Ideally, the electric field inside the analyzer should point axially along the direction in which the velocity component is to be analyzed. To achieve this, the hole size h of the mesh forming the grid and the spacing s between adjacent electrodes must be of the order of 1 - 10λ_D. Each grid then forms an equipotential surface with the discriminating electric field oriented perpendicular to the gird surface. At higher plasma densities or larger mesh sizes such that h, s > > λ_D, the plasma in between grid wires shields out the potential of each wire, giving rise to short-range radial electric fields between plasma and grid wires. Particles going through the grids no longer see an axial discriminating electric field and poor resolution of the ion distribution results. The finest mesh presently available satisfies the above size criterion up to a plasma density of $10^{12}/cm^3$. If the first grid is made of such a fine mesh it lowers the plasma density inside the analyzer by as much as two orders of magnitude and increases λ_D there by an order of magnitude. As a result, the allowable mesh size of the second grid is somewhat larger. The lowering of plasma density inside the analyzer is a desirable feature, as long as the collector current is within the limit of detectability, since the plasma behaves more like a collection of single particles whose trajectories are easily predicted. If the ion energy exceeds 10 eV sputtering and secondary emission from the electrodes must be taken into account. A fourth grid might have to be introduced in front of the collector and biased slightly more negatively than the collector in order to repel secondary electrons released from the collector surface due to ion bombardment. If allowed to escape from the analyzer probe, this secondary electron emission will result in a stray, positive collector current.

2) Analysis of Measurements

After the electrons have been screened out by the discriminator grid, the ion current reaching the plate collector of area A is given by

$$I(\phi) = eA\int_{\left(\frac{2e\phi}{M}\right)^{1/2}}^{\infty} v\,F(v)dv$$

$$= \frac{eA}{M}\int_{\left(\frac{2e\phi}{M}\right)^{1/2}}^{\infty} F(v)\,d\left(\frac{Mv}{2}\right) = \frac{eA}{M}\int_{e\phi}^{\infty} F(v)\,dE \quad where\; E = \frac{1}{2}Mv^2 \tag{1}$$

Differentiating (1) with respect to ϕ, we get an expression for the velocity distribution function F(v) or G(ϕ) in terms of the first derivative of the current-voltage characteristic, I(ϕ) vs ϕ, namely

$$F(v) = -\frac{M}{e^2 A}\frac{dI}{d\phi} \tag{2}$$

Let us consider a typical characteristic of I(ϕ) vs ϕ as in Figure III-4a. The derivative $\frac{dI}{d\phi}$ obtained by methods mentioned below is represented in Figure 4b. This gives us the ion distribution as a function of energy. If the velocity distribution function F(v) vs v is desired the abscissa must be re-scaled according to the relation $v = \sqrt{\frac{2e\phi}{M}}$, as in Figure 4c. It should be pointed out that the I(ϕ) characteristic should not be taken seriously at very low discriminating voltage ϕ, when the electric fields introduced by the analyzer grids are comparable to the fluctuating fields inside the analyzer. In practice the shape of the distribution is taken to be the curve starting from the right side in Figure 4b and rising to a maximum near ϕ = 0 V. The left side of the maximum is discarded on account of the poor resolution of the analyzer.

Ion Temperature

If F(v) is a Maxwellian function then, according to (1). I(ϕ) =

$$I(\phi) = (constant)\,\mathrm{Exp}\left(-\frac{e\phi}{KT_i}\right) \quad or$$

$$\ln I(\phi) = (constant) - \frac{e\phi}{KT_i}$$

The plot of

$$\ln I(\phi) \text{ vs. } \phi$$

should be a straight line ant the inverse of its slope gives the ion temperature KT_i directly.

Plasma Potential

The analyzer also measures the plasma potential, i.e. the potential at which all ions are collected. Experimentally this potential is given by the value at which $\frac{dI(\phi)}{d\phi}$ reaches a maximum.

a)

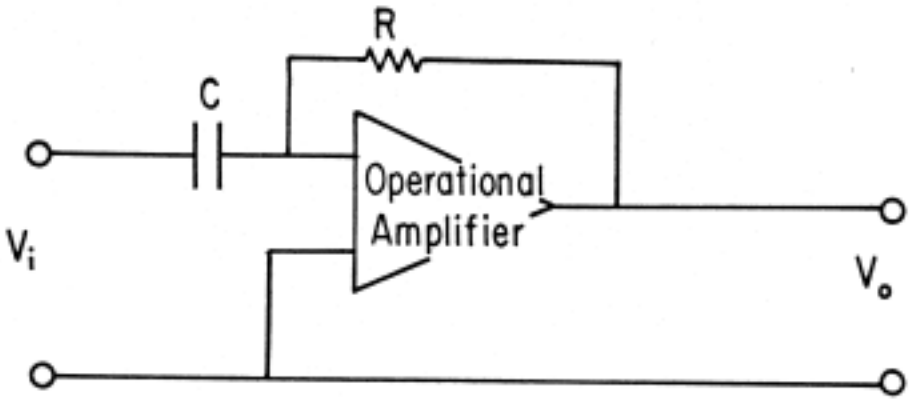

b)

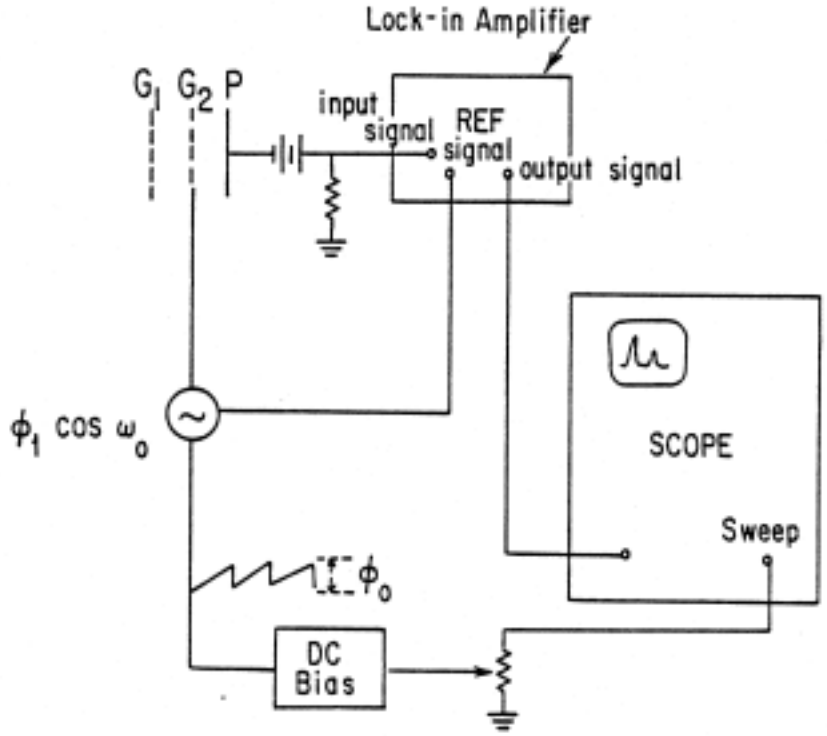

Figure 5.

a) Differentiating circuit using high gain operational amplifier A.
b) Schematic diagram for the measurement of ion distribution functions.

3) Experimental Methods of Differentiation of Current-Voltage Characteristics

Ion distribution functions can be obtained from electronic circuits which differentiate the normal current-voltage characteristic of the analyzer with respect to ϕ, Figure III-4b. Experimentally, this differentiation can be carried out in two different ways: with a simple R-C differentiating circuit, Figure III-5a, or a more sophisticated method using a lock-in detector, Figure III-5b.

i) R-C differentiation

This method requires a very linear variation of the discriminator voltage ϕ with time t. With the R-C differentiator synchronized with the discriminator voltage ramp, differentiation is carried out with respect to time and therefore indirectly with respect to ϕ. The advantage of this method is ifs fast response and instant display of the distribution function.

An oscilloscope plug-in unit which has an operational amplifier differentiation circuit is used. When the analyzer's collector signal V_i is put into the circuit, shown in Figure III-5a, the output is simply

$$V_o \cong -RC \frac{dv_i}{dt}$$

ii) Differentiation by synchronous detection

In this method a small sinusoidal voltage $\phi_1 \cos \omega_0 t$ is applied to the discriminator grid biased at potential ϕ_0 and the synchronous variation of the current as a function of energy selection potential is measured. The current collected is

$$I(\phi) = \frac{eA}{M} \int_{e\phi}^{\infty} G(E) dE \tag{5}$$

Adding a small amplitude modulation $\phi_1 \cos \omega_0 t$ to the linear variation of discriminator bias ϕ_0 we define

$$\phi \equiv \phi_0 + \phi_1 \cos \omega_0 t, \text{ with } \phi_1 << \phi_0.$$

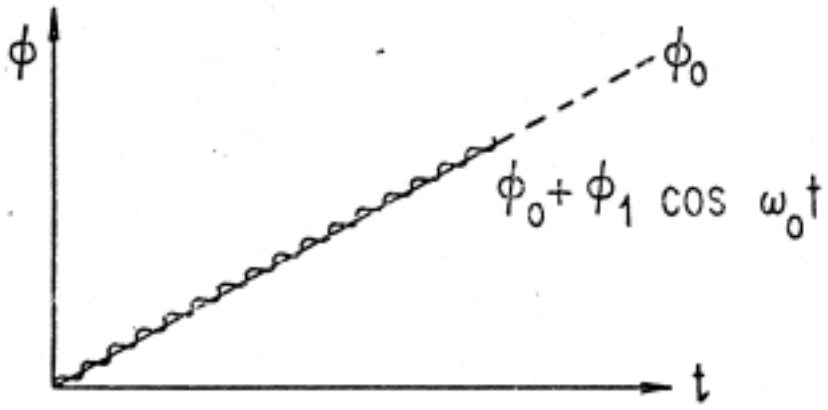

Then expanding (5) in a Taylor Series about ϕ_0 produces

$$I(\phi)\_I(\phi_0)+(\phi_1\cos w_0 t)\frac{dI}{d\phi}\Big|_{\phi_0}+\frac{(\phi_1\cos\omega_0 t)^2}{2}\frac{d^2I}{d\phi^2}\Big|_{\phi_0}+\ \ldots \tag{6}$$

By looking at the coefficient of the time varying component $\phi_1 \cos\omega_0 t$ we can find $\frac{dI}{d\phi}|_{\phi_0}$ and hence the distribution function $G(e\phi_0)$ according to (5).

Figure III-5b shows a schematic diagram for the measurement of ion distribution functions with the aid of a lock-in detector.

A lock-in detector is a ultra-sensitive instrument, capable of detecting a small signal (signal-to-noise ration as low as 40 db), provided this signal varies at the same frequency as a known reference signal. It is generally used to multiply some input signal $\Sigma_n A_n \cos\omega_n t$ by a reference signal $B_r\cos\omega_r t$ and then time-average the product: the lock-in output signal S is then

$$\begin{aligned} S &= <(\Sigma_n A_n\cos\omega_n t)[B_r\cos(\omega_r t+\theta)]> \\ &= <A_r B_r\cos(\omega_r t)\cos(\omega_r t+\theta)> \\ &= \lim_{T\to\infty}\frac{1}{T}\int_0^T A_r B_r\cos^2 w_r t\cos\theta\,dt \\ &\quad -\lim_{T\to\infty}\frac{1}{T}\int_0^T A_r B_r\cos w_r t\sin w_r t\sin\theta\,dt \end{aligned} \tag{7}$$

This final term time averages to zero, hence

$$S=\frac{A_r B_r}{2}\cos\theta. \tag{8}$$

The final result is proportional to the signal strength at the frequency ω_r and is related to the angle θ between the reference and its corresponding harmonic in the input signal. All other frequency components do not maintain a constant phase relationship with the reference signal and are time averaged to zero.

To relate this lock-in output S to the measurement of $\frac{dI}{d\phi}\big|_{\phi_0}$ in (6), write the reference component in (7) as $B_r \cos \omega_r t = \phi_1 \cos \omega_0 t$ and the input signal as $\Sigma_n A_n \cos \omega_n t = I(\phi)$. According to (8) the detector output

$$S = \frac{\phi_1^2}{2} \frac{dI}{d\phi}\Big|_{\phi_0} \quad \propto (e\phi_0)$$

is proportional to the ion energy distribution function.

4) Experiments with the Ion Energy Analyzer

Perform each of the following experiments in the double plasma (DP) device described in Chapter 1, Appendix B.

a) Ion temperature measurement: Monitor the probe characteristics on both sides of the DP device and

vary the known bias between the two chambers to balance the plasma potentials[1] so that ion beams are not present in either chamber. Obtain an analyzer I-V characteristic for at least two different neutral pressures. Replot the characteristic on semi-log paper and determine the ion temperature. Determine the plasma potential according to the potential ϕ at which $\frac{dI}{d\phi}$ reaches a maximum [Figure III-4(b)]. Compare this measurement with the one made by the Langmuir probe.

b) Observation of ion beams: Bias the source chamber positive with respect to the target chamber to launch an ion beam. The beam energy is determined by the difference in plasma potentials between the source and target plasmas. Record an I-V characteristic to determine T_i and T_b, the temperature of the beam, from the slope of a semi-log plot of this data.[2] An example is given in Figure III-6, 7 in which the I-V characteristics ant the corresponding ion distributions are depicted. When a beam is directed into the analyzer, all the beam ions are collected whenever the discriminator potential ϕ is such that $e\phi < E_b$, where E_b is the beam energy. For $e\phi > E_b$, the beam ions are repelled so the I-V characteristic has the step function shape as in Figure

[1]Because of slight density gradients near the DP interface, plasma potentials are most easily balanced when each Langmuir probe is placed about 10 cm from the launching grid.

[2]See Appendix A

III-6b and III-6c. When the I-V characteristic is differentiated to obtain the ion velocity distribution function, F(v) vs. E, the ion beam appears as a bump on the tail centered around the beam's energy as in Figure III-7b and III-7c.

Obtain similar ion velocity distribution functions for beam energies such as 2 eV, 4 eV, 10 eV, using the operational amplifier plug-in for R-C differentiation. Verify the beam energy obtained from the analyzer against the potential difference between target and source chambers.

In preparation for the next chapter, monitor the density fluctuation ($\delta n/n$) in the target chamber with a Langmuir probe and see if there is a correlation between the fluctuations and the beam energy. What beam energy and corresponding ion beam velocity maximizes the amplitude of the fluctuations?

c) Ion beam decay-measurement of the charge exchange cross-section: The ion beam decays spatially due to charge exchange collisions[1] and elastic collisions with the background neutral atoms. To derive an expression for this spatial decay, we note that a decrease dI_b in the beam current in a distance dx at the point where the beam current is I_b is proportional to $-N_o I_b dx$, where N_o is the neutral density. The proportionality constant is the charge exchange cross-section, σ, which may be visualized as the effective area a neutral atom presents to an incident beam ion for undergoing a charge exchange collision.

---

[1]When a beam ion A^+ collides with a cold neutral A, the ion A^+ may capture an electron from the atom A in accordance with

$$\begin{array}{ccccccc} A^+ & + & A & \rightarrow & A & + & A^+ \\ \text{(fast ion)} & + & \text{(slow neutral)} & \rightarrow & \text{(fast neutral)} & + & \text{(slow ion)} \end{array}$$

resulting in a fast (beam) neutral and a cold ion. This charge-exchange process is utilized in current plasma fusion studies where intense neutral beams are produced from fast ion beams for the purpose of injection heating.

Figure III-6.

Current-voltage characteristics.

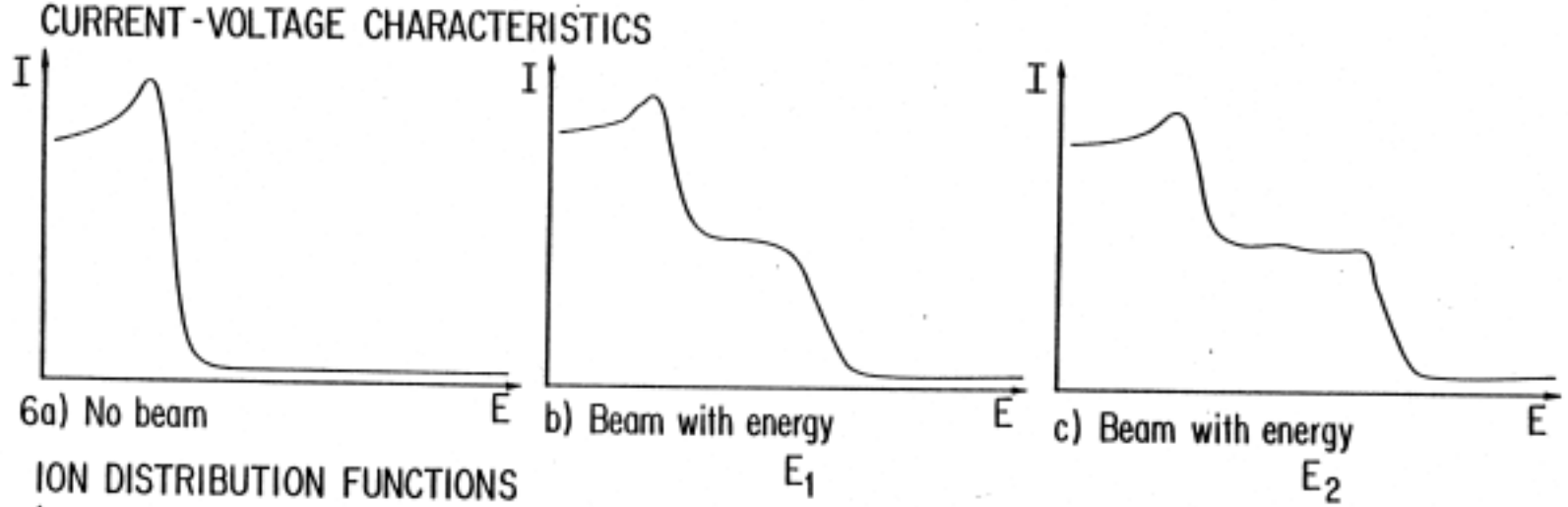

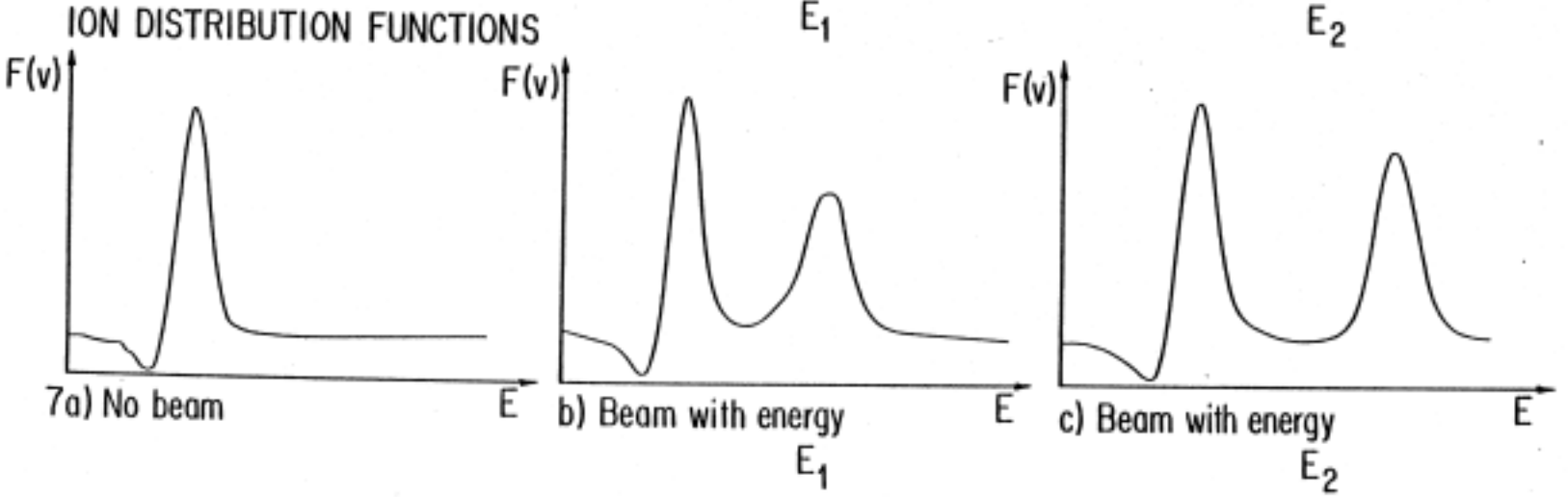

Figure III-7.

Ion distribution functions.

Thus

$$dI_b = -I_b N_0 \sigma dx$$

Integrating we have

$$\ln I_b = \ln I_0 - N_0 \sigma x$$

or

$$I_b = I_0 \text{ Exp } (-N_0 \sigma x). \qquad (9)$$

The beam current therefore decays exponentially. The cross-section can be computed by simply measuring the e-folding decay length of the beam with the energy analyzer and assuming the cool neutrals to be at room temperature.

Experiment

Vary the axial position of the analyzer for one beam energy and plot the spatial decay of the beam for at least two different neutral pressures (10^{-4} and 8×10^{-4} torr for example). Use (9) above to measure the collision cross-section for the beam energy you choose and compare it with the cross-section for both elastic and charge exchange collisions in Reference 8 or 9. According to your data, which collision process dominates?

References

1. J. Brophy, Basic Electronics for Scientists, 2nd Ed. (McGraw-Hill, 1972) p. 318.
2. S. Brown, Basic Data of Plasma Physics (MIT Press, 1967).
3. E. McDaniel, Collision Phenomena in Ionized Gasses (Wiley, 1964).

5) Appendix A: Ion Beam Temperature in Double Plasma Device

The ion beam-plasma system is formed in the DP device by biasing the source chamber anode positive with respect to the target chamber anode. This results in a source plasma space potential which is higher than the potential of the target plasma. If the difference between the source and target space potentials is ?, then we have the situation shown in Figure III-B, where the space potential is[1]

$$\phi(x) = \begin{cases} 0 & x \le 0 \\ \phi(x) & 0 < x < L \\ -\phi & x \ge L \end{cases}$$

Because the dynamics of the accelerated beam ions is of interest, a kinetic treatment (rather than fluid theory) is appropriate. We start with the collisionless, steady state $\left(\frac{\partial f}{\partial t} = 0\right)$ Boltzmann equation given by

$$v_x \frac{\partial f}{\partial x} + \frac{qE}{m} \frac{\partial f}{\partial v_x} = 0$$

for each component plasma species, where $E = -\frac{\partial \phi}{\partial x}$. This equation is satisfied by the distribution function

$$f(x,v) = C \, \mathrm{Exp}\left(-\frac{mv^2}{2KT} - \frac{q\phi(x)}{KT}\right),$$

with C ≡ constant, as can be verified by direct substitution.

In the source chamber, the plasma ion distribution function is just a Maxwellian (Figure III-9a):

$$f_i(v) = C \, \mathrm{Exp}\left(-\frac{Mv^2}{2\,KT_i}\right)$$

From Figure III-8 it is obvious that only those source plasma ions (near the plasma-grid sheath interface at x = 0) with $v_x > 0$ can enter the grid sheath to become accelerated beam ions hence, the restricted velocity distribution of Figure III-9b.

As these extracted plasma ions proceed as beam ions down the potential "hill" plotted in Figure III8, they will all gain the same amount of energy E_b, where $E_b \equiv e\phi$. Because of this, the beam ions arriving at the end of the sheath (x = L) will have a minimum velocity v_o given by

$$v_o \equiv \sqrt{\frac{2E_b}{M}}$$

[1]Source plasma potential is chosen as ground reference to simplify the mathematical analysis which follows.

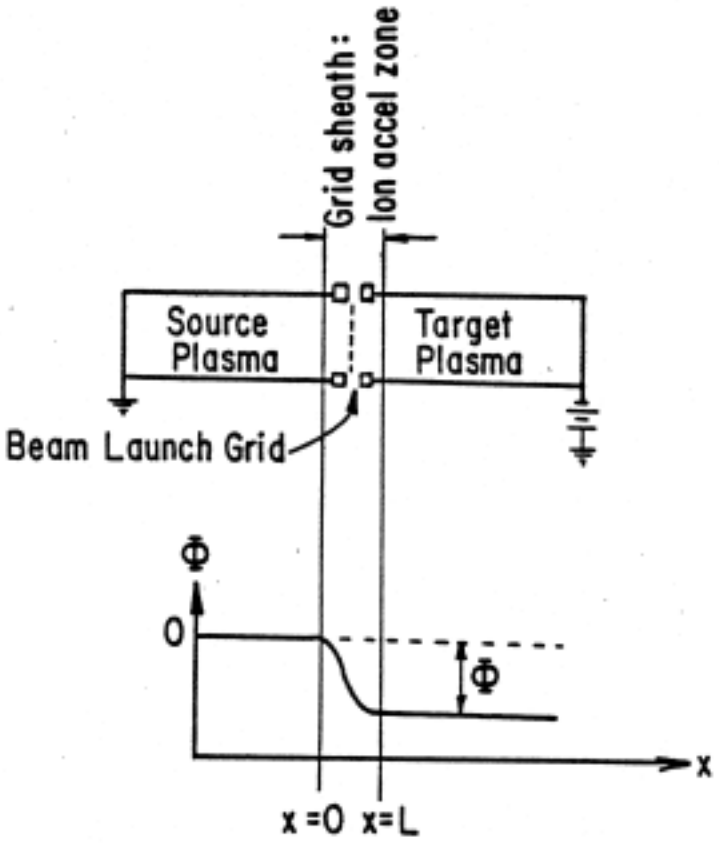

Figure-8.

Space potential profile along axis of DP device biased to launch an ion beam.

Also,

$$N_b = \int_{v_0}^{\infty} C\ Exp\left(\frac{{v_0}^2 - v^2}{{a_i}^2}\right) dv$$

$$= C\ Exp\left(\frac{{v_0}^2}{{a_i}^2}\right) \int_{v_0}^{\infty} Exp\left(\frac{v^2}{{a_i}^2}\right) dv$$

$$= C a_i\ Exp\left(\frac{{v_0}^2}{{a_i}^2}\right) \frac{\sqrt{\pi}}{2} erfc\left(\frac{v_0}{a_i}\right)$$

where

$$erfc(z) \equiv \frac{2}{\sqrt{\pi}} \int_z^{\infty} Exp(-u^2) du$$

with z denoting the minimum beam ion velocity normalized to plasma ion thermal velocity $z \equiv \frac{v_0}{a_i}$..

$$KT = < m(v - \bar{v})^2 >$$

$$\frac{1}{N} \int_{v_1}^{v_2} m(v - \bar{v})^2\ f(v) dv,$$

(10)

where v_1 and v_2 are the lower and upper velocity limits, respectively; the normalization factor, N, is given by

$$N \equiv \int_{v_1}^{v_2} f(v) dv$$

and the average velocity, $\bar{v}$, is

$$\bar{v} = \frac{1}{N} \int_{v_1}^{v_2} v f(v) dv$$

In the source chamber, <u>plasma</u> ions have $v_1 = -\infty$, $v_2 = +\infty$ and

$$f_i(v) = \left(\frac{M}{2\pi K T_i}\right)^{\frac{1}{2}}\ Exp\left(\frac{Mv^2}{2KT_i}\right).$$

Equation (10) yields an identity for this case.

However, for the accelerated <u>beam</u> ions at $x \geq L$, we have (referring to figure III-9c) $v_1 = v_0$, $v_2 = +\infty$, and

$$f_b(v) = C\ Exp\left(\frac{Mv^2}{2KT_i} + \frac{E_b}{KT_i}\right),$$

where C is a constant.

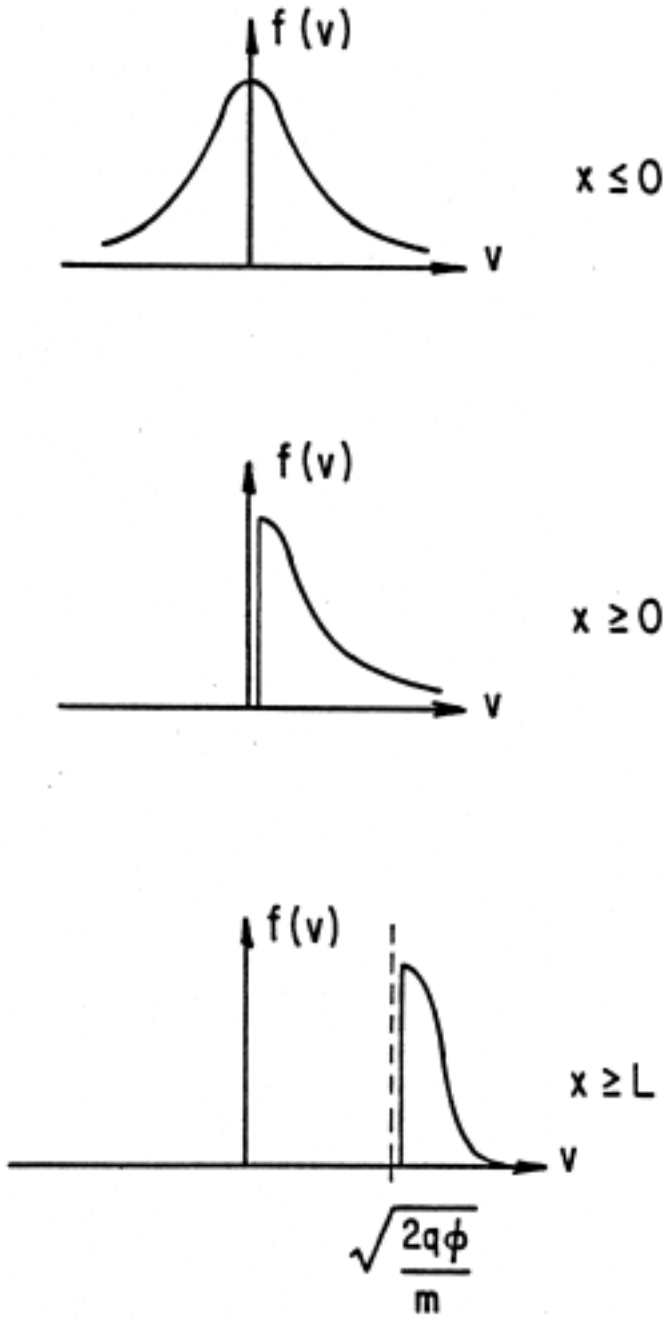

Figure III-9.

a) Velocity distribution function of source plasma ions.
b) Velocity distribution function of beam ions near x = 0.
c) Velocity distribution function of beam ions for x ≥ L.

(11)

We also need to find the average beam ion velocity $\overline{v_b}$ before KT_b can be computed from (11):

$$\bar{v}b = \frac{C}{N_b}\int_{v0} v\ Exp\left(\frac{v_0{}^2 - v^2}{a_i{}^2}\right)dv$$

$$= \frac{C}{N_b} Exp(z^2)\int_{z^2} \frac{1}{2} a_i{}^2\ Exp(-y)\,dy, y = \frac{v^2}{a_i{}^2}$$

$$= \frac{Ca_i^2}{2N_b}\mathrm{Exp}\,(z^2)\,\mathrm{Exp}\,(-z^2)$$

$$= a_i\ \frac{\mathrm{Exp}\,(-z^2)}{\sqrt{\pi}\ erfc\,(z)}$$

With the definition

$$\xi(z) \equiv \frac{Exp(-z2)}{\sqrt{\pi}\ erfc(z)}$$

we proceed to evaluate v:

$$< v^2 >= \frac{C}{N_b}\int_{v_0}^{\infty} v^2\ Exp\left(\frac{v_0{}^2 - v^2}{a_i{}^2}\right)dv$$

$$= \frac{\int_{v_0}^{\infty} v^2\ Exp\left(-\frac{v^2}{a_i{}^2}\right)dv}{a_i\frac{\sqrt{\pi}}{2}\ erfc(z)}.$$

Changing the variable in the last integral to $w \equiv \frac{v}{a_i}$ and integrating by parts gives

$$< v^2 >= \frac{1}{2}a_i^2 + v_0 a_i \xi\left(\frac{v_0}{a_i}\right)$$

Using these expressions we can evaluate $< (v - \overline{v_b})^2 >$ in (11) above by noting that

$$< (v - \overline{v_b})^2 > = < v^2 - 2v\overline{v_b} + \overline{v_b^2} >$$

$$= < v^2 > - 2\,\overline{v_b} < v > + \overline{v_b^2}$$

$$= < v^2 > - \overline{v_b^2}.$$

Thus according to (10):

$$KT_b = M[\ \frac{1}{2}a_i^2 + v_0\, a_i \xi\left(\frac{v_0}{a_i}\right) - [\ a_i \xi\left(\frac{v_0}{a_i}\right)\ ]^2\ ]$$

$$= \frac{Mv_0^2}{2z^2}[1 + 2z\xi(z) - 2\xi^2(z)]. \qquad (12)$$

The low ion temperature T_i typical of DC discharges implies that

$$a_i << v_0 \qquad \text{or} \qquad z >> 1.$$

The following asymptotic expression can be used:

$$\sqrt{\pi}z\ Exp(z^2)\ erfc(z) \sim 1 + \sum_{i=1}^{\infty} \frac{1\cdot 3\cdot 5\cdots(2i-1)}{(2z^2)^i}$$

Keeping only the terms of order $1/z^4$ or larger in the denominator we get:

$$\xi(z) \_ \frac{z}{1 - \frac{1}{2z^2} + \frac{3}{4z^4}} = \frac{4z^5}{4z^4 - 2z^2 + 3}$$

Placing this expression for $\xi(z)$ into (12) gives

$$KT_b = KT_i \left[\frac{8z^6 + 28z^4 - 12z^2 + 9}{(4z^4 - 2z^2 + 3)^2}\right] \qquad (13)$$

(Since z is large, the term inside the brackets is clearly positive, as it should be.) Note also as $z \to \infty$ we get

$$KT_b \sim \frac{KT_i}{2z^2} = \frac{KT_i}{2\left(V_0 / A_i\right)^2} = \frac{\left(KT_i\right)^2}{2e\phi_0} \to 0_+.$$

Hence the temperature of the beam is less than the source temperature KT_i and approaches zero as $\frac{V_0}{a_i} \to \infty$.

Chapter IV. Ion Acoustic Waves

In this and in the following chapters, we are going to examine the excitation and propagation of plasma wave modes. ln a plasma with no applied magnetic field, the wave phenomena are particularly simple because such a plasma has only two electrostatic normal modes--a high and a low frequency mode. The high frequency mode is one in which the electrons oscillate rapidly about stationary ions and is called the electron plasma wave. In the low frequency mode, ions and electrons oscillate in phase producing longitudinal density perturbations called ion acoustic waves. They were first predicted in 1929 on the basis of a fluid analysis by Tonks and Langmuiral[1] who found, for frequencies well below the ion plasma frequency and for isothermal changes, that the phase velocity v_p should be given by

$$v_p^2 \cong \left(\frac{KT_e + KT_i}{M} \right).$$

These waves differ from ordinary sound waves in that the coupling between electrons and ions arises from electric fields resulting from small charge separations. More recently, a number of authors[2,3] have shown on the basis of the collisionless Boltzmann (Vlasov) equation that ion waves can exist in a plasma even in the absence of collisions. The collisionless equations also predict an interesting feature of the ion waves namely, that they should be damped by interaction with ions moving with velocities close to the phase velocity of the wave.[4] This damping, which was first predicted by Landaus for electron plasma waves, is strong in the ease of ion acoustic waves even for wavelengths large compared with the Debye length, if the ion and electron temperatures are comparable.

Ion acoustic waves can be excited by producing a density perturbation with a conducting launch grid immersed in the plasma. Two commonly used techniques are described as follows:

i) Absorption method:[6] Consider a grid immersed in the plasma as shown in Figure IV-la. If the ion-collection region (approximately 10 λ_d) is a significant fraction of the interwire spacing, then a modulation of the grid bias will produce a varying amount of absorption, i.e., a small density perturbation is created in the transmitter probe vicinity and propagates down the plasma column.

ii) Velocity acceleration: A second method uses velocity accelerations produced by biasing the potential of one plasma with respect to another as shown in Figure IV-lb. The inflow of plasma

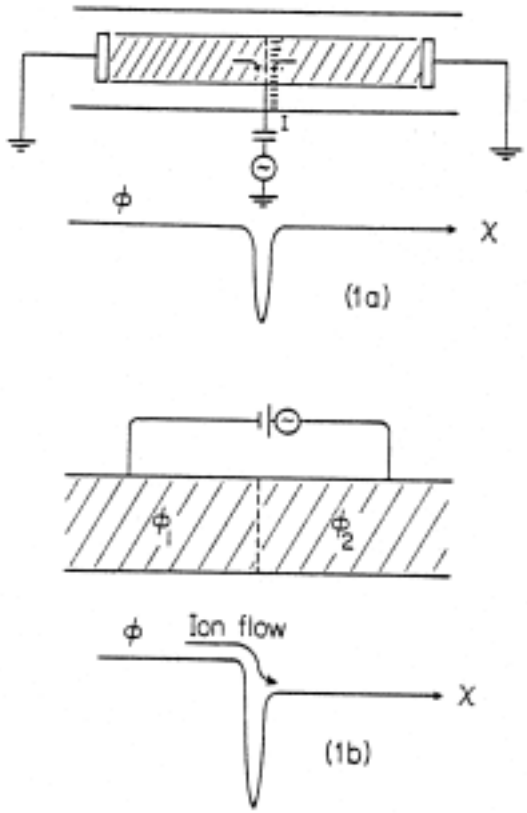

Figure IV-1.

particles from one chamber to another sets up a density perturbation. In this case, a floating wire-mesh grid defines the interface of the two plasmas.

Most excitation schemes create a propagating density perturbation by a combination of these two methods. However, there are more advanced methods which do not require grids in the main region where ion waves are excited and detected. For example, a slow electron drift can cause ion waves to grow spatially from one end of a device to the central region by an order of magnitude a large amplitude electron plasma wave excited by electron beams or externally imposed electromagnetic waves can decay into an ion acoustic wave ant another electron plasma wave of slightly lower frequency. These advanced methods will be treated in Volumes II ant III.

1) Physical Description

Ion acoustic waves derive their name from the similarity they bear to sound waves in a gas. Sound waves are longitudinal density oscillations in which the compressions and rarefactions are driven by collisions among the gas atoms. Ion acoustic waves are also longitudinal density oscillations, but they are driven by collisionless effects--namely, the electric fields that arise from the space charge developed by the slight displacements between ion and electron density perturbations. Since the ions and electrons oscillate in phase, the ion space charge, which would normally tend to push the ion compressions apart, is neutralized or shielded by the electrons. However, due to their thermal motion, some electrons overshoot the ion charge clouds hence the shielding is incomplete and an electric field is developed which then drives the wave. The higher the electron temperature, the more incomplete the charge neutralization and the greater the wave electric field and the phase velocity.

If the electron-to-ion temperature ratio is such that $T_e/T_i >> 1$, a condition that can be met in laboratory plasma, the dominant driving force comes from the electron pressure, and the ion acoustic speed is simply given by $C_s = [\gamma_e K T_e/M]^{1/2}$. The ratio of specific heats, γ_e and γ_i, can be assigned values from simple thermodynamic arguments. Since the frequency of the ion waves is so low, the electrons move several wavelengths in one period and thus carry away any heat developed

within that period. Therefore, the isothermal condition is valid for electrons, and $\gamma_e = 1$. The ion compressions, however, are one-dimensional, γ_i is generally assumed to be 3. A comparison of fluid theory and the more exact kinetic theory (Appendix A) of ion acoustic waves shows that the above values of γ_e and γ_i give an excellent approximation to the exact result.

2) Simple Theoretical Derivation

a) Linear dispersion of ion acoustic waves: We will first present a very simple fluid model, which reveals the wave motion carried by the bulk of the two charged species: ions and electrons. Various refinements are then added to explain experimental observations. A more complete kinetic theory, which includes interactions between waves and resonant particles as well as boundary conditions at the exciter, is treated in Appendix A.

i) Elementary analysis: We shall first present a simple analysis of ion acoustic waves under the following assumptions:

1) $T_i = 0$, which to a good approximation describes our plasma with $T_i << T_e$.
2) Assume charge neutrality $n_i = n_e = n$. This is a good assumption for low frequency waves in which ions and electrons move very nearly together.
3) Ions provide the main inertia since $M_i >> m_e$. Neglect electron inertia.
4) One-dimensional analysis since our plasma has a large cross section and the excited wave is very nearly a plane wave.

Ions and electrons are described as charged fluids according to the following equations:

$$nM \frac{dv_i}{dt} = neE \tag{1}$$

$$nm \frac{dv_e}{dt} = -neE - \frac{\partial p_e}{\partial x} \tag{2}$$

Adding equations (1) and (2), and using assumptions (2) and (3), we obtain:

$$nM \frac{dv_i}{dt} = -\frac{\partial p_e}{\partial x} = -\gamma_e KT_e \frac{\partial n}{\partial x},$$

where the adiabatic assumption $p_e \propto n^{\gamma}_e$ is used:

γ_e = ratio of specific heats for electrons = (r+2)/r,

where r is the number of degrees of freedom.

Using the continuity equation for ions, assuming small wave amplitudes and linearizing (making use of $n_1/n_0 << 1$, where n_1 is the time dependent density term, and neglecting second order terms), we obtain the wave equation:

$$\frac{\partial^2 n}{\partial t^2} = \frac{\gamma_e KT_e}{M} \frac{\partial^2 n}{\partial x^2}.$$

Assuming one-dimensional plane waves of the form Exp i(kx - ωt) yields the following dispersion relation:

$$\omega^2 = k^2 C_s^2,$$

where the phase velocity

$$C_s^2 = \frac{\gamma_e KT_e}{M}.$$

ii) Refinements:

1) Including the ion temperature and hence the ion pressure in equation (1) we obtain:

$$\frac{\omega^2}{k^2} = C_s^2 = \frac{\gamma_{eKT_e} + \gamma_i KT_i}{M} \qquad (3)$$

2) Next we include the wave electric field from the Poisson's equation

$$\frac{\partial E}{\partial x} = 4\pi e(n_i \quad n_e). \qquad (4)$$

Under the assumption of small electron inertia, equation (2) yields a relationship between n_e and the local plasma potential ϕ:

$$n_e = n_0 \ \text{Exp} \ [\frac{e\pi}{KT_e}]. \qquad (5)$$

Inserting the relation (5) into equation (4) we obtain

$$\frac{\partial^2 \pi}{\partial x^2} = 4\pi e(n_1 \quad n_o \ \text{Exp} \ [\frac{e\phi}{KT_e}]).$$

Writing $n_i = n_0 + n_1$, and noting that plasma density ($n_0 k_{De}^{-3} >> 1$) justifies the assumption $e\phi/KT_e << 1$, we have for the wave potential

$$\phi = \frac{4\pi e n_i}{k^2 + k_{De}^2}, \qquad (6)$$

Now we include the finite ion temperature in equation (1) and rewrite it as

$$nM\frac{\partial}{\partial t}\left(\frac{\partial v_i}{\partial x}\right) = n_o e\frac{\partial E}{\partial x} - \gamma_i KT_i \frac{\partial^2 n_i}{\partial x^2}$$

$$= n_o e\frac{\partial^2 \phi}{\partial x^2} - \gamma_i KT_i \frac{\partial^2 n_i}{\partial x^2} \qquad (7)$$

Again using the continuity equation,

$$\frac{\partial^2 n_i}{\partial t^2} = \frac{n_o e}{M}\frac{\partial^2 \phi}{\partial x^2} + \frac{\gamma_i KT_i}{M}\frac{\partial^2 n_i}{\partial x^2}.$$

Fourier transforming and using (6)

$$\frac{\omega^2}{k^2} = \frac{KT_e}{M}\sum\frac{1}{1 + (k^2/k_{De^2})} + \frac{\gamma_i KT_i}{M} \approx C_s^2, \qquad (8)$$

which lacks the factor γ_e of equation (3) because of the assumption of equation (5), i.e., $\gamma_e = 1$.

This dispersion relation is plotted below in Figure IV-2. At low frequencies and small wavenumbers, the dispersion curve is linear and has intercept at $\omega = 0$ so that in this region the phase and group velocities are identical. Since we have not considered any dissipation process in our theoretical treatment so far, the wavenumber k is real. At higher frequencies and wavenumbers, the curve bends over and the wave becomes dispersive that is, the phase velocity becomes a function of k (it decreases with increasing k).

b) Wave damping:

i) Collisional damping by neutrals: ln a weakly ionized laboratory plasma where the neutral density is much higher than the plasma density, the dominant damping mechanism of ion acoustic waves is ion-neutral collisions. We may derive an expression for the spatial damping rate by including a collision term in the equation of motion for the ions,

$$Mn_i\left(\frac{\partial v_i}{\partial t} + v_i\frac{\partial v_i}{\partial x}\right) + Mn_i\, \nu_{in} v_i = en_i E - \frac{\partial p_i}{\partial x}, \qquad (9)$$

where ν_{in} is the ion-neutral collision frequency.

Using equation (9) to replace equation (7) in our previous derivation and solving for the dispersion relation, we obtain for the weak damping case

$$k \approx \frac{+}{-}\left(\frac{\omega}{C_s} + i\,\frac{\nu_{in}}{2C_s}\right). \qquad (10)$$

Equation (10) shows that for weak damping the wavenumber has a real and an imaginary part. Since the wave varies in space as Exp ikx, the imaginary part of the wavenumber will produce spatial exponential damping proportional to $\mathrm{Exp}[-\upsilon_{in}x/2C_s]$. The distance the wave travels before its amplitude

is reduced to e^{-1} of its initial value is then

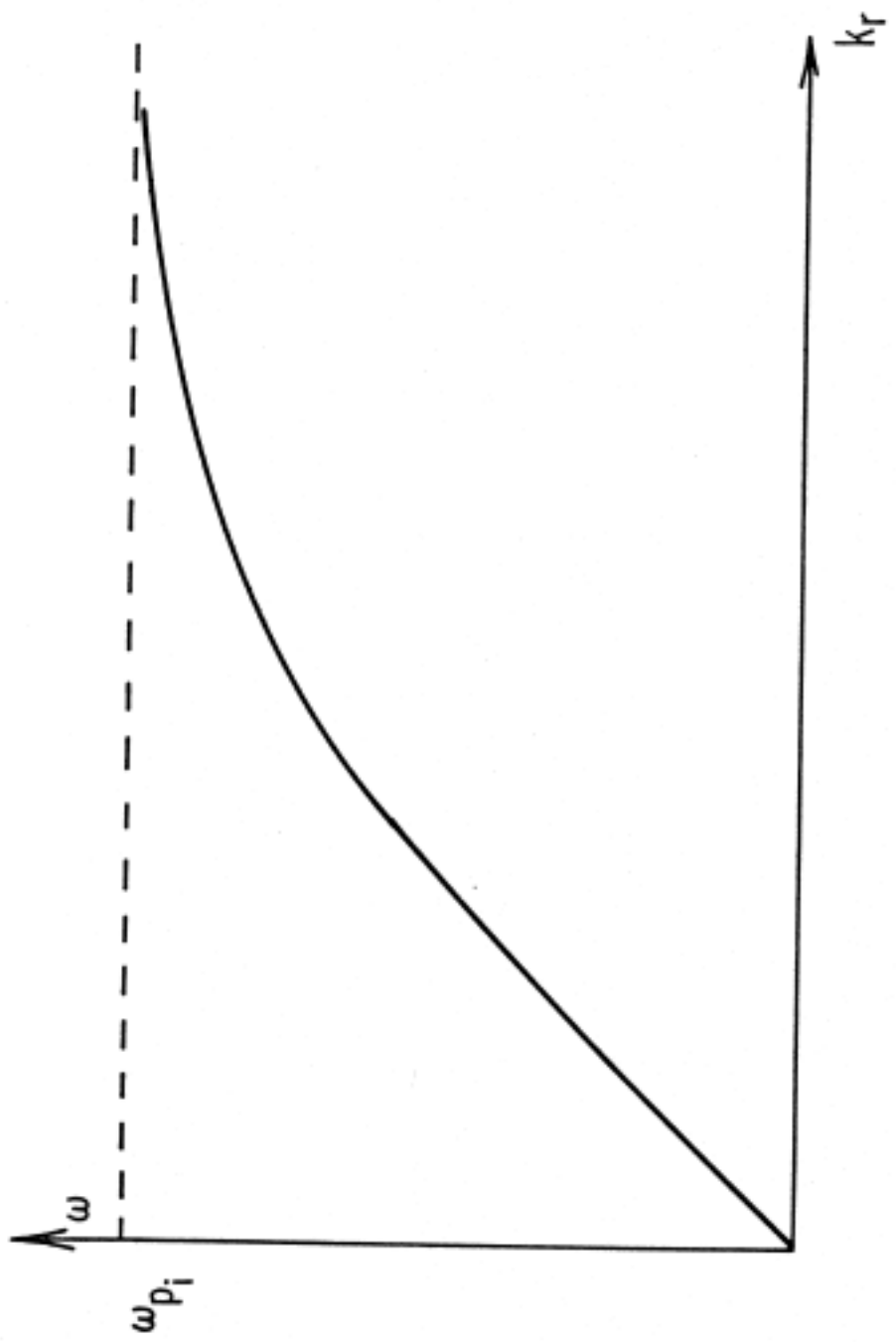

Figure IV-2.

Dispersion relation for ion acoustic waves (real wavenumber dependence).

$$\delta \equiv 2C_s/\nu_{in},$$

and the number of wavelengths in this distance is

$$\frac{\delta}{\lambda} \equiv \frac{1/k_i}{2\pi/k_r} = \frac{\omega}{\pi\nu_{in}},$$

where

$$k = k_r + ik_i$$

If $\nu_{in} << \omega$, $\delta/\lambda >> 1$ and we expect to see many wavelengths over the e-folding distance. In particular, if the frequency is raised, the collisional damping will effectively decrease.

ii) Ion Landau damping: The total damping of ion acoustic waves will not continue to decrease as ω approaches ω_{pi} because the phase velocity becomes comparable to the ion thermal velocity and there are resonant wave-particle interactions. Ions moving slightly slower than the wave can be accelerated and transfer energy out of the wave, thus damping it collisionlessly. Similarly, ions moving slightly faster than the wave can transfer their energy to the wave and make its amplitude grow. In a Maxwellian plasma there are more ions moving slightly slower than the wave and the net effect is damping. This collisionless damping due to the resonant wave-particle interaction is called Landau damping and is named after the discoverer of a similar effect for electron plasma waves. Kinetic theory (Appendix A) shows that the rate of Landau damping is proportional to the slope of the ion distribution function $\partial f_o(\nu) \Big/ \partial\nu \Big|_{\nu_p}$ evaluated at the phase velocity:

$$k_i = (\text{attenuation distance})^{-1} \propto \frac{\partial f(\nu)}{\partial \nu}\Big|_{v_p}$$

$$\propto \nu_p \ \text{Exp}\ [-\nu_p^2 \Big/ a_i^2] \propto \text{Exp}\ \frac{-1}{2}\frac{T_e}{T_i}\left(1 - \frac{\omega^2}{\omega^2_{pi}}\right),$$

where equation (8) has been used for the expression of the phase velocity v_p. The above expression holds only in regimes where the damping is weak, $k_i/k_r << 1$; for example $T_e/T_i >> 1$, $v_p >> a_i$.

As the excitation frequency ω approaches the ion plasma frequency ω_{pi}, the phase velocity v_p is reduced (Figures IV-2 and IV-3) and moves closer to the region of maximum slope in the velocity distribution function, giving rise to a larger ion Landau damping. Physically this can be explained by the increasing difference between the number of particles traveling slower than the wave (which takes energy from the wave) and the number traveling faster (giving energy to the wave).

If the attenuation distance normalized to a wavelength, δ/λ, is plotted against ω we would expect the collisional damping to decrease and thus δ/λ to increase linearly with ω until ω approaches ω_{pi}, where Landau damping begins to dominate. At that point δ/λ should decrease. This behavior is illustrated below in Figure IV-4. It is worth pointing out that with a certain temperature range, T_e/T_i

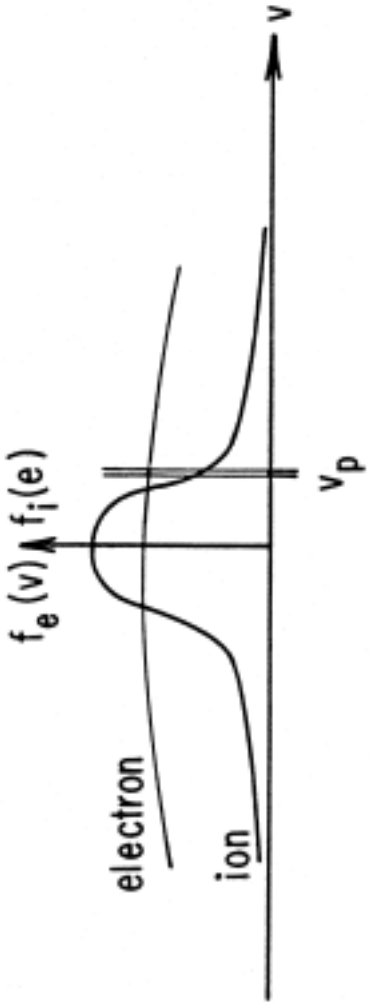

Figure IV-3.

Location of the phase velocity v_p with reference to the ion and electron distribution functions.

≤ 5, the electron Landau damping is smaller than the ion Landau damping[7] because the slope of the electron velocity distribution function at the phase velocity v_p is nearly flat (Figure IV-3) since the phase

velocity is much less than the electron thermal velocity, $v_p \approx (KT_e/M_e)^{1/2} << a_e$.

3) Experimental Method

The experimental arrangement is described in Figure IV-5. A grid made of stainless steel mesh partitions the plasma chamber into two independent halves. In this double plasma (DP) device, the separation grid is negatively biased to prevent electrons of one half from going to the other half. To insure that there is no ion beam in the target chamber, the plasma potentials are closely matched (as observed by Langmuir probes in each half). The driver chamber's plasma potential is made to oscillate at frequency ω relative to the target plasma potential by applying a signal to the driver anode. The possibility of controlling the plasma potential by the anode lies in the fact that when the anode is biased more positively than the plasma potential, it draws a larger electron current, depleting the plasma of electrons and there-by raising the plasma potential. When a potential difference is established between the source and target chambers, plasma particles flow from one chamber into another, setting up a density perturbation.

The ion acoustic wave is then detected by a small disc probe (approximately 5 mm diameter). Since perturbed ion and electron densities in an ion acoustic wave are very nearly equal ($\delta n_e \_ \delta n_i$) and the electron current $\delta n_e e v_{es}$ is much larger than the ion current $\delta n_i e v_{is}$ by the ratio $\sqrt{\frac{M}{m}}$, the most sensitive detection [1] of ion acoustic waves by a probe is achieved when it is biased positively to collect electron saturation current. Another advantage of biasing the receiving probe at or above the plasma potential is the resulting fast probe response the electron-rich sheath surrounding the probe permits good communication between the plasma proper and the probe surface. Two diagnostic techniques which effectively discriminate between the wave signal and extraneous high and low frequency noise are: tone burst time-of-flight measurements and signal interferometry.

a) Tone burst or time-of-flight method: In this scheme a short burst of rf is pulsed onto the exciter grid to launch an ion acoustic wavepacket of several cycles in duration. This traveling wavetrain reaches a movable Langmuir probe (placed at a distance *x* from the grid) in a time longer than the duration of the burst to facilitate a positive identification of the propagating signal. The phase velocity v_p is computed from the time delay τ_p:

$$v_p = x/\tau_p ,$$

[1] in an unmagnetized plasma only.

where the time development of a selected peak in the wavetrain is followed

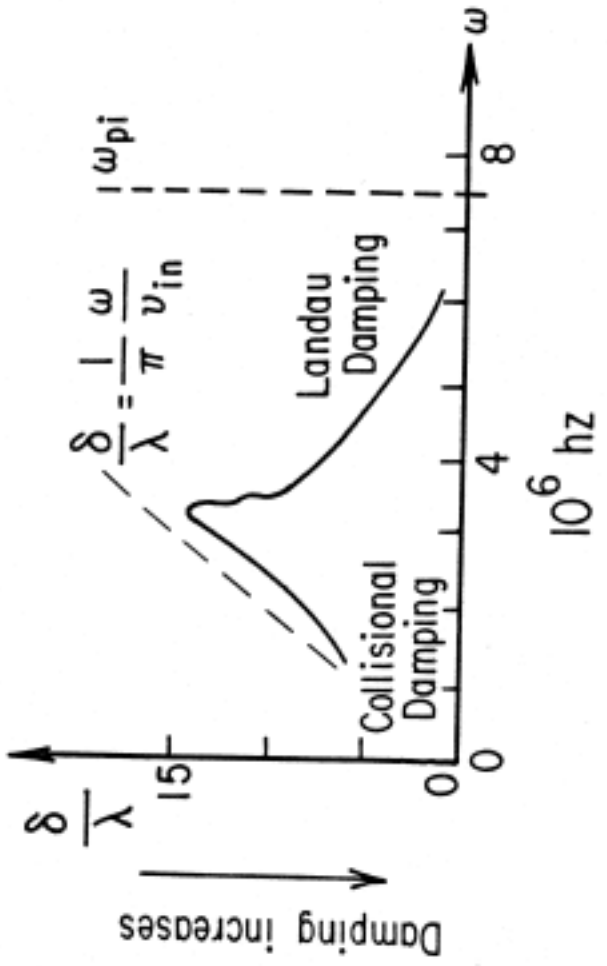

Figure IV-4.

Sample data (solid line) with comparison to collision theory (dashed line). $P_n = 5 \times 10^{-5}$ torr, $\frac{T_e}{T_i} \sim 10$.

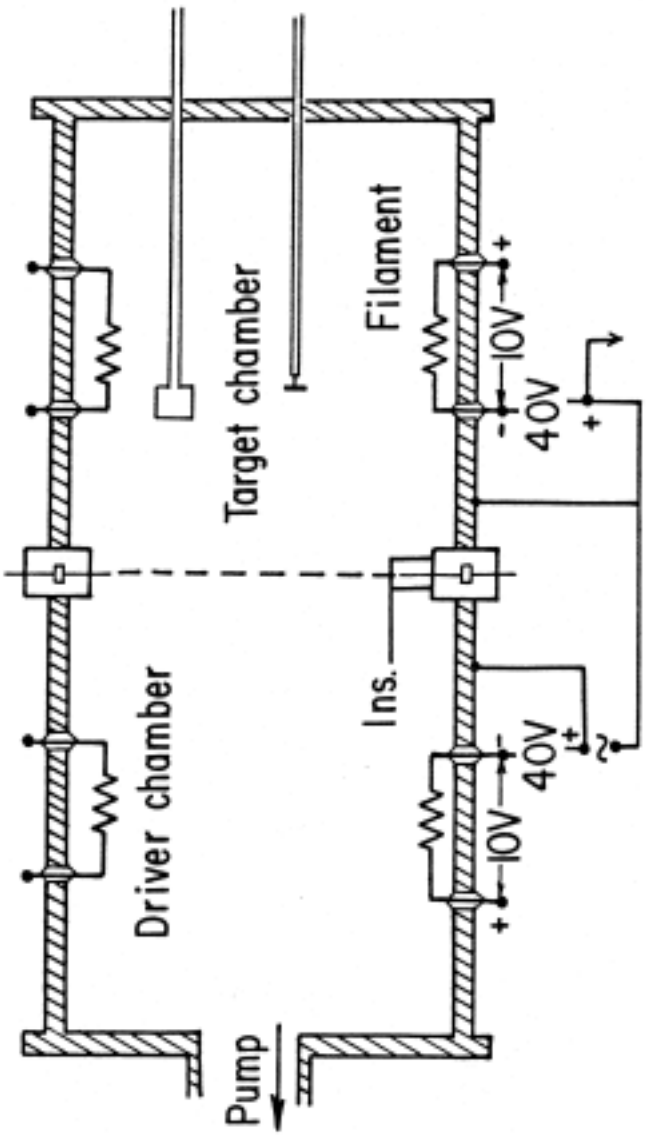

Figure IV-5.
The double plasma device arranged to excite ion acoustic waves.

to determine τ_p.

On the other hand, the group velocity $\frac{\partial\omega}{\partial k_r}$ is just

$$v_g = x/\tau_b ,$$

where τ_b is the time delay measured at the center of the wavepacket. If the wave propagation is dispersive $v_g \neq v_p$, i.e., the selected peak in the wave-train will undergo a noticeable shift in phase within the packet. (The total phase of all cycles within the packet, however, remains constant.)

The real component of the wavenumber k_r follows from the above measurement of v and the

known excitation frequency ω via the definition of phase velocity $v_p = \omega/k_r$.

Information about damping is also available in the tone burst data. The spatial damping rate is the inverse distance over which the wave packet amplitude decays by e^{-1}.

The tone burst method has the advantages of: 1) Separating waves or disturbances with different speeds, thus reducing the possible confusion arising from the superposition of directly coupled signals, ion acoustic and ballistic effects (see Appendix B) 2) Separation of temporal behavior from spatial behavior, and 3) Direct observation of wave forms and group velocities. The principal disadvantage is that since it is a pulsed technique, the detection is more difficult if the signal is near or below the background noise level. However, if the excitation is repetitively pulsed, electronic processors such as the "box-car integrator" or sampling scopes are now available which can extract signals out from the background noise (see data in Figure IV-6d).

The set-up of equipment and sample data for the tone burst method appear in Figure IV-6.

b) Interferometer method: Instead of observing the response of the plasma to a wavetrain burst, we now apply a continuous sinusoidal signal via the exciter grid at the double plasma interface. Again the positively biased probe detects the launched ion acoustic wave only now other continuous signals (directly coupled, etc.) are superimposed on it.

With the continuous signal applied, the relative phase of the detected signal is measured point-by-point in the plasma as the probe is steadily moved away from the exciter grid. In order to separate the ion acoustic wave signal $f(x,t) = A \sin(kx - \omega t)$ from the direct coupled exciter signal $f(t) = B \sin \omega t$, a synchronous detection scheme similar to that described in Chapter III is used.

In this method a mixer multiples the total probe signal with the reference signal from the rf oscillator to give the following output:

$$g(x,t) = AB \sin \omega t \, [\sin \omega t + \sin(kx - \omega t)]^1.$$

An R-C integrating circuit (low-pass filter) integrates this composite signal $g(x,t)$ in time producing the resultant space dependent direct current signal (frequency independent)

$$h(x) \propto A_{ion}(x) \cos (kx + \alpha),$$

---

[1] The two signals placed into the mixer must be of comparable, although small, amplitude to avoid damaging this device. Usually the reference signal must be attenuated and the probe signal amplified to achieve this condition. A 0.5 V maximum tolerable input is typical.

where $A_{ion}(x)$ is the spatially dependent ion wave amplitude, $k = 2\pi/\lambda$, and α is an arbitrary constant phase. This processed signal h(x) is the spatial profile of the wave modes launched in the plasma. This is plotted on the chart recorder by transducing axial detecting probe positions into potentials calibrated to the x-sweep function of this instrument.

a)

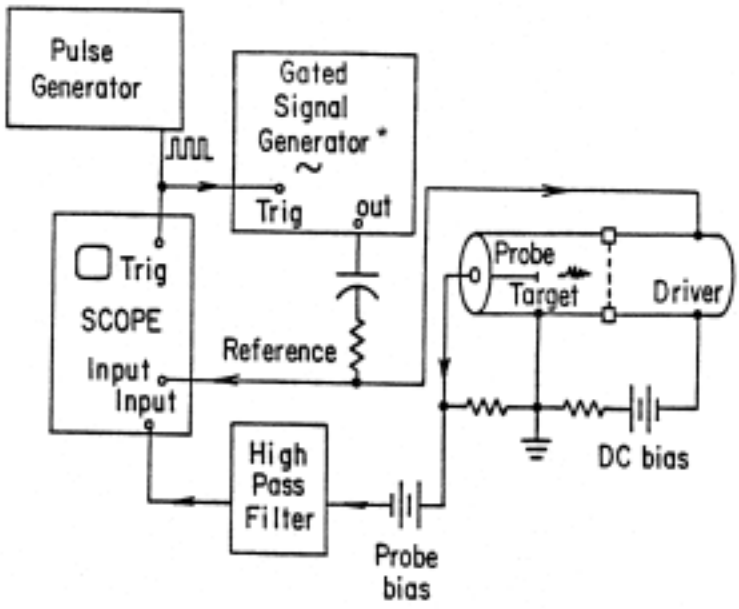

a) Simple tone burst circuit for oscilloscope data. *Function Generator Model 110 (Wavetek Instruments, San Diego, CA)

b) Tone burst circuit using box-car averager to slowly scan the probe signal in time, averaging out all high frequency noise. This time scan is performed for each setting of probe distance x.

b)

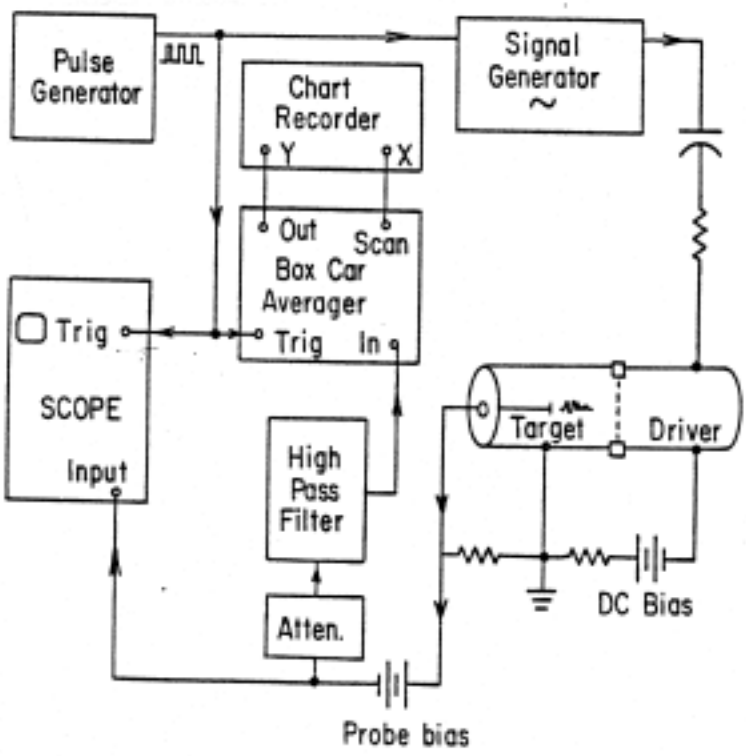

Figure IV-6.

T

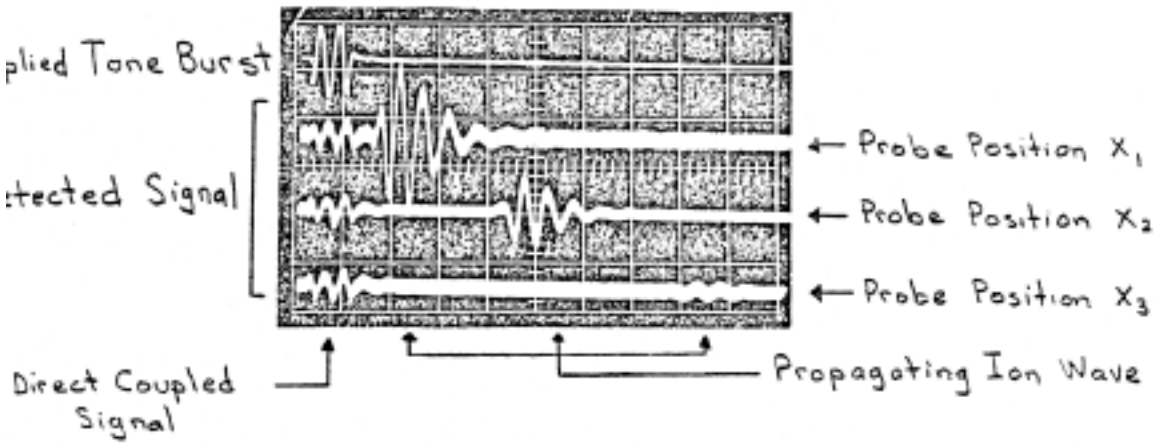

Figure IV-6c.

Typical oscilloscope data showing the applied signal, the directly coupled components and the time-delayed ion acoustic wave signals.

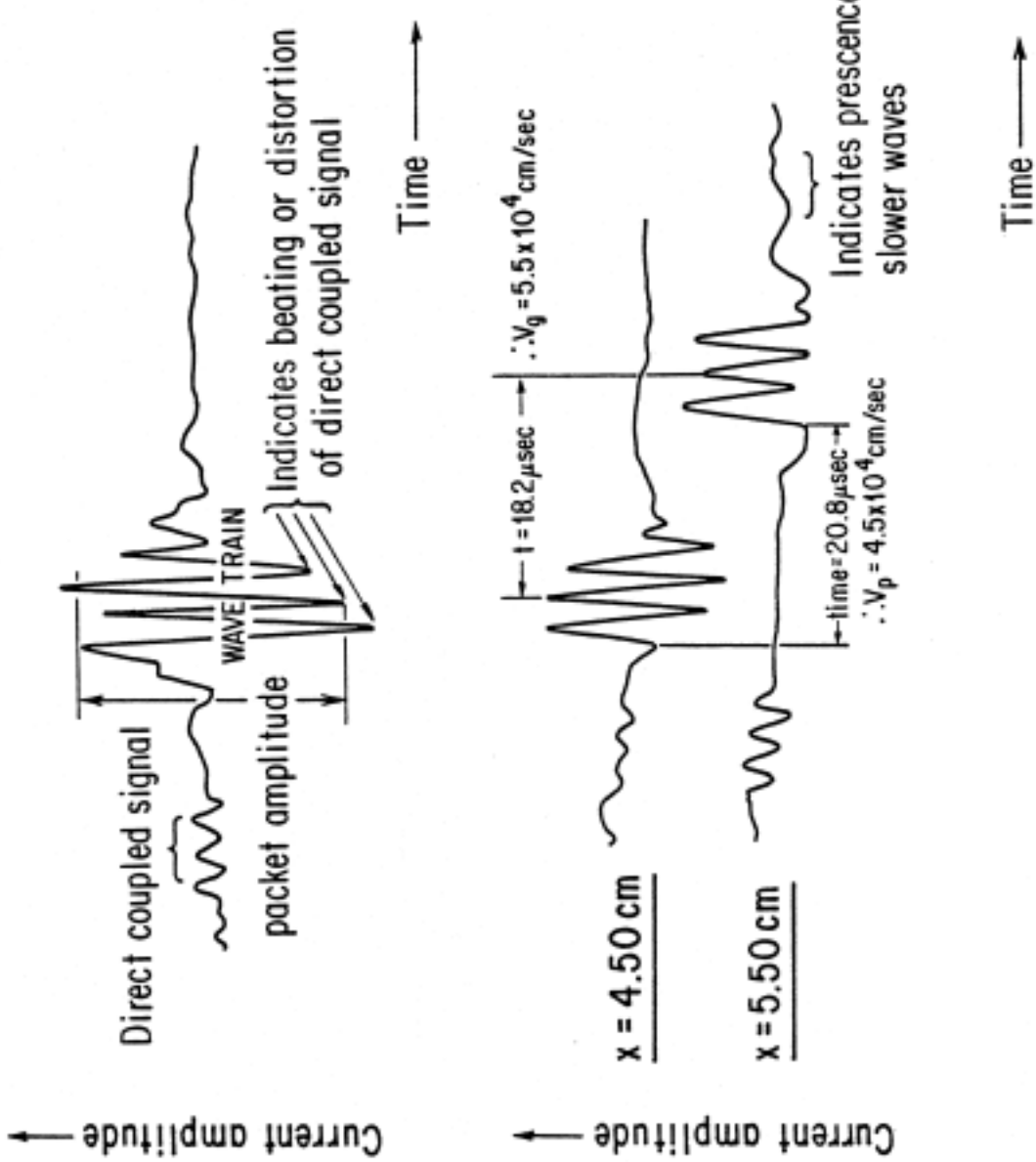

Figure IV-6d.

Sampled tone burst data obtained with box-car integrator. $\omega = 2.5 \times 10^6$ sec^{-1}.

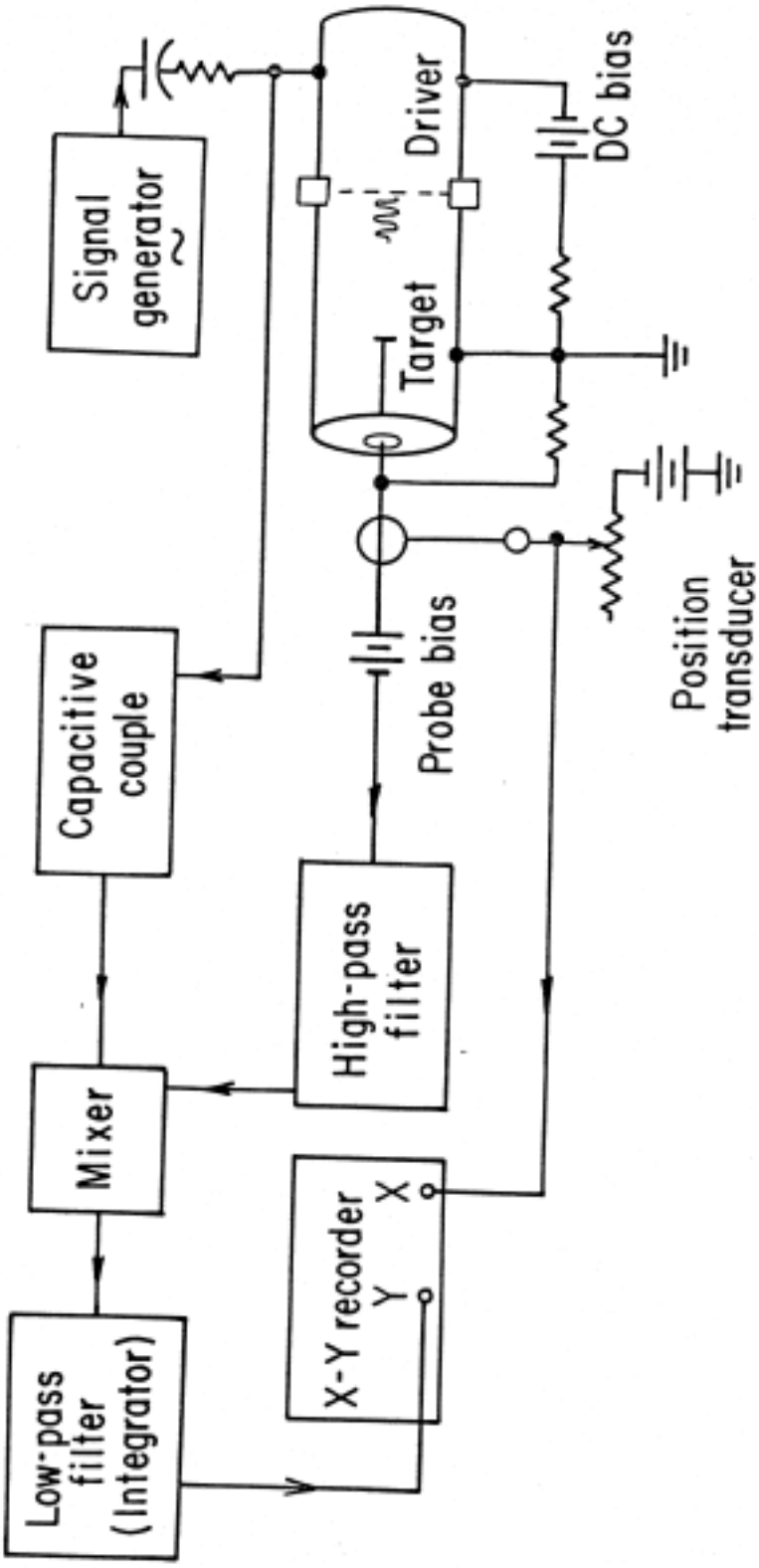

Figure IV-7a.

Interferometry Apparatus. Capacitive coupling protects mixer from DC level on target anode.

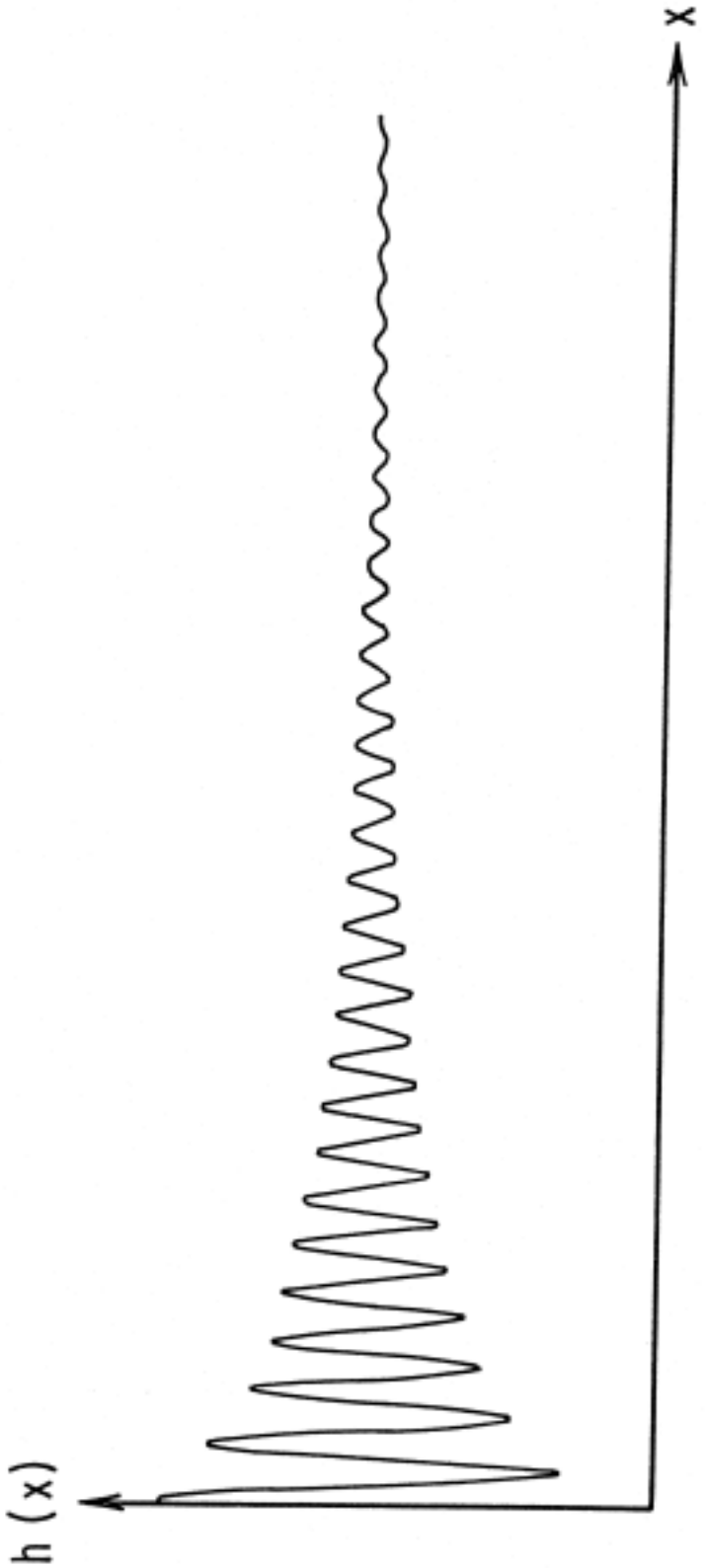

Figure IV-7b.

Typical interferometer data.

his interferometer apparatus is summarized in Figure IV-7 along with a sample interferometer trace of the ion acoustic signal h(x). Wavelengths and spatial damping rates are measured directly from such recorder plots of h(x) vs. x. This diagnostic method holds the principal advantage of a long time constant in the R-C filter, which averages out noise (uncorrelated signals) producing a good signal-to-noise ratio.

4) Experimental Procedure

a) Tone burst: Set up the tone burst circuit of Figure IV-6 using an rf source to generate an oscillating potential between the component chamber of the DP device.

i) Before activating the tone burst,

1) Monitor the ion distribution function to make sure no ion beam is present.

2) Double check the match of driver and target plasma potentials with Langmuir probes positioned ~ 10 cm from the exciter grid.

3) Measure T_i to verify $T_i << T_e$.

ii) Use the tone-burst generator to launch a wavetrain of sinusoidal oscillations. Observe the propagation of the wavepacket with the disc probe (biased to collect electron saturation current).

1) Measure $\delta n/n$ by noting the density perturbation on a Langmuir trace or by biasing the probe at a fixed potential above the plasma potential and monitoring the fluctuations in the electron current $\delta I_e/I_e$, which is proportional to $\delta n/n$, assuming there is no fluctuation of temperature.

b) Measure $\delta n/n$ by monitoring the ion wave signal at the floating potential,[1] V_f, using the capacitive probe of Appendix F.

3) Measure V_s, the plasma potential using a sampling technique. Collect the entire Langmuir trace at a particular phase in the oscillating ion signal. Obtain V_s directly from the shape of the Langmuir curve.

iii) For a selected exciter frequency, find[2]

1) v_p, the propagation velocity of the envelope of the wavepacket (group velocity), and

---

[1] Convince yourself that if we assume the fluctuation of the floating potential is the same as the fluctuating plasma potential, then

$$\delta n/n \_ e\delta V_s/KT_e \_ e\delta V_f/KT_e$$

Check this relation for several values of δn and V_f.

[2] Both phase and group velocities are computed by displaying the applied exciter grid signal and the received probe signal on the same scope trace and noting the time delay of corresponding features of the wave form as a function of the axial distance between the receiving probe and separation grid.

2) v_g, the propagation velocity of a given peak within the wavepacket. Whenever this traveling peak shifts phase (position) within the propagating packet, $v_p \neq v_g$ (dispersive wave propagation).

iv) Check the parametric dependence of the signal investigated in step iii):

1) Is damping getting stronger as ω approaches ω_{pi}?

2) Compute the ion acoustic speed C_s by measuring T_e in the target plasma with the Langmuir probe. Does this value agree with the experimentally measured speed?

v) Carry out step iii) over as wide a frequency range as possible so that you can plot

1) ω vs. k_r, the dispersion relationship, and

2) ω vs. δ/λ, where δ/λ is the spatial damping rate of the ion acoustic wave.

vi) Repeat the procedure in step v) for several different neutral pressure settings.

b) Interferometer: Set up the interferometer circuit as shown in Figure IV-7a. Again verify that no ion beam is present and record interferometer traces with the continuous signal applied to the exciter for a wide range of frequencies. Using this technique, replot the dispersion relation, ω vs. k_r, and the spatial damping dependence, ω vs. δ/λ, for several neutral pressure settings. Record any irregular patterns in the waveforms and attempt to interpret your data in terms of more than one mode propagating in the plasma (see Appendices B and E).

Appendix A: Landau Damping of Ion Acoustic Waves

1) General Dispersion Relation

We shall describe a more detailed theory of ion acoustic waves which includes the boundary conditions at the excitation source. Ion dynamics will be included in this treatment to describe the collisionless damping of ion waves.

In most experiments on ion acoustic waves, the frequency is much less than the electron-electron collision frequency but greater than the ion-ion collision frequency. We shall therefore follow the analysis of Jensen[8] in treating the electrons as a fluid but shall describe the ions by a collisionless Boltzmann equation in the manner of Fried and Gould.[3] The electrons are characterized by an average electron density n_e, and average velocity v_e, and isotropic pressure P_e. The equation of motion for electrons is

$$nm\frac{dv_e}{dt} = -neE\ \frac{\partial p_e}{\partial x} \tag{A-1}$$

where $P_e = nKT_e$ and E is the total electric field present at x at time t. The ions are described by a velocity distribution function f_i satisfying the one-dimensional collisionless Boltzmann equation

$$\frac{df_i}{dt} = \frac{\partial f_i}{\partial t} + v\frac{\partial f_i}{\partial x} + \frac{eE}{M}\frac{\partial f_i}{\partial v} = 0. \tag{A-2}$$

A separate theoretical analysis[10] has shown that axially propagating ion acoustic waves are insensitive to radial boundary conditions because the strong shielding by electrons greatly reduces the influence of electric fields at the boundary on the central propagating region. A one-dimensional analysis should provide a reasonably good description of the propagation of ion acoustic waves.

We shall linearize (A-l) and (A-2) by letting

$$n = n_0 + n_1(x,t)$$

and

$$f_i(x,v,t) = f_{0i}(v) + f_{1i}(x,v,t),$$

where $f_{oi}(v)$ is the Maxwellian ion velocity distribution function. Since no external electric fields are applied to the plasma volume (except at the exciter, located on the x = 0 boundary) the total electric field E is just the self-consistent field due to the separation of the local plasma charges,

$$E = E_1 (x,t).$$

Neglecting electron inertia (m/M << 1) and assuming isothermal conditions in equation (A-l) and linearizing both equation (A-l) ant (A-2), one obtains

$$n_0 e E_1 \approx KT_e \frac{\partial n_1}{\partial x} \tag{A-3}$$

$$\frac{\partial f_{1i}}{\partial t} = \nu \frac{\partial f_{1i}}{a x} + \frac{eE}{M} \frac{\partial f_{1i}}{\partial \nu} = 0 \tag{A-4}$$

Next, Fourier analyze ant Laplace transform each of the first order terms in (A-3) and (A-4) into (k,ω) space, as in the following steps, which involve integrations by parts:

$$\int_{-\infty}^{\infty} dt \int_{o}^{\infty} dx \frac{\partial n_1(x,t)}{\partial x} e^{-i(kx - \omega t)} = \left| \int_{-\infty}^{\infty} dt \; e^{i\omega t} \| n_1(x,t) \; e^{-ikx} \right|_0^{\infty}$$

$$- \int_0^{\infty} dx(-ik) \; n_1(x,t) \; e^{-ikx} \Big|$$

$$= - \int_{-\infty}^{\infty} dt \; n_1(0,t) \; e^{i\omega t} + ikn_1(k,\omega)$$

$$\int_{-\infty}^{\infty} dt \int_0^{\infty} dx \frac{\partial f_1(x,v,t)}{\partial t} e^{-i(kx - \omega t)} = \int_{-\infty}^{\infty} dt \frac{\partial f_1(k,v,t)}{\partial t} e^{i\omega t}$$

$$= \underbrace{f_1(k,v,t) \, e^{i\omega t} \Big|_{-\infty}^{\infty}}_{\Uparrow = 0 \text{ (See footnote [1])}} - \int_{-\infty}^{\infty} dt \; i\omega \; f_1(k,v,t) \; e^{i\omega t}$$

$$= - i\omega \, f_1(k,v,\omega).$$

Solving the Fourier and Laplace, transformed versions of (A-3) and (A-4) for $n_1(k,\omega)$ and $f_{1i}(k,v,\omega)$, respectively, produces

$$n_1(k,\omega) = \frac{in_o eE_1(k,\omega)}{kKT_e} - \frac{iq(\omega)}{k} \qquad \text{(A-5)}$$

and

$$f_{1i}(k,v,\omega) = \frac{i}{(kv - \omega)} \left(\frac{eE_1(k,\omega)}{M} \frac{\partial f_{0i}(v)}{\partial v} \quad vg_i(\omega,v) \right), \qquad \text{(A-6)}$$

where

$$q(\omega) \equiv \int_{-\infty}^{\infty} dt \; n_1(0,t) \; e^{i\omega t}$$

and

$$g(\omega,v) \equiv \int_{-\infty}^{\infty} dt \; f_1(0,v,t) \; e^{i\omega t}.$$

Note that $n_1(0,t)$ and $f_1(0,v,t)$ are the boundary values of the electron and ion perturbations at the exciter

---

[1] This term is zero because $f(k,v,-\infty) = 0$ and the excitation is turned on very slowly at $t > -\infty$; there is a very small positive imaginary frequency component in $\omega = \omega_r + i\delta$ such that the entire term vanishes at $t = +\infty$.

(x=0), and q(ω) and g(ω,v) are their respective Fourier transforms.

The Poisson's equation,

$$\frac{\partial E_1}{\partial x} = 4\pi e(n_{1i} - n_1) = 4\pi e\left(\int_{-\infty}^{\infty} dv\, n_o\ f_{1i}(x,v,t) - n_1(x,t)\right), \qquad \text{(A-7)}$$

can also be Fourier-Laplace transformed to give

$$ikE_1(k,\omega) - E_1(0,\omega) = 4\pi e\left(\int_{-\infty}^{\infty} dv\ n_0\ f_{1i}(k,v,\omega)\ n_1(k,\omega)\right), \qquad \text{(A-8)}$$

where E (0,ω) is the field at the exciter grid (x = 0). Substituting (A-6) and (A-8) into (A-7) yields an expression for the total electric field in the plasma

$$E_1(k,\omega) = \frac{1}{ik\varepsilon(k,\omega)}\left[E_1(0,\omega) + 4\pi e\left(\int_{\infty}^{\infty} \frac{vg_i(\omega,v)\,dv}{i(kv - \omega)} - \frac{q(\omega)}{ik}\right)\right] \qquad \text{(A-9)}$$

Source electric field	Perturbed ion distribution at source	Electron density perturbation at source

where ε(k,ω) is defined as the dielectric constant for longitudinal waves, which describes the collective response of the plasma to excitations of frequency ω and wave number k

$$\varepsilon(k,\omega) = 1 + \frac{4\pi n_o e^2}{Mk^2}\int_{-\infty}^{\infty} \frac{f'_{oi}(v)dv}{\omega/k - v} + \frac{4\pi n_o e^2}{k^2 Kt_e} \qquad \text{(A-10)}$$

$$= 1 + \frac{\omega_{pi}^2}{k^2}\int_{-\infty}^{\infty} \frac{f'_{oi}(v)dv}{\omega/k - v} + \frac{k_{De}^2}{k^2}. * \qquad \text{(A-11)}$$

ion contribution electron contribution

The contribution of electrons (k_{De}^2/k^2) to shielding is large (since $k << k_{De}$ under most experimental conditions), as is expected from their high degree of mobility.

As indicated by the form of (A-9), the dominant contributions to the total plasma (wave) electric field come from the set of ω's and k's which satisfy the dispersion relation ε(k,ω) = 0. The solution to ε(k,ω) = 0 contains terms similar to those already derived in the fluid theory (equation 8 of Chapter IV), plus an additional, imaginary part, which depends on the shape of the ion distribution function $f_{oi}(v)$ and pertains to wave damping.

To see this dependence, let us solve for the roots (zeros) of the dispersion relation $\varepsilon(k,\omega) = 0$ for a case of experimental interest, $T_e >> T_i$, and $a_i << \omega/k << a_e$, consistent with temperatures typically observed in the DP device. first, rewrite the ion contribution to (A-11), which is an integration along the real axis, using the identity

$$\frac{1}{\omega/k\ v} = P\left(\frac{1}{\omega/k\ v}\right) + i\pi\delta(\omega/k\ v) \qquad \text{(A-12)}$$

where P denotes the Cauchy principal value and δ the delta function. Substitution of (A-12) into (A-11) gives us a more explicit expression of the dielectric constant:

$$\varepsilon(k,\omega) = 1 + \frac{\omega_{pi}^2}{k^2} P \int_{-\infty}^{\infty} \frac{f_{oi}^{\copyright}(v)dv}{\omega/k - v} - i\pi \frac{\omega_{pi}^2}{k^2} f_{oi}^{\copyright}(\omega/k) + \frac{k_{De}^2}{k^2} \qquad \text{(A-13)}$$

valid for small damping $k_i << k_r$. Solving for $\varepsilon(k,\omega) = 0$ using the relation

$$P\int_{-\infty}^{\infty} \frac{f_{oi}^{\copyright}(v)dv}{\omega/k - v} = -\frac{1}{\omega^2/k^2}\left(1 + \frac{3\frac{KT_i}{M}}{\omega^2/k^2}\right)$$

we obtain analytic expressions for the real and imaginary wavenumbers k_r and k_i:

$$\frac{\omega^2}{k_r^2} \cong \frac{\omega_{pi}^2\left(1 + \frac{3KT_i}{M}\frac{1}{\omega^2/k^2}\right)}{k_r^2 + k_{De}^2}$$

or

$$\frac{\omega^2}{k_r^2} \cong \frac{KT_e}{M}\frac{(1 + 3T_i/T_e)}{1 + k_r^2/k_{De}^2} \qquad \text{(A-14)}$$

and

The phase velocity calculated from the kinetic theory essentially agrees with the result of the fluid theory (equation 8 of Chapter IV), since the wave motion is carried on by the main plasma moving as a whole. The new result of the kinetic treatment lies in the imaginary wave number k_i which describes the contribution of the resonant particles traveling at the wave phase velocity. For a Maxwellian plasma $f_{oi}(v) = \pi^{-1/2}\ a_i^{-1}\ \text{Exp}\ (-v^2/a_i^2)$,

$$k_i = \frac{\pi^{1/2}}{2} \frac{\omega}{a_i} \frac{\omega_{pi}^2}{\omega^2} \frac{T_e}{T_i} \mathrm{Exp}\left\{\frac{T_e}{2T_i}\left(1 - \frac{\omega^2}{\omega_{pi}^2}\right)\left(1 + \frac{3T_i}{T_e}\right)\right\} \qquad \text{(A-15)}$$

and the attenuation distance normalized to one wavelength is:

$$\frac{\delta}{\lambda} = \frac{1}{2\pi}\frac{k_r}{k_i} \cong \frac{\left(\frac{T_i}{T_e}\right)^{3/2} \mathrm{Exp}\left\{\frac{T_e}{3T_i}\left(1 - \frac{\omega^2}{\omega_{pi}^2}\right)\left(1 + \frac{3T_i}{T_e}\right)\right\}}{2\pi^{3/2}\left(1 - \frac{\omega^2}{\omega_{pi}^2}\right)^{1/2}} \qquad \text{(A-16)}$$

where the approximation $\frac{1}{1 + k^2/k_{De}^2} = 1 - \omega^2/\omega_{pi}^2$ has been used.

Appendix B: Collective and Free-streaming Contributions to Propagating Ion Acoustic Waves

When a grid is used to produce a local density perturbation and thereby launch an ion acoustic wave, particles near the grid are accelerated and a perturbation on the velocity distribution function is produced. This perturbation is carried by particles free-streaming contribution. When these particles are collected by the detecting probe, their modulated velocity distribution makes a contribution to the probe signal. This is called the free-streaming contribution to distinguish it from the collective plasma behavior in ion acoustic waves derived in a homogeneous plasma. In the following we shall discuss the collective and free-streaming behaviors in an experimental situation and their relative importance. It is possible to distinguish one contribution from another through a systematic variation of plasma parameters such as T_e, T_i, n, the concentration of lighter ions, etc. This series of tests is summarized in a table at the end of this appendix.

1) Free-streaming Ions and Spatial Landau Damping

In the laboratory, ion waves are detected by either collecting ions by a probe or energy analyzer, or by monitoring the wave electric field by an electron beam diagnostic technique or a high impedance probe. As explained below, each detection method emphasizes different aspects of ion waves. First, we shall consider a method in which ion flux is detected.

a) Detection of ion flux: If the receiving probe is biased negatively to detect ion flux, J_1, the spatial variation of the detected signal is obtained via the inverse transform of the spatial Fourier spectrum of the current:

$$J_1(x,\omega) = \frac{1}{2\pi}\int_c dk\, J_1(k,\omega)\, e^{ikx} = \frac{1}{2\pi}\int_c dk \int_{-\infty}^{\infty} dv\ v f_{1i}(k,\omega,v)\, e^{ikx} ,$$

where c denotes the appropriate contour of integration in k space from the inverse Laplace transform. Using the expression of $f_{1i}(k,\omega,v)$ from equation (A-6), we obtain two types of contributions to the current:

$$J_1(x,\omega) = \underbrace{\frac{i}{2\pi}\int_{-\infty}^{\infty} dv \int_c \frac{dk}{\left(k - \frac{\omega}{v}\right)} \frac{e}{M} E_1(K,\omega)\ f'_{oi}(v)\ e^{ikx}}_{\text{i) collective term}} - \underbrace{\frac{i}{2\pi}\int_{-\infty}^{\infty} dv \int_c \frac{v\,dk}{\left(k \pm \frac{\omega}{v}\right)} g_i(\omega,v)\ e^{ikx}}_{\text{ii) free-streaming term}} \quad \text{(B-1)}$$

i) Collective term: spatial Landau damping. In the collective term, the wave electric field E_1 accelerates the ions, ant together with the gradient of the ion distribution function produces and ion flow in the velocity space. Integration over the entire velocity range $-\infty < v < \infty$ sums up the contribution of ion flow at each velocity to the overall ion flux. The collective effects are contained in the dielectric constant term $\varepsilon(k,\omega)$ of the expression for the self-consistent field $E(k,\omega)$, as given in equation (A-9).

The collective term is calculated by substituting (A-9) into (B-1) and performing the integration over complex k space:

$$J_1 \text{ collective}^{(x,\omega)} = E_1(0,\omega)\underbrace{\left|\int_{-\infty}^{\infty} dv \frac{i\frac{ve}{M}f_{oi}^{\copyright}(v)}{\partial\varepsilon/\partial k\big|_{k_{res}}} \frac{\text{Exp}\left(ik_{res}x\right)}{k_{res}^2\left(v-\frac{\omega}{k_{res}}\right)}\right.}_{\text{Type A}}$$

$$\left. + \int_{-\infty}^{\infty} dv \frac{i\frac{ve}{M}f_{oi}^{\copyright}(v)\ \text{Exp}\left[i\ \frac{w}{v}\ x\right]}{\omega\varepsilon\left(\frac{\omega}{v},v\right)}\right|$$

Type B

+ similar terms with $E(0,\omega)$ replaced by $\int_{-\infty}^{\infty} \frac{vg(o,\omega,v)\ dv}{i(kv\ \ omegta)}$

+ similar terms with $E(0,\omega)$ replaced by $q(0,\omega)$. (B-2)

Here each boundary condition at x = 0[$E_1(0,\omega)$, $g(0,\omega,v)$, and $q(0,\omega)$] is propagated toward the detector with a spatial phase Exp [$ik_{res}x$], where k_{res} is determined from the dominant root of $\varepsilon(\omega,k) = 0$. This behavior is represented by the type A terms in equation (B-2) and corresponds to the wave-particle interaction proposed by Landau. A second spatial behavior Exp [$ik_{eff}x$] is obtained from the integration of the type B terms. It is similar to the phase mixing process to be discussed below except for the plasma shielding term $\frac{1}{\varepsilon(\omega/v,v)}$ in the integrand.

Let us now consider the physical picture of free-streaming and phase-mixing processes. We shall present an x-t diagram which illustrates the free-streaming behavior of the perturbed particle distribution at the boundary. A simple argument gives a good estimate of the effective attenuation distance $x = (k_{err})^{-1}$ due to phase-mixing among particles traveling at different velocities.

Consider an idealized grid which acts as a gate that either lets particles go through or absorbs them completely. In Figure IV B-1, the grid located at x = 0 allows short bursts of particles to pass through at intervals of τ. The lowest harmonic of this modulation corresponds to the frequency of our exciter. The response of the receiver which detects ion flux I(t) as shown on the right is obtained by an integration over velocity, i.e., $I(t) = q\int_{-\infty}^{\infty} vf(v)\,dv$. The velocity spread causes particles to overtake one another or phase mix resulting in a loss of the original oscillating signal. An estimate of the effective attenuation distance x_0 at which phase mixing begins to occur is made by computing the

time $\Delta\tau$ required by the fastest ion (velocity v_2) to overtake the slowest ion (velocity v_1) of a previous cycle. Referring to Figure IV B-!:

$$v_2\Delta\tau = v_1 (\tau + \Delta\tau) = x_0.$$

This gives

$$\Delta\tau = \frac{\nu_1}{\Delta\nu}\tau \wedge x_0 = \frac{\nu_1\nu_2}{\Delta\nu}\tau = \frac{\nu_m^2 (\Delta\nu/2)^2}{\Delta\nu}\tau - \frac{\nu_m^2}{\Delta\nu}\frac{2\pi}{\omega}$$

where

$$\nu_m = \frac{\nu_1 + \nu_2}{2}, \quad \Delta\nu = \nu_2 \quad \nu_1$$

or

$$k_i = \frac{\omega}{2\pi v_m}\frac{\Delta v}{v_m} \tag{B-3}$$

smaller the attenuation distance x_0. As the frequency increases or the period shortens, the phase mixing occurs over a shorter distance as expected. If v_m is replaced by the thermal velocity a_i and assuming a velocity spread $\Delta v \_ a_i/2$ then $k_i \_ \omega/4\pi a_i$.

ii) Free-streaming term in the detection of ion flux. Returning to (B-1) we note that the second term describes how a perturbation of the velocity distribution function at the exciter, $g(x = 0,\omega,v)$, propagates out from the source. If the perturbed ion distribution $g(\omega,v)$ can be assumed to be Maxwellian, the free-streaming term in equation (B-1) takes on the following form:

$$J_{1\ \text{freestream}}(x,\omega) \propto \left(\frac{\omega x}{a_i}\right)^{2/3} [\text{Exp}\ (\omega x/a_i)^{2/3}\ (1\ \ i\sqrt{3})]. \qquad \text{(B-4)}$$

The above expression gives an effective decay constant $k_i \_ \omega/a_i$, which is similar to the result derived from our physical model.

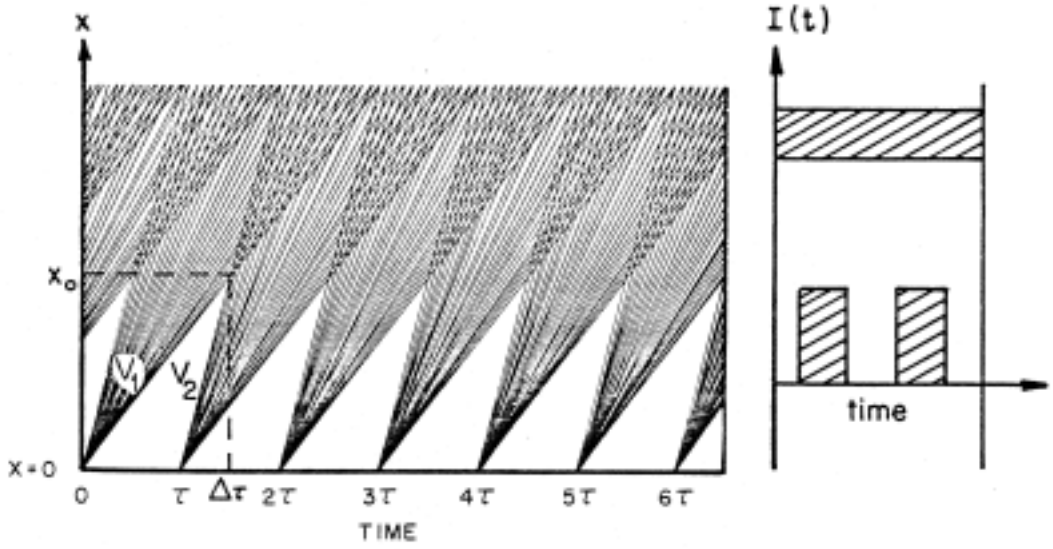

Figure IV B-1
Space-time trajectories of gated particles showing phase mixing that causes spatial damping of ballistic ion perturbations. The probe response at various distances is shown at the right.

b) Detection of wave electric field $E_1(x,\omega)$: If the fluctuation of plasma potential is monitored by a probe technique or the wave electric field is directly measured by an electron beam method, the detected quantity expressed in terms of the wave electric field $E_1(x,w)$ is just the spatial transform of equation (A-9):

$$E_1(x,\omega) = \frac{1}{2\pi}\int_c dk\ E_1(k,\omega)\ e^{ikx}$$

$$= \frac{1}{2\pi}\int_c dk\ \left[\frac{E_1(0,\omega) + 4\pi e\left[\int_{-\infty}^{\infty} dv\ \frac{g_i(0,\omega,v)}{i(k\ \omega/v}\ \frac{q(0,\omega)}{ik}\right]}{ik\varepsilon(k,\omega)}\right]e^{ikx}.$$

In using the residue theorem to evaluate this integral, we notice that there are again two kinds of poles, a "free-streaming" pole at $k = \omega/v$ and a "collective" pole k_{res} derived from the solution to $\varepsilon(k,\omega) = 0$. Summing these residues gives

$$E_1(x,\omega) = \frac{Exp\ [ik_{res}x]}{k_{res}\frac{\partial\varepsilon}{\partial k}|_{k_{res}}}\left[E_1(0,\omega) + 4\pi e\left\{\int_{-\infty}^{\infty}\frac{g_i(\omega,v)\,dv}{i(k_{res}\ \omega/v)}\ \frac{q(\omega)}{ik_{res}}\right\}\right]$$

$$- i4\pi e\int_{-\infty}^{\infty}\frac{v\,dv\ g_i(\omega,v)\ e^{i(\omega/v)x}}{\omega\varepsilon(\omega/v,v)} \qquad \text{(B-5)}$$

The first bracket contains the boundary conditions of the electric field, perturbed ion distribution function and perturbed electron density, which propagate toward the electric field detector with the spatial phase variation Exp $[ik_{res}x]$; the last term of (B-5) is the contribution of the perturbed ion flux generated at the exciter; those particles with a given free-streaming velocity v propagate with an equivalent wavenumber $k = \omega/v$. Summation over the entire velocity distribution taking the electron shielding into account through the dielectric constant $\varepsilon(\omega/v,v)$ gives the total contribution of the free-streaming ions to the wave field.

An estimate of the relative importance of the collective contribution and the free-streaming contribution can be made. The former decays as Exp $[-k_i x]$ (where k_i = Im k_{res}) while the latter approximately as Exp $[-(\omega/a_i)x]$. For our experimental conditions of high electron temperatures $T_e/T_i >> 1$ and a correspondingly high phase velocity, the Landau damping is weak for $\omega << \omega_{pi}$ and $k_i \equiv$ Im $k_{res} << \omega/a_i$. The collective behavior therefore dominates at distances $x > a_i/\omega$. Since the wavelength of ion acoustic waves is given by:

$$\lambda = 2\pi\frac{a_i}{\omega}\left(\frac{T_e}{T_i}\right)^{1/2} >> \frac{a_i}{\omega}$$

we can safely state that at distances beyond one wavelength from the source the collective behavior

makes the dominant contribution to the detected wave electric field.

2) Pseudo-ion waves

These are wave-like signals detected by the receiver probe, which are ion bursts emitted at regular intervals by an excitation grid driven to large amplitudes ($e\phi 0/KT_e >> 1$ where ϕ_0 is the oscillating potential of the grid with respect to the surrounding plasma).

Consider an exciter grid located at x = 0 with a typical sheath thickness of 20 λ_D in Figure IV 8-2. Particles at thermal velocities $(KT_i/M)^{1/2}$ enter the sheath region from below and are accelerated if they encounter the correct phase of the oscillating electric field $E(t) = E_0 \cos \omega t$. The trajectories of certain particles are altered in such a way that upon crossing the grid they are further accelerated to a maximum velocity v_0 which can be estimated as follows:

$$\frac{1}{2} M v_o^2 \leq 2e\phi_0$$

or

$$v_o \leq 2(e\phi_0 / KT_e)^{1/2} (KT_e/M)^{1/2}$$

We note that only at a particular phase of the cycle are particles accelerated to the maximum velocity v_0 proportional to $(e\phi_0/KT_e)^{1/2}$. These fast ions can become the dominant contribution to a probe biased to collect ion flux. As can be easily verified in the diagram, there is an associated wavelength $\lambda = 2\pi v_0/\omega$. Unlike ion acoustic waves, the wavelength and hence the phase velocity of this pseudo wave are strongly dependent on the exciter amplitude. The attenuation arises from phase mixing among the bursts in a manner similar to that in the free-streaming contribution discussed previously for ion acoustic waves.

3) Experimental Differentiations Between Collective and Free-streaming Contributionsto Ion Acoustic Waves

These two major contributions to ion acoustic waves can be distinguished from each other by an examination of their dependence on various plasma parameters. By "free-streaming contributions" we imply both the small amplitude free-streaming mode and the large amplitude pseudo ion waves For example, for frequencies near ω_{pi}, ion acoustic waves are strongly Landau damped, while ballistic contributions and pseudo waves are easily observed for $\omega \sim \omega_{pi}$. Another important distinction is their parametric dependence on the electron temperature. The collective behavior driven by electron pressures is more sensitively dependent on T_e than the free-streaming behavior.

As we shall discuss in Volume III, when there is an electron drift of velocity comparable to the ion acoustic phase velocity, only the collective mode can grow spatially there are more electrons traveling faster than the wave than those traveling slower. The free-streaming contribution and the pseudo ion wave do not undergo any spatial growth at all as they are not dependent on resonant particles. This is an example of using an external free energy source to distinguish the collective ant

free-streaming contributions, These differences in parametric dependence are summarized in Table IV B-l.

TABLE IV B-1

Experimental differentiation between collective and free-streaming behaviors.

	ION ACOUSTIC WAVES	
	Collective Contribution	Free-streaming Contributi
Description	Ion density perturbation driven by electric field, which is caused by charge separation between ions and electrons.	Individual particles in perturbed distribution $f_1(v)$ free-stream at tl respective velocities from the sou the exciter
Dependence on T_e/T_i	Landau damping (wave particle interaction) decreases with increasing T_e/T_i. $V_p = \left(\frac{3KT_i + KT_e}{M}\right)^{1/2}$.	δ/λ does not depend on T_i or T_e/ Apparent v_p increases with T_i; $v_p = \frac{2}{\sqrt{3}} a_i \left(\frac{\omega x}{2a_i}\right)^{1/3}$.
ϕ Amplitude of exciter	V_p independent of ϕ in linear regime	V_p is independent of ϕ.
Effects of ion-ion collisions	Landau damping is decreased, because ion-ion collisions prevent wave-particle interaction.	Phase-mixing increases with ν_{ii}.
Addition of impurity ions traveling at v_{ph}.	Landau damping increased drastically.	Negligible change in damping.
Frequency range.	Waves cannot be observed near ω_{pi} because of severe Landau damping.	Observable near and above ω_{pi}
Methods of detections.	Best observed if electric fields are detected.	Best observed if ion current is de

δ/λ = damping distance normalized to the wavelenght

V_p = phase velocity

Appendix C: Damping of Ion Acoustic Waves in Presence of a Small Amount of Light Ions[12]

The collisionless interactions between ions and ion acoustic waves can be increased by the addition of a lighter ion species whose thermal velocity is close to the wave phase velocity in other words, the population of resonant ions can be controlled by varying the amount of light ions. If the amount of light ions is small, the wave phase velocity remains virtually the same, because the wave is carried by the bulk plasma. Theoretically the only addition to the dielectric constant in equation (A-13) is an imaginary term due to the newly added resonant ions: $-i\pi\,(\omega^{*}_{pi}{}^{2}/k^{2})\,f^{*}_{oi}(\omega/k)$ where the * quantities refer to the new species. Carrying out the same procedure as in Appendix A, we find

$$k_i = -\frac{\pi}{2}\frac{\omega_{pi}{}^{2}}{k_r}\left[f_{oi}'(\omega/k_r) + \frac{n^*}{n}\,\frac{M^*}{M}\,f_{oi}^{*\prime}(\omega/k_r)\right]$$

contribution of light ions

If both the background ions and the light species have Maxwellian distributions and are at the same temperature, then

$$k_i = \frac{\pi^{1/2}}{2}\frac{\omega}{a_i}\frac{\omega_{pi}^2}{\omega^2}\frac{T_e}{T_i}\left[\mathrm{Exp}\left(\frac{1}{2}\frac{T_e}{T_i}\left(1 - \frac{\omega^2}{\omega_{pi}^2}\right)\right) + \frac{n^*}{n}\left(\frac{M^*}{M}\right)^{1/2}\mathrm{Exp}\left(\frac{1}{2}\frac{T_e}{T_i}\frac{M^*}{M}\left(1 - \frac{\omega^2}{\omega_{pi}^2}\right)\right)\right]$$

contribution of light ions

The mass dependence in the exponential term can make the contribution of light ions to damping comparable to the background ions. For example, the addition of 3% Helium to an Argon plasma of $T_e/T_i \_ 10$ would approximately double the spatial damping rate. A qualitative picture of the two ion distributions together with the phase velocity is depicted in Figure IV C-l, which shows a larger number of lighter ions traveling near the wave velocity.

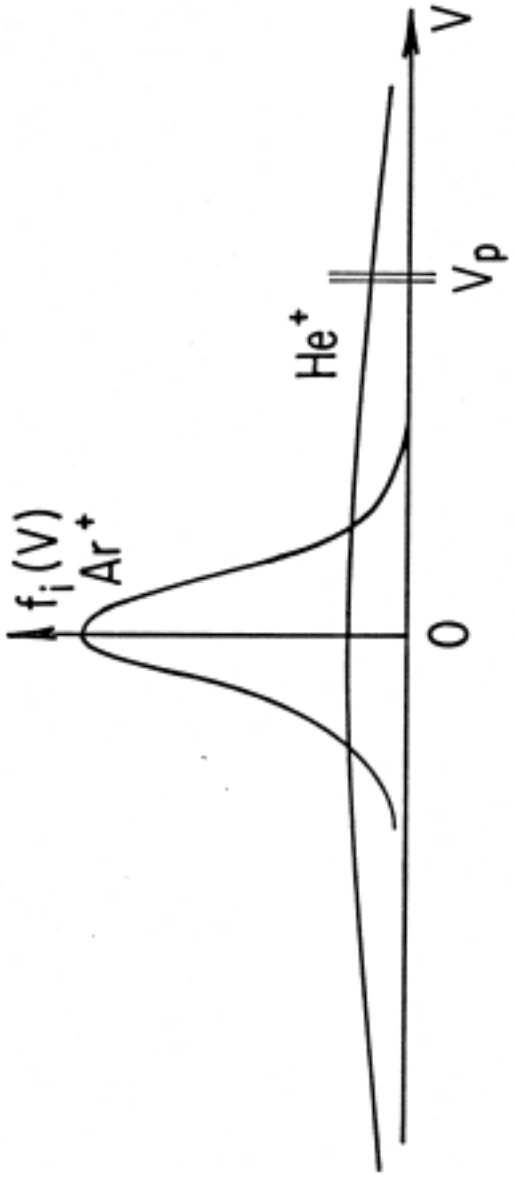

Figure IV C-1.

Appendix D: Ion Acoustic Shocks

This section deals with a nonlinear state[13,14] which develops when the amplitudes of density or potential perturbations become large ($e\phi/KT_e$ or $\Delta n/n_0 \geq 10\%$). It can be looked upon as a propagating discontinuity which separates two regions of different densities, potentials and temperatures. The propagating speed of this shock, v_s, is always greater than v_p of an ion acoustic wave and a Mach number $M = v_s/v_p > 1$ is associated with a shock of a given amplitude. We shall first point out the nonlinearity in a simple fluid treatment which is supplemented by a kinetic argument showing the importance of particle reflections from the shock front.

1) Theory

a) Fluid equations with nonlinear terms: In obtaining the linear dispersion [equation (3)] for ion acoustic waves using the fluid approximation, we have neglected the nonlinear term $v_i \frac{\partial v_i}{\partial x}$ in equation (1), the equation of motion for ions the inclusion of this term together with the equation of motion for electrons gives:

$$\frac{dv_i}{dt} = \frac{\partial v_i}{\partial t} + v_i \frac{\partial v_i}{\partial x} = \frac{1}{n} C_s \frac{\partial n}{\partial x} \qquad \text{(D-1)}$$

for $T_e >> T_i$ and negligible electron inertia at ion frequencies.

When the fluid density and velocity n, v_i are expressed as function of a single variable, u = x/t, a simple relation exists between them. Let us rewrite (D-l) in terms of this new variable u using the transformations $\frac{\partial}{\partial x} = \frac{1}{t}\frac{d}{du}, \frac{\partial}{\partial t} = \frac{u}{t}\frac{d}{du}$:

$$nu \frac{dv_i}{du} + nv_i \frac{dv_i}{du} + C_s^2 \frac{dn}{du} = 0 \qquad \text{(D-2)}$$

or

$$(u - v_i) dv_i = C_s{}^2 \frac{dn}{n}. \qquad \text{(D-3)}$$

A similar analysis of the equation of continuity for ions gives:

$$dv_i = (u - v_i) \frac{dn}{n}. \qquad \text{(D-4)}$$

Equations (D-3) and (D-4) have compatible solutions if $u = v_i \pm C_s$ is used in (D-2), and after integration one obtains:

$$v_i = C_s \ln \frac{n}{n_0} = C_s \frac{e\phi}{KT_e}. \qquad \text{(D-5)}$$

The Boltzmann distribution $n = n_0$ Exp (ef/KTe) has been used in the above expression. Equation (D-

5) states that the fluid velocity is proportional to the plasma potential or to ln (n/n0); in other words, the larger is the potential or density perturbation, the faster the local fluid element. As shown in Figure IV D-1a, a large amplitude ion wave can steepen to form a sharp front because the higher density or potential region travels faster.

ii) Second case: u = vi - Cs. The student can verify that this case does not give rise to a shock formation; instead a rarefaction wave is developed.

The student will observe in the laboratory that ion acoustic shocks maintain approximately constant shapes only over a rather limited distance on account of charge exchange collisions, plasma inhomogeneities, and other processes.

b) Ion reflections from the shock front: The plasma in which a shock travels is composed of ions of a range of velocities. Ions are reflected from the shock front if their relative velocities, v, with respect to the shock, are small enough such that 1/2 Mv2 £ qf0, where f0 is the potential jump in the shock, Figure IV D-1. Let us consider a frame moving with the shock speed vs in which the shock front appears stationary. Those background ions with v < vs in front of the shock will appear flowing toward the shock front, Figure IV D-1a, with a relative speed v' = vs - v. The ion distribution f(v') in the moving frame is depicted fin Figure IV D-1b which shows the range of velocities of ions to be reflected: 0 < v' < (2qf0/M)1/2. After reflection, ions move in a direction away from the shock front as shown in Figure IV D-1c. In the laboratory frame, these ions travel faster than the shock by the same amount as they were traveling slower before reflection. In the experiment, the student is expected to observe a density bump at the foot of the shock front as in Figure IV D-1c. An analysis of the velocity distribution at this bump will show a beam-like distribution consisting of faster ions. The percentage of fast ions observed experimentally could be checked against a theoretical estimate which integrates over the shaded velocity range of Figure IV D-lb, once the ion temperature and the shock speed v_s are measured. Since the number of reflected particles is a sensitive function of the location of $v_s \cong M(KT_e/M)^{1/2}$ with respect to the ion distribution, another experimental check of the theory can be made by measuring the number of reflected particles as a function of T_e/T_i.

c) Consequences of reflected ions: Ion reflections from the shock front result in a net extraction of energy from the propagating front. In a plasma with infrequent collision, this reflection process is the dominant dissipation process which leads to the formation of shocks (see the Sagdeev potential of Chapter 8 in Chen's book, "Introduction to Plasma Physics".)

Secondly, the beam-like distribution that is formed by ion reflections from the shock front can give rise to ion acoustic instabilities, similar to those in ion beam-plasma interactions. Ion wave turbulence has indeed been observed ln the shock front as a result of such interactions.[14]

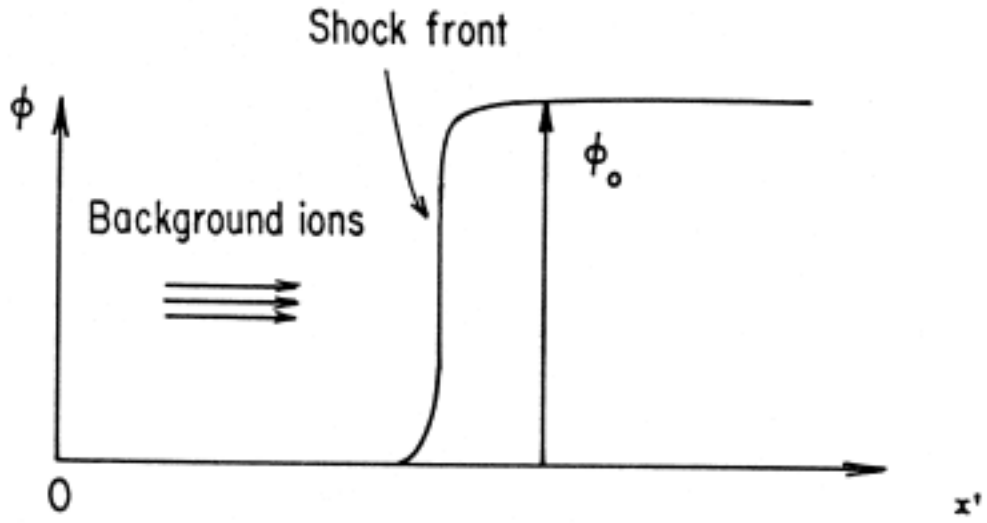

Figure IV D-1a.

In a frame moving with the shock from right to left, the potential jump in the shock appears stationary and the background ions traveling slower than the shock appear to be moving towards the shock front.

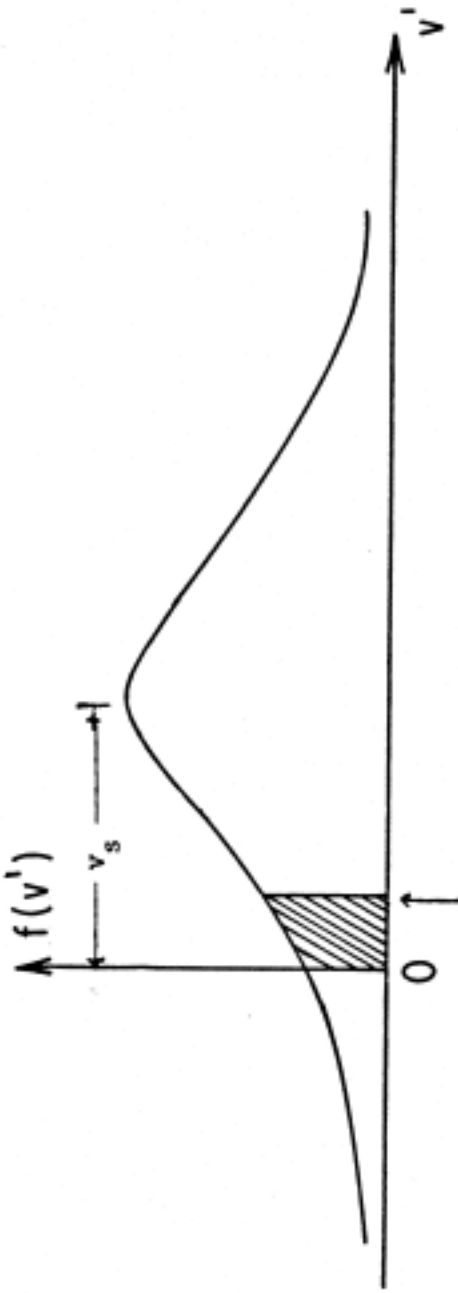

Figure IV D-1b.

Velocity distribution of background ions as seen in a frame moving with the shock speed v_s. The cross-hatched region represents the group of ions which will be reflected at the shock front.

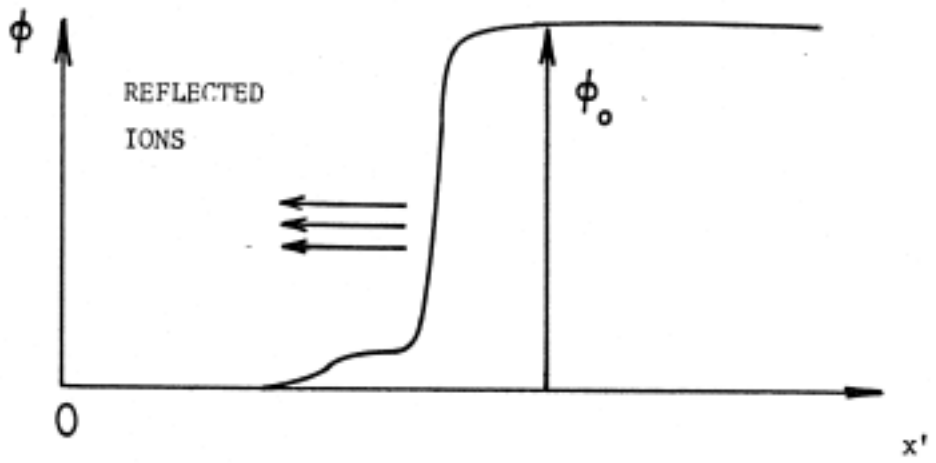

Figure IV D-1c.

Immediately after reflection at the shock front, the ions move in the -x' direction, appearing as a bump just in front of the shock.

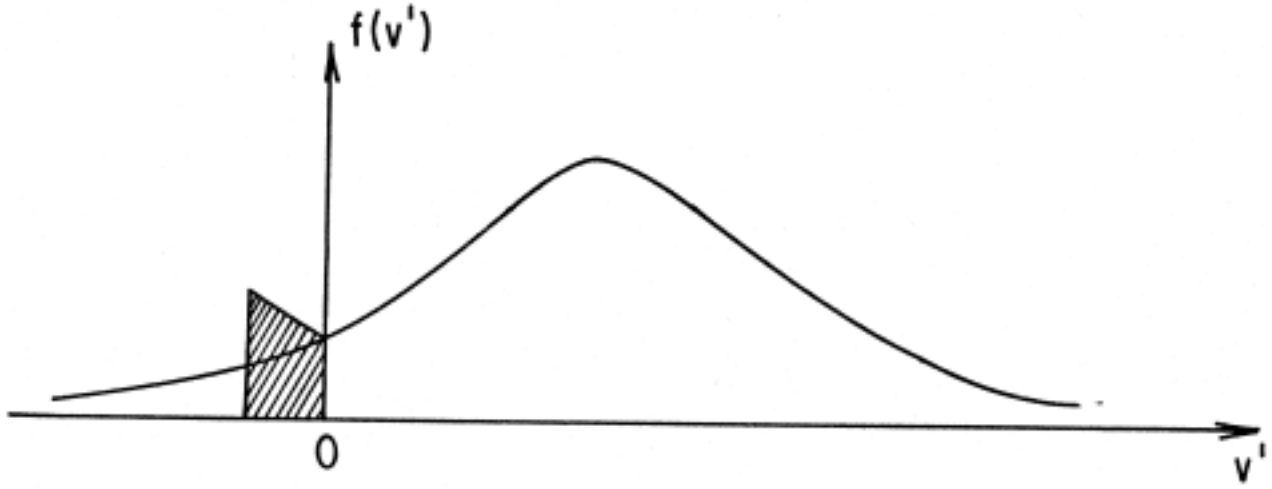

Figure IV D-1d.

Upon reflection from the shock, the ions reverse their directions, corresponding to a reflection of the cross-hatched region in Figure IV D-1b about the v' = 0 axis.

2) Experiment

Adapt the tone-burst configuration outlined in Figure IV-6 to set-up diagrammed in Figure IV D-2a. A long (~ 100 μsec) pulse is applied between the two chambers. The capacitor C_0 across the output of the pulser increases the rise time of the pulse so that a more gradual steepening of the ion acoustic disturbance can be observed. The following experiments are suggested.

a) Vary the amplitude of the applied pulse and observe the plasma response. Verify that for small density perturbations the response is linear --that is, the launched ion acoustic pulse has approximately the same shape as the applied pulse. How large does the density perturbation have to be before the edge of the pulse begins to steepen? Observe the plasma response for several values of initial density perturbations $\delta n/n$. Under the most optimum conditions, when the spatial steepening of the shock front can be clearly seen, record the evolution by making several exposures on one film.

b) Launch a small amplitude, linear ion acoustic tone burst and measure v_p. Then launch a shock and measure the shock speed, v_s, as a function of the shock density perturbation. Plot v_s vs. $\delta n/n$. find out the range of Mach numbers, $M = v_s/C_s$, that can be obtained in the experiment.

c) Observe the bump in front of the shock. record the characteristics of the shock, as a function of T_e/T_i, giving special attention to the bump just ahead of the shock. Use an ion energy analyzer and a sampling scope to record the distribution function at the location of this bump. Does the number of reflected particles and the shape of the distribution agree with the theoretical expectation? Be as quantitative as you can.

d) Record the characteristics of the wave-train trailing behind the shock front. Study Chapter 8 in Reference 2 and explain the wave train in terms of the Sagdeev potential.

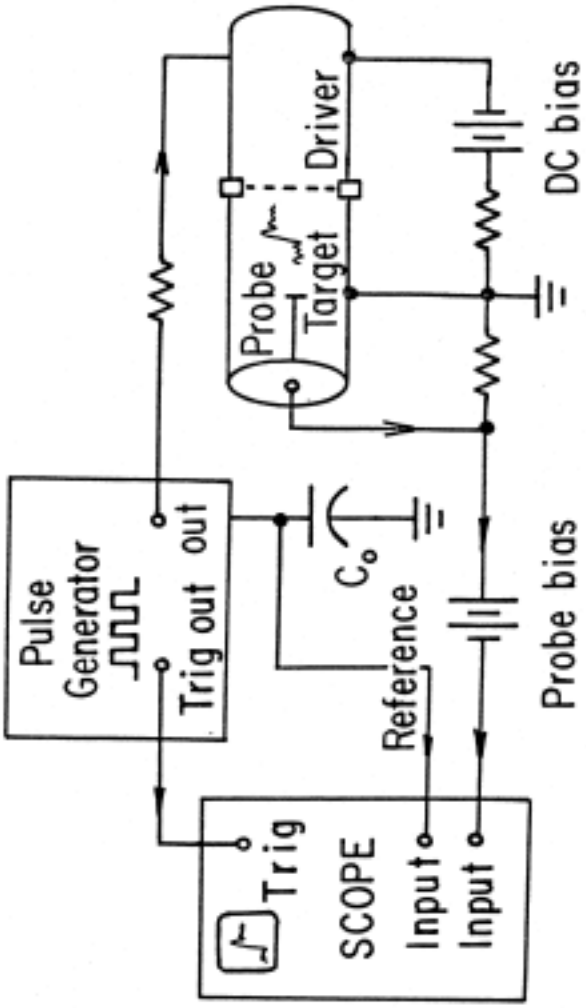

Figure IV D-2a.

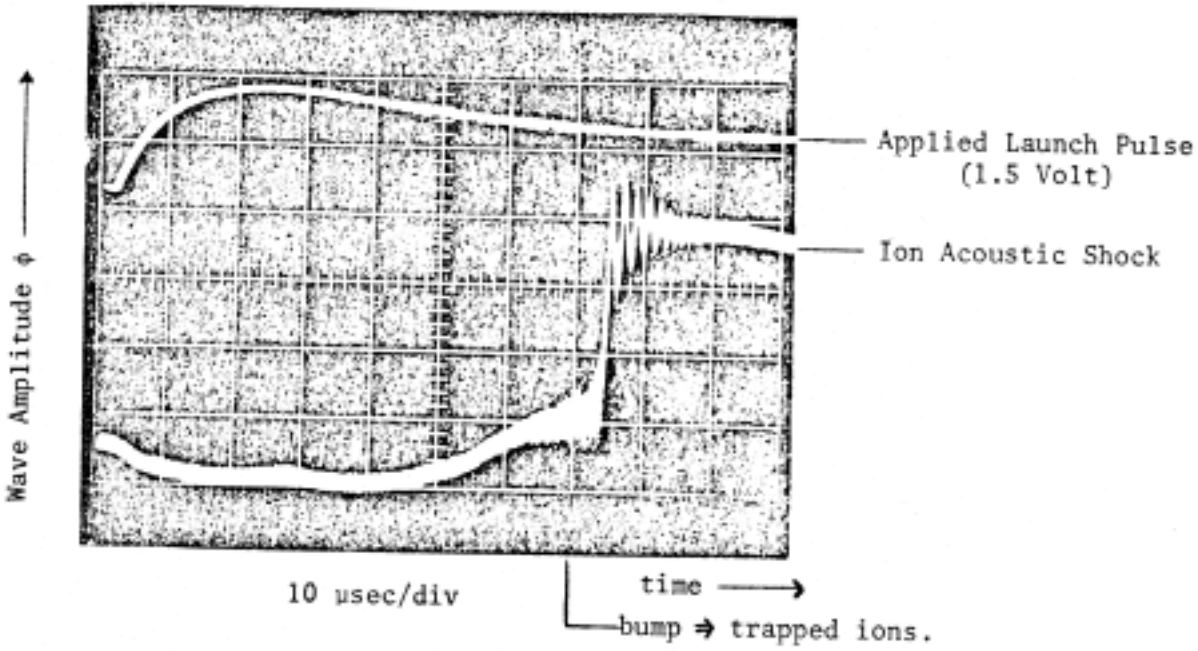

Figure IV D-2b.

Waveform of an ion acoustic shock. Observe the trailing wave train, the "foot" in front of the shock and the low level of turbulence.

Reference

1. L. Tonks and I. Langmuir, Phys. Rev. 33, 195 (1929).
2. J. D. Jackson, J. Nucl. Energy: Pt. Cl, 171 (1960); I. B. Berstein, E. A. Frieman, R. M. Kulsrud, and M. N. Rosenbluth, Phys. Fluids 3, 136 (1960); E. A. Jackson, Phys. Fluids 3, 786 (1960); I. B. Bernstein and R. M. Kulsrud, Phys. Fluids 3, 937 (1960).
3. B. D. Fried and R. W. Gould, Phys. Fluids 4, 139 (1961).
4. T. H. Stix, The Theory of Plasma Waves (McGraw-Hill Book Company, Inc., New York 1862), p. 132.
5. L. Landau, J. Phys. (USSR) 10, 25 (1946).
6. A. Y. Wong, R. W. Motley and N. D'Angelo, Phys. Rev. 133, A 436 (1964).
7. G. Sessler and G. Pearson, Phys. Rev. 162, 110 (1967).
8. V. O. jensen, Risö Rept. No. 54, Risö, Roskilde, Denmark, 1962 (unpublished).
9. The collisionless contribution by electron is treated theoretically in R. W. Gould Phys. Rev. 136, A991 (1964); and experimentally by A. Y. Wong, Phys. Rev. Lett. 14, 252 (1965).
10. A. Y. Wong, Phys. Fluids 2, 1261 (1966).
11. B. D. Fried and S. D. Conte, The Plasma Dispersion Function, (Acad. Press, New York, 1961).
12. I. Alexeff, W. Jones, and D. Montgomery, Phys. Rev. Lett. 19, 422 (1967).
13. R. Taylor, H. Ikezi and D. Baker, Phys. Rev. Lett. 24, 206 (1970).
14. A. Wong and R. Means, Phys. Rev. Lett. 27, 973 (1971).
15. T. E. Stringer, Plasma Physics 6, 267 (1964).
16. B. D. Fried and A. Y. Wong, Phys. Fluids 9, 1084 (1966).
17. N. Sato, H. Sugai, R. Hatakeyama, Phys. Rev. Lett. 34, 931 (1975).
18. D. R. Baker, Phys. Fluids 16, 1730 (1973).

Appendix E: Ion Beam-Plasma Interactions in a One Dimensional Plasma

We have seen that in a magnetic field free plasma, with $T_e >> T_i$, there exists a low frequency ($\omega < \omega_{pi}$) normal mode, the ion acoustic wave, with phase velocity

$$v_p = \omega/k = = \pm \frac{C_s}{\left(1 + k^2\lambda_D{}^2\right)^{1/2}}, \quad C_s \equiv (KT_e/M)^{1/2}.$$

If a cold ion beam with velocity v_b is injected into such a plasma, we find, in addition to the background ion modes, two ion beam modes. The dispersion relation for the four low frequency modes is given by the fluid theory as

$$\varepsilon(\omega, k) = 1 \frac{\omega_{pi}{}^2}{\omega^2} - \frac{\omega_{pb}{}^2}{(\omega \ kv_b)^2} + \frac{1}{k^2\lambda_D{}^2} = 0 \qquad \text{(E-1)}$$

or

$$1 + k^2\lambda_D{}^2 - \frac{n_i}{n_e}\frac{C_s{}^2}{v_p{}^2} \quad \frac{n_b}{n_e}\frac{C_s{}^2}{(v_p \quad v_b)^2} = 0 \qquad \text{(E-2)}$$

Exercise: Obtain equation (E-l) by treating the plasma as a three fluid system with $T_i = T_b = 0$ and proceeding in the spirit of the ion acoustic wave derivation given in Chapter IV.

The nature of the solutions of equation (E-2) will be discussed for two cases of interest, $v_b >> C_s$, and $v_b \sim C_s$.

1) Case 1: $v_b >> C_s$

If the beam velocity is much greater than the sound speed, the beam and background ions are not strongly coupled. The background ions support slightly modified ion acoustic waves and the berm ions support ion acoustic waves whose phase velocities are shifted by the beam velocity. The velocity distributions are sketched in Figure IV E-l.

For this case, approximate solutions to equation (E-2) may be obtained by making the assumptions outlined above, to be justified a posteriori. A second order equation for the background ion modes may be obtained from (E-2) by neglecting v_p ($<< v_b$) in the last (beam ion) term, yielding the solutions:

$$v_p = + \frac{(n_i/n_e)^{1/2} C_s}{\left(1 + k^2\lambda_{De}{}^2 \frac{nb}{n_e}\frac{C_s{}^2}{v_b{}^2}\right)^{1/2}} = \pm \; C_s{}^{\copyright} \qquad \text{(E-3)}$$

To obtain approximate solutions for the beam modes, a simple transformation to the beam frame yields an equation similar to (E-2) but with the roles of n_i and n_b interchanged. The solution is:

$$\left(v_p - v_b\right) = \pm \frac{(n_b/n_e)^{1/2} C_s}{\left(1 + k^2\lambda_D{}^2 - \frac{n_i}{n_e}\frac{C_s{}^2}{v_b{}^2}\right)^{1/2}} \qquad \text{(E-4)}$$

We see that the background ion modes no longer propagate with speed C_s, but with reduced speed $Cs' \sim (n_i/n_e)^{1/2} C_s$. The acoustic waves carried by the beam are similarly modified. A full kinetic treatment of the problem reveals that all four modes are weakly damped by ion Landau damping when $T_e >> T_i$ and $v_b >> c_s$.

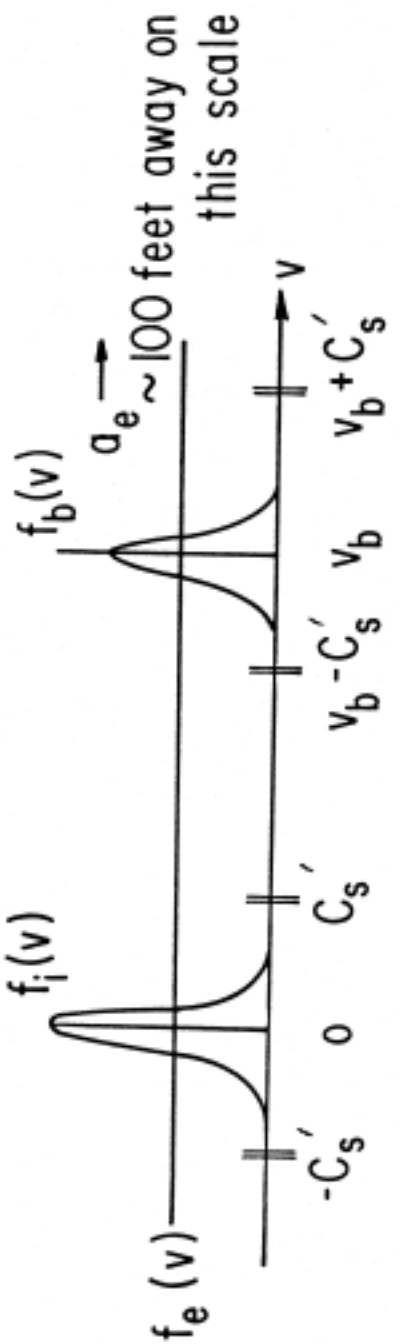
$f_e(v)$
$f_i(v)$
$f_b(v)$
$a_e \longrightarrow$ ~ 100 feet away on this scale
v
$-C_s'$
0
C_s'
$v_b - C_s'$
v_b
$v_b + C_s'$

Figure IV E-1.

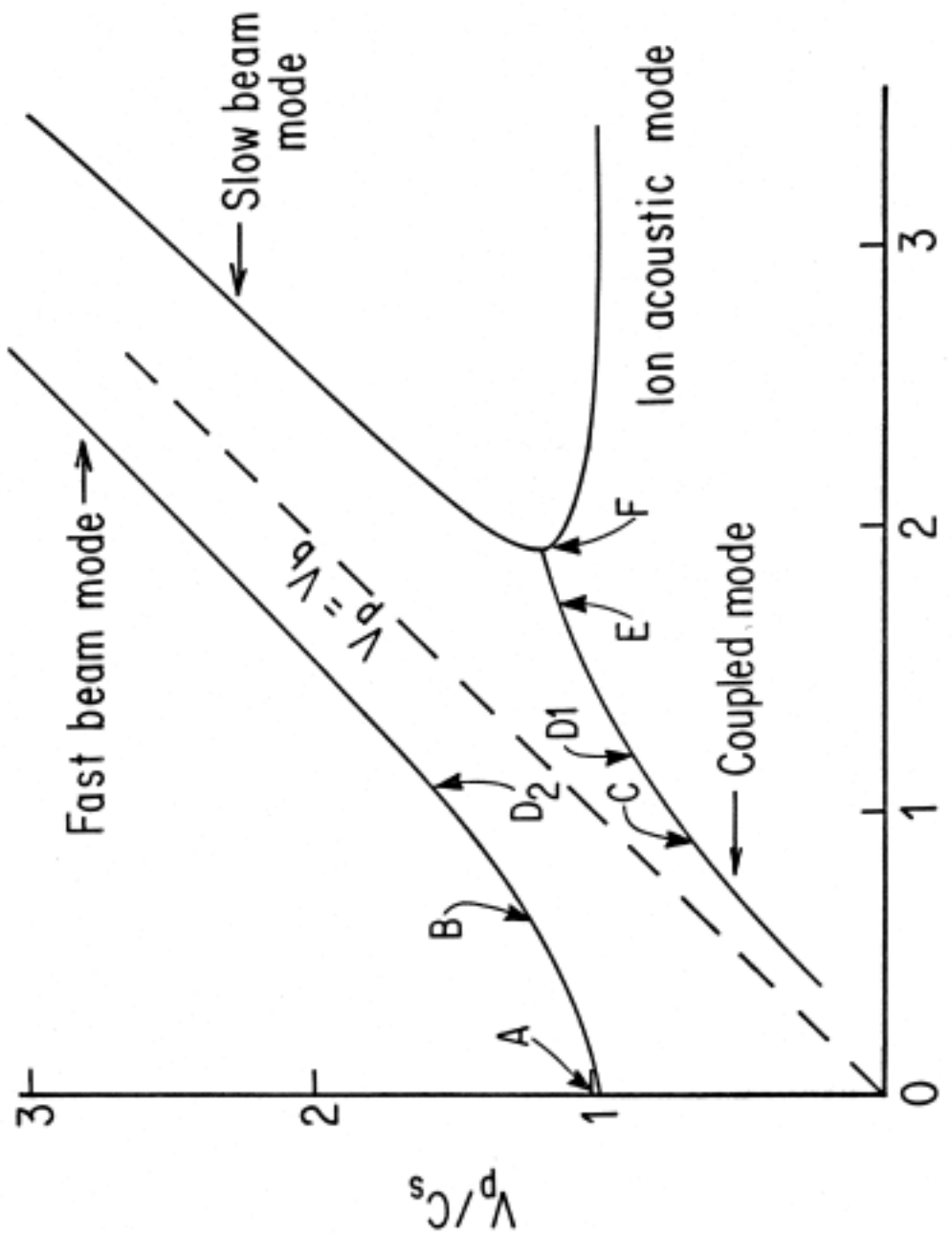

Figure IV E-2
Phase velocities of low frequency normal modes in an ion beam-plasma system as a function of beam velocity. Lettered points are referred to in Figure IV E-5.

2) Case 2: $v_b \sim C_s$

When the beam velocity is approximately equal to the sound speed, the beam and background ions are strongly coupled. An unstable ion wave grows by absorbing free-streaming energy from the beam ions. This "ion-ion instability" is a member of the important class of electrostatic two stream instabilities,[15] which arise whenever a relative drift exists between two plasma components.

Figure IV E-2 illustrates typical results of a numerical solution of the ion beam plasma dispersion relation derived from fluid theory, including the finite ion temperature. For $v_b > 2C_s$, the fast and slow beam modes and the background ion acoustic wave discussed under case 1 appear. For beam velocities below about twice the sound speed, $0.7\ C_s \leq v_b < 2C_s$, the slow beam wave and the background wave couple to form an unstable wave with a finite growth rate. The fast mode continues to exist in a stable form.

The lower limit of $v_b \_ 0.7\ C_s$ for the instability is a finite ion temperature effect the system becomes stable when the beam and background ions overlap sufficiently in velocity space. Below this limit the fluid theory is no longer adequate for the coupled mode with phase velocities $0 < v_p < v_b$ kinetic theories,[2,16] which take into account wave particle interactions, show that this mode is strongly Landau damped.

3) Experiment 1 - Observation of Beam Ion Acoustic Waves

In this experiment we shall observe the fast and slow beam waves discussed under Case 1 ($v_b >> C_s$) in the theory section. The double plasma device is adjusted to obtain a beam in the target chamber, $v_b >> C_s$, and small-amplitude test waves are launched by varying the potentials between the two chambers or by applying modulation to the separation grid. This excitation launches both fast and slow beam waves so the tone burst method (described earlier in the chapter) must be used to separate the responses. The two modes, traveling with different velocities, will become separated in space away from the excitation point.

We may compute the propagation distances for complete separation of the responses, referring to Figure IV E-3. A tone burst of length τ occupies a spatial extent $\Delta x = v_b\tau$.

The responses will be fully separated when the distances x_f and x_s travelled by the fast and slow modes are separated by Δx:

$$x_f - x_s = v_b\tau$$

which occurs in a time τ,

$$v_f t - v_s t = v_b\tau$$

$$t = \frac{v_b}{v_f - v_s}\tau = \frac{v_b\tau}{2(n_b/n_e)^{1/2}C_s}$$

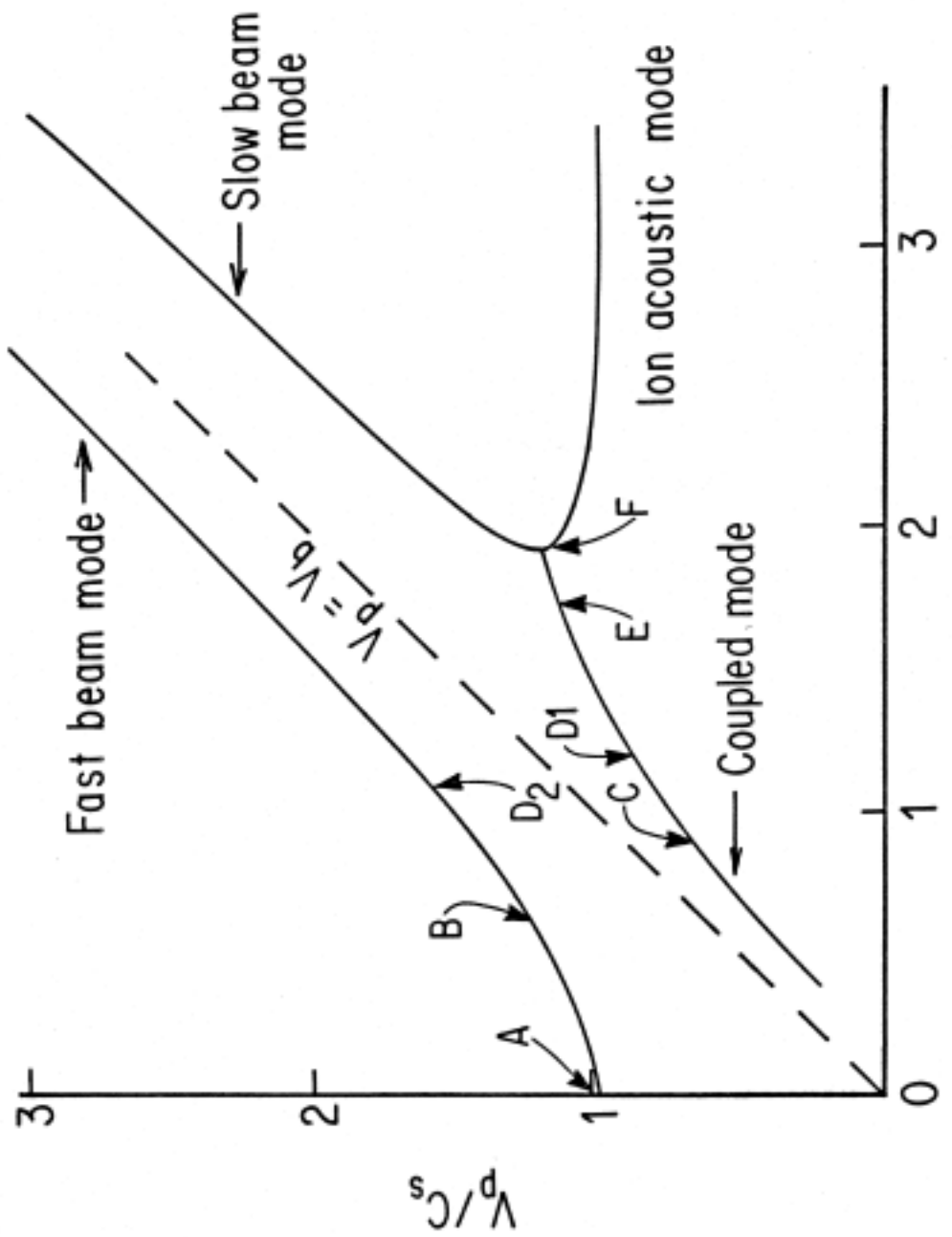

Figure IV E-2
Phase velocities of low frequency normal modes in an ion beam-plasma system as a function of beam velocity. Lettered points are referred to in Figure IV E-5.

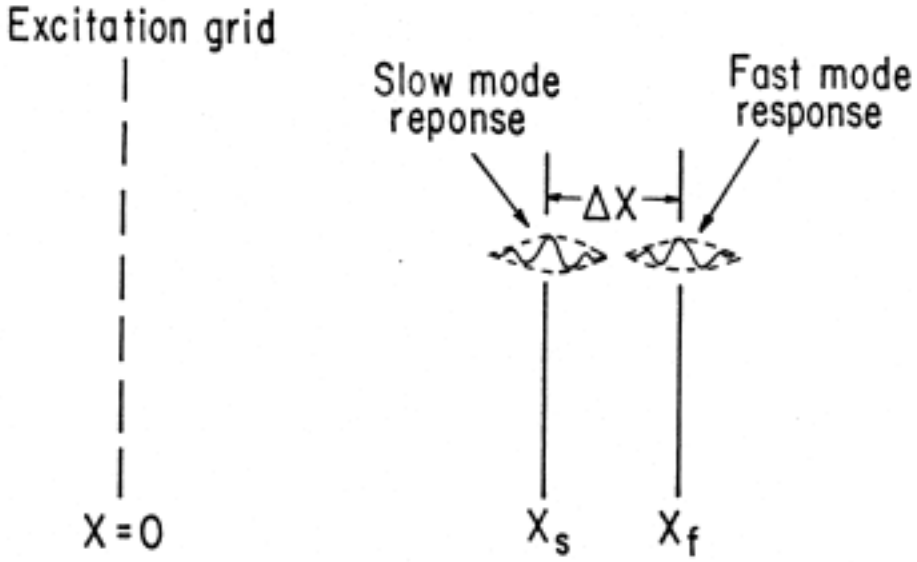
Excitation grid
Slow mode
reponse
Fast mode
response
ΔX
X=0
X_s
X_f

Figure IV E-3.

where the subscripts f and s refer to the fast and slow modes, respectively.
Thus the beam travels a distance

$$x = v_b t = \frac{v_b^2 \tau}{2(n_b/n_e)^{1/2} C_s}. \qquad \text{(E-5)}$$

Examination of (E-5) reveals the optimum experimental conditions for the identification of the two beam modes:

a) τ short: Use a tone burst of a few cycles try one or two cycles at 400 kHz, or even a pulse.

b) n_b large: Adjust the source and target chambers to obtain the maxi-mum beam density.

c) v_b small: Choose $3C_s \leq v_b \leq 5C_s$ to satisfy our criterion of a fast beam.

The beam waves will be strongly damped if the beam is scattered by ion neutral collisions, so the neutral pressure should be kept as low as possible, preferably below 10^{-4} torr.

An example of tone burst detection of fast and slow beam waves and the background ion acoustic wave is shown in Figure IV E-4. Note that the beam waves are much more weakly damped than the ion acoustic waves. The student should compare his beam wave observations with the ion acoustic wave observations made in a previous experiment. Relate the damping rates to the observed background and beam ion temperatures.

The two beam modes may also be observed by interferometry using our excitation signal as a reference. The two waves, with wave numbers k_1 and k_2, form a spatial beat pattern.[3,17]

4) Experiment 2 - Ion-ion Two Stream Instability[18] (v_b _ C_s)

The purpose of this experiment is to study some of the characteristics of the ion-ion two stream instability. Stability limits and growth rates will be determined by the test wave method. The student should thoroughly understand the results of the ion acoustic wave and energy analyzer experiments before attempting this experiment.

Set up the DP device for the interferometric observation of ion acoustic waves. A CW signal source is used to apply an excitation to the separation grid. Position the energy analyzer about 3 cm from the separation grid and adjust the source chamber potential to obtain a beam of energy about 10 V. Set the beam current to about one-tenth the background ion current by adjusting the source and target chamber densities.

Now readjust the beam energy to zero by varying the potential of the anode and obtain the propagation of an ion acoustic wave in the absence of a beam as a reference.

Apply a CW excitation signal at 1/3 the ion plasma frequency and obtain an interferometer trace by moving the Langmuir probe (biased above the plasma potential) axially starting at the separation grid. The excitation amplitude should be kept as small as possible to avoid nonlinear

effects. An excitation amplitude of 10 - 500 mV_{pp} should be sufficient. This interferometer trace should indicate the presence of a damped ion acoustic wave.

Increase the beam energy in steps of 0.25 V or less taking an interferometer trace at each step. The student should look for the smooth transition (as a function of beam energy) of the ion acoustic wave to the fast beat wave (refer to Figure IV E-2) and for the appearance of the spatially growing wave.[1] Continue increasing the beam energy until the instability is no longer observed. An example of interferometer traces in the range of beam energies $0 < E_b < 7$ V is given in Figure IV E-5.

Plot the observed phase velocities and the damping or growth rates as a function of beam velocity. Compare your results to Figure IV E-2 or to the experimental or theoretical results presented in references 16 and 18.

5) Other Suggested Experiments

a) Spontaneous noise behavior: In the absence of a test wave, spontaneous density fluctuations in the unstable frequency range ($\omega \leq \omega_{pi}$) will grow in the direction of beam propagation. Obtain unstable beam conditions and measure the spatial growth rate and saturation amplitude of the noise by biasing the Langmuir probe above the plasma potential and measuring the ac probe current fluctuations. If a spectrum analyzer is available, the frequency dependence of the noise behavior may be studied.

c) Ion velocity distribution: As the unstable waves grow, absorbing energy from the beam, the beam particles are slowed down. The beam spreads in velocity space and eventually merges with the background ions, saturating the instability. Use the energy analyzer to study the spatial development of the ion distribution as a function of distance from the beam injection point (separation grid). Correlate the behavior of test waves or noise with the modification of the distribution. Reference 18 is highly recommended in connection with this experiment.

d)

---

[1]Note: The excitation amplitude should be substantially reduced when observing the unstable wave to prevent nonlinear saturation of the wave and resulting erroneous measurement of the growth rate.

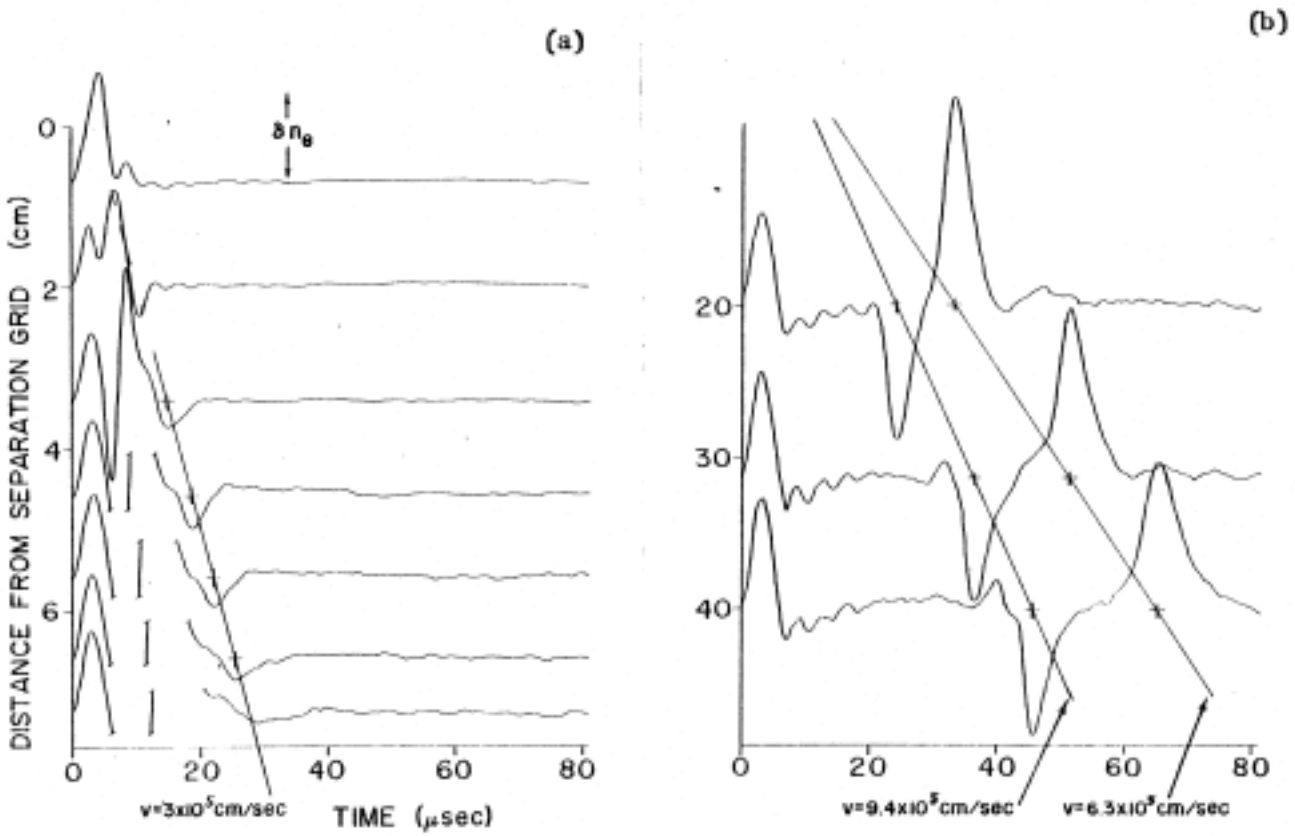

Figure IV E-4

"Tone burst" observation of ion acoustic wave and fast and slow beam waves. A one volt, 4 μsec pulse was applied to the separation grid and the resulting density fluctuations measured with a Langmuir probe. The probe signal as a function of time at distances from 0 to 8 cm from the grid is shown in a), illustrating the ion acoustic response. Probe signals at 20, 30, and 40 cm are given in b), showing fast and slow wave responses. The "direct coupled" response is visible in all traces, near t = 0.

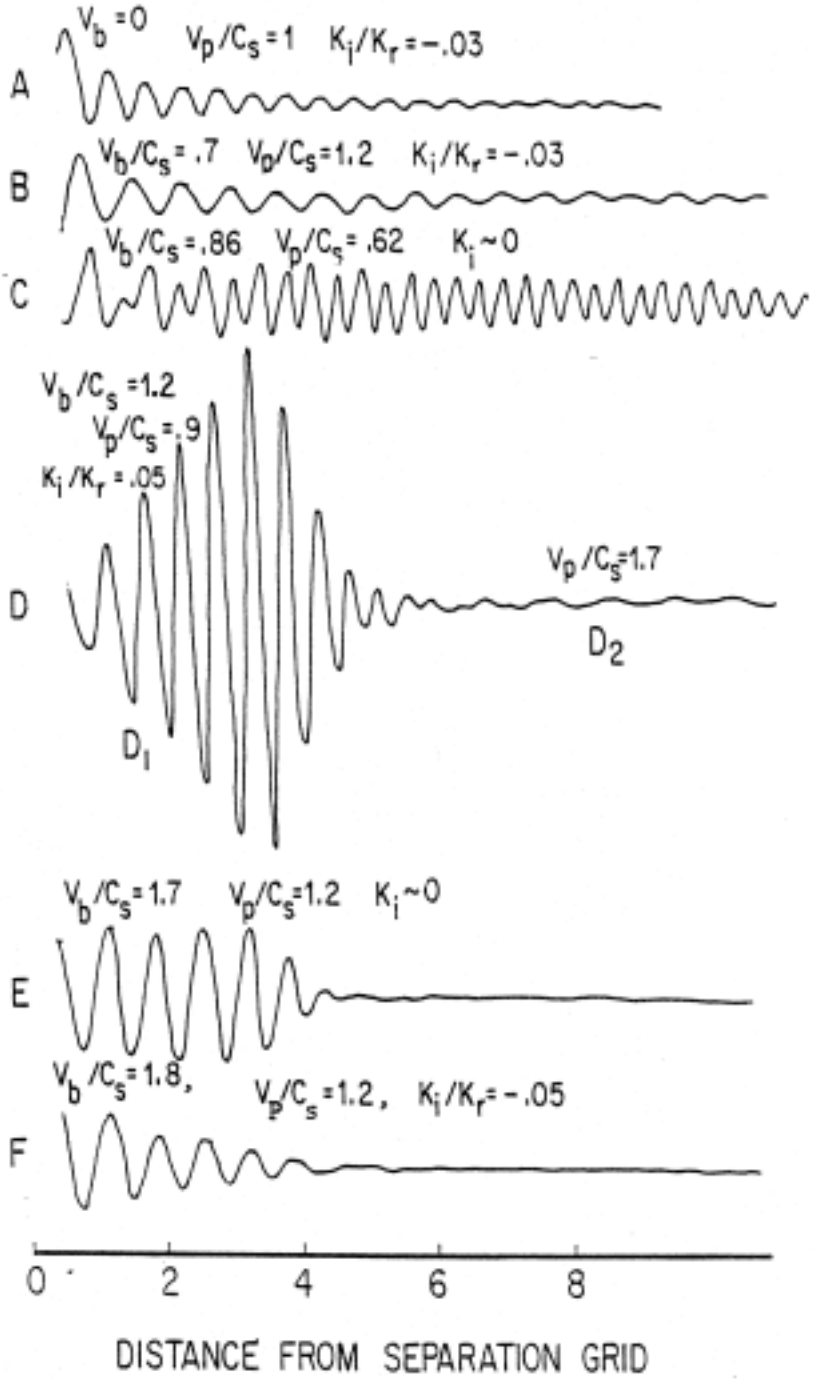

Figure IV E-5

Interferometer traces at various beam velocities from $v_b = 0$ to $v_b = 1.8\ c_s$. A 400 KHz cw, 50 mV_{pp}, excitation signal was applied to the separation grid. Beam velocity was measured with an energy analyzer. Approximate position of each trace in a plot of phase velocity versus beam velocity is indicated in Figure IV

Chapter V. Electron Plasma Waves

1) Introduction

The electron plasma density oscillation is one of the most fundamental excitations in plasmas. In the simplest approximation it is driven by electric fields caused by displacements of electrons from the background ion distribution. Although it is easy to derive this mode theoretically for uniform plasmas (is the dispersion) the experimental verification of the simple theoretical formulation is a rather difficult task. The electric field arising from the out-of-phase motion between electrons and ions in electron plasma waves (hereafter referred to as EPW) is significantly larger than that in ion acoustic waves in which ions and electrons move in near synchronism. This electric field makes the $\omega^2 = \omega_p^2 + 3k^2\overline{v}_e^2$ wave characteristics very sensitive to the radial boundary conditions or how the E-field is terminated at the wall. Wave reflections at the wall set up radial modes which complicate the subsequent analysis.

Secondly, the collective behavior of electrons depends on the plasma density. The propagation of EPW is very sensitive to the density profile or any local density perturbation, created by probes for example. These considerations require a large plasma in which a good density uniformity is maintained in the propagation region. In addition caution must be exercised in the excitation and detection of these waves since the probe sheath itself, a density and potential inhomogeneity, might play a significant part in the data, again making a straight forward interpretation impossible. Special diagnostics, such as a collimated electron beam, are used to measure the absolute amplitude of these waves, as an independent check on the conventional probe diagnostics.

EPW can be excited along with free steaming modes at the excitation source. Electrons streaming through a grid to which the excitation signal is applied can be modulated to form free-streaming modes which propagate at the streaming velocity. If the excitation signal is large bursts of electrons are generated at the grid similar to the ballistic mode discussed in Chapter IV.

The experiments described in this chapter are designed to excite the collective mode, commonly discussed in basic theories, while avoiding the other modes which can be excited at the source. It is hoped that the experimental results thus achieved will be sufficiently universal in character to be relatively independent of the characteristics of the particular experimental device used. In the following an experimental method is described which emphasizes the excitation of the collective mode and which produces waves in a region many wavelengths from the exciter.

Our experimental method takes advantage of the fact that among the possible electron modes which can be excited by $(e\phi_{ex} >> kT_e)$ the grid, only the collective mode can grow spatially in the presence of the electron beam, Free-streaming and ballistic modes decrease in amplitude as they move away from the source as a result of phase-mixing among particles of different velocities; the spatial phase of each velocity class varies according to exp (i ϖ/ψξ). It will be shown that the most unstable waves have frequencies and wave numbers near the intersection of the dispersion curves (Figure V-1) for uniform plasmas $\left(\omega^2 = \omega_{pe}{}^2 + 3kT_e/mk^2\right)$ and electron beams $(\omega = kv_D)$. for such spatially growing modes a very small excitation signal can be used and the detector placed well away from the exciter, thereby reducing the direct coupling between the exciter and receiver. In the plasma proper where the density profile has the highest uniformity, we can measure the EPW wavelengths and amplitudes using the interferometry technique and compare the results with the predictions of the theory of EPW in a spatially uniform plasma.

2) Theory of Electron Plasma Waves in the Presence of an Electron Beam

The one dimensional dispersion relation governing the propagation of Electron Plasma Waves (EPW) in a uniform plasma has been derived in many texts[1] and given by

$$\omega^2 = \omega_{pe}^{\ 2} + 3k^2\bar{v}_e^{\ 2}$$

To treat growth or damping of EPW in the presence of an electron beam we must resort to kinetic theories which include the interaction of the beam with the waves. One such kinetic description has been given by O'Neil and Malmberg[2] who started with the one dimensional dispersion relation for a beam-plasma (assuming stationary ions)

$$1 + \left(\frac{\omega_{pe}}{k}\right)^2 \int_{-\infty}^{+\infty} \frac{k\left(\frac{\partial f_e}{\partial v}\right)dv}{(\omega - kv)} + \frac{n_b}{n}\left(\frac{\omega_{pe}}{k}\right)^2 \int_{-\infty}^{+\infty} \frac{k\left(\frac{\partial f_b}{\partial v}\right)dv}{(\omega - kv)} = 0 \tag{1}$$

where f_e and f_b are the background and beam electron velocity distribution functions respectively, (n_b/n) is the ratio of the beam and background plasma densities, and all first order quantities are assumed to vary as exp [i (kx- ϖt)].

To proceed with this theory we assume a Maxwellian distribution for the background electrons and a Lorentzian distribution for the beam electrons[3]. Equation (1) then gives for our dispersion relation

$$\varepsilon_p(k,\omega)\left[\omega - kv_D + ik\bar{v}_b\right]^2 = \left(\frac{n_b}{n}\right)\omega_{pe}^{\ 2} \tag{2}$$

where $\varepsilon_p(k,\omega)$ is the background plasma dielectric function

$$\varepsilon_p(k,\omega) = 1 + \left(\frac{\omega_{pe}}{k}\right)^2 \int_{-\infty}^{+\infty} \frac{k\left(\frac{\partial_{fe}}{\partial_v}\right)dv}{(\omega - kv)}$$

and $v_D \equiv$ beam drift velocity, $\bar{v}_b \equiv$ beam thermal spread.

In the following we shall treat a variety of beam plasma interactions ranging from a very fast beam with a relatively small thermal spread (cold beam) to a slow beam with a broad thermal spread (warm beam). In our discussion we will restrict ourselves to the weak beam limit, $(n_b/n) << 1$. In this limit we can separately treat three cases according to equation (2):

(i) $\varepsilon_p(k,\omega) \approx 0,\ |\omega - kv_D + ik\bar{v}_b| >> 1$

---

1 Chen, F., Introduction to Plasma Physics.

2 O'Neil and Malmberg, Phys. Fluids 11, 8 (1968), p.1756.

3 $f_0 = (\ _e)^{-1} \exp(-v^2/\ _e^2)$, $f_v = \ _b/\ [(v-v_D)^2 + \ _b^2]^{-1}$

(ii) $\left|\varepsilon_p(k,\omega)\right| >> 1,\ (\omega - kv_D + ik\bar{v}_b) \approx 0$

(iii) $\varepsilon_p(k,\omega) \approx 0$ and $(\omega - kv_D + ik\bar{v}_b) \approx 0$

(i) If $\varepsilon_p(k,\omega) \approx 0$ and $\left|\omega - kv_D + ik\bar{v}_b\right| >> 1$, equation (2) describes an EPW propagating in the background plasma according to the uniform plasma dispersion relation with phase velocity ϖ/k very different from the beam drift velocity v_D. This wave is unaffected by the presence of the electron grow since it does not couple to the free energy carried by the electron beam.

(ii) If $\varepsilon_p(k,w) \approx 0 \, and \, |\omega - kv_D + ik\bar{v}_b| >> 1$, we have a beam mode traveling near the beam velocity whose propagation characteristics are very different from the EPW in (i). Solving equation (2) for k, we obtain

$$k = \frac{\omega \pm \omega_{pe}\left(\frac{n_b}{n}\frac{1}{\varepsilon_p}\right)^{1/2}}{\left(v_D{}^2 + \bar{v}_b{}^2\right)}(v_D + i\bar{v}_b)$$

Writing

$$\alpha \equiv \left(\frac{n_b}{n}\frac{1}{\varepsilon_p}\right)^{1/2} << 1, \text{ we have}$$

$$k_r = \omega v_D \frac{\left(1 \pm \frac{\omega_{pe}}{\omega}\frac{\bar{v}_b}{v_D}|\alpha|\right)}{(v_D{}^2 + \bar{v}_b{}^2)}$$

$$k_i = \omega v_D \frac{\left(\frac{\bar{v}_b}{v_D} \pm \frac{\omega_{pe}}{\omega}\right)|\alpha|}{(v_D{}^2 + \bar{v}_b{}^2)}$$

for $\left|\varepsilon_p\right| >> 1,\ \varepsilon_p < 0$.

For our choice of notation on (exp [i(kx- ϖt)]) spatial growth of the waves occurs when $k_i < 0$. Thus the cold beam case $\left(\bar{v}_b / v_D \approx 0\right)$ yields weakly growing waves with

$$\frac{k_i}{k_r} = -\left(\frac{\omega_{pe}}{\omega}\right)|\alpha| = -\left(\frac{\omega_{pe}}{\omega}\right)\left(\frac{n_b}{n}\frac{1}{|\varepsilon_p|}\right)^{1/2} << 1.$$

(iii)

We have seen that the two modes $\varepsilon_p \approx 0$ and $\left(\omega - kv_D + ik\bar{v}_b\right) \approx 0$ taken separately either under go damping or do not grow significantly. If we wish to excite a mode which is easily observed experimentally we must look for a mode which exhibits strong growth. Such a mode corresponds to the third case, $\varepsilon_p \approx 0,\ \left(\omega - kv_D + ik\bar{v}_b\right) \approx 0$ where the phase velocity of the beam

mode matches the phase velocity of the EPW of the background plasma as depicted in Region A of Figure V-1. The solution of the dispersion relation [equation (2)] for this case can be obtained by Taylor expansion in the region A about the intersection point (ω_o, k_o), (see Appendix 1). In this derivation a dimensionless parameter *s* has been found useful in describing the entire range from warm to cold beams.

$$\text{S = scaled thermal speed} = \frac{\bar{v}_b}{v_D}\left(6\frac{n}{n_b}\frac{\bar{v}_e^{\,2}}{v_D^{\,2}}\right)^{1/3}$$

The cold beam case is represented by $s \approx 0$ and the warm beam case by $s \geq 0$.

For comparison the qualitative behaviors of the solutions of the dispersion relation for the limiting cases of warm and cold beams s=2, s=0, have been plotted in Figure V-2. (s=2 is considered a limiting case since the numerical results are essentially unaltered when s exceeds this value.) The regions where spatial growth takes place are cross hatched. The physical significance of these two results will be explained in the following sections.

3) Physical Pictures of the Beam-Plasma Instability

Although it is difficult to describe a physical picture which is generally applicable to the beam plasma instability it is possible to understand the physical mechanism of the instability in two limiting cases corresponding to cold and warm beams.

The parameter *s* which characterize the beam conditions can be varied in several ways. We will, however, concern ourselves with constant but small beam density $n_b / n << 1$, constant beam $\bar{v}_e / v_D$ and assume that s has variations due only to changes in the thermal spread, $\bar{v}_b / v_D$.

Warm Electron Beam

Figure V-2a summarizes graphically the numerical results obtained from the solution of equation (2) for a warm beam. The warm beam-plasma instability corresponds to the picture of inverse Landau damping. When a wave has a phase velocity v_p less than the beam drift velocity, v_D, there are more beam electrons with v > v_p than with v < v_p (since the beam distribution function has a positive slope for $v < v_D$, see Figure V-3). There is a net transfer of energy from the beam to the wave which then grows. This situation is also described in figures V-1 and V-2a: on the curve $\varepsilon_p(k,\omega) = 0$, points with $\omega > \omega_o$ correspond to waves with phase velocity $v_p = \omega / k < v_D$ which are calculated to be growing waves according to equation (2).

Cold Electron Beam

For a very cold electron beam we take the beam thermal spread $\bar{v}_b = 0$ and write equation (2) as

$$\varepsilon_p\left(\omega - kv_D\right)^2 = \frac{n_b}{n}\omega_{pe}^{\,2}$$

or

$$k = \frac{\omega}{v_D} \pm \frac{\omega_p}{v_D}\left(\frac{n_b / n}{\varepsilon_p(k,\omega)}\right)^{1/2}$$

Since the Fourier components of the electric field have been assumed to vary as exp [i (kx - ϖt)], spatial growth will occur if k has a negative imaginary part corresponding to $\varepsilon_p(\omega, k) < 0$.

Referring to Figure V-4 we can understand the physical mechanism for the cold beam

plasma interaction as follows:

In the beam frame beam electrons in a density trough will experience a stationary electric field due to the bunched electrons on both sides of the trough. If there is no background plasma the vacuum electric field, E_{vac}, will be such that electrons in the trough feel a force $F = -eE_{vac}$ which is repulsive and tends to keep them in the trough. However, in the presence of a background plasma characterized by the dielectric function ε_p the total field seen by the beam electrons is $E_T = E_{vac} / \varepsilon_p$. If ε_p is negative E_T is opposite to E_{vac} in direction the electrons are expelled from a trough causing further bunching of electrons at each side of a given trough. Therefore, the initial perturbation on the beam grows under the condition that the dielectric function of the background plasma is negative.

4) Experimental Apparatus

The experimental apparatus used for the study of EPW is the double gridded double plasma (D.P.) chamber as shown in figure V-5.

In the D.P. device, the source and target plasmas are independently produced in separate chambers by primary electron bombardment of a neutral gas. The potentials are arranged in such a way as to cause the target plasma to be at a positive potential with respect to the source plasma. The target chamber wall and grid 2 are grounded. The source chamber grid (grid 1) is biased negatively at $-V_{bias}$ with respect to grid 2. This negative bias on grid 1 inhibits the flow of electrons from the source to the target chamber, thus permitting the establishment of two different plasma potentials in the source and target plasmas. The wall of the source chamber is not anchored to any external DC potential; it adopts a negative potential with respect to the source plasma potential because electrons are lost to the wall at a faster rate than ions. The source plasma then has a positive potential with respect to the wall and grid 1 but is negative with respect to the target plasma. The resulting potential profile as depicted in Figure V-5b accelerates electrons from point A to point B, creating an electron beam for our experiment. It should be pointed out that only the tail of the source electron distribution can overcome the negative potential barrier at A and is then accelerated in the region between the grids to B.

The drift velocity, v_D, of the beam is controlled by varying the voltage bias between the grids. The ratio n_b / n can be changed either by varying the target plasma density, n, or by indirectly varying the beam density, n_b, through variations in the source plasma density. The thermal spread $\bar{v}_b$ of the beam is controlled by both the source temperature and the drift velocity (or the bias V_{bias}). The reduction of the thermal spread with increased drift velocity is the same as described in Appendix A of Chapter II.

Typical operating parameters are: $n_o \approx 10^8 - 10^9$ cm^{-3}, $v_e \sim (KT_e/m)^{1/2} \sim 6 \_ 10^7$ cm/sec, $n_b / n \sim$(5-10) % and $v_D / v_e \sim$(5-10), $\bar{v}_b / v_D \sim$10-50%. The plasma frequency lies in the convenient range of 100-300 MHz where the standard laboratory test equipment is available.

As we have seen in the physical pictures, the beam-plasma instability is initiated by modulating the beam density and thereby creating the associated spatially oscillating potential along the beam. Experimentally this is achieved by applying an oscillating voltage of the desire frequency in addition to the DC bias between the grids. The RF and DC voltages are independently applied to a grid signal mixer (GSM) which in turn applies the combined signal to the grid. The function of the GSM is to provide isolation between the DC and RF supplies. The typical applied RF signal strength is 0.1 V peak-to-peak and in general should be as small as possible in order to avoid ballistic modes produced at the excitation grid.

5) Diagnostics

Three diagnostics are used in this study of EPW. They are the two-sided Langmuir

probe, the RF pickup probe, and the diagnostic electron beam. The two-sided Langmuir probe consists of two, identical, separate metal discs (typically 5 mm diam., 0.5 mm thick) placed back to back in the target plasma (see Figure V-6a). These discs are oriented such that one disc faces the grids. The probe has separate electrical connections for each disc. Each disc can separately be voltage-swept in the usual manner to obtain Langmuir characteristics. By means of electronic differentiation (OP-AMP or Lock-in Amplifier; see Chapter II) the electron distributions are obtained. The distribution of the background plasma is obtained from the disc facing away from the grids while the combined beam and background distribution is obtained from the disc facing the grids. By electronically subtracting (Beam + Background) - (Background), we can extract the beam-electron distribution. This provides a method for the experimental determination of the quantities n/n_b, $\bar{v}_b/v_D$, $\bar{v}_e/v_D$ and therefore the scaled thermal spread "s" for the experiment. The experimental data for the EPW can then be compared with the theory using the same "s" value.

Experimental dispersion curve data are obtained using the interferometry technique (cf Figre IV-7a). In this method the relative amplitude and phase measurements are carried out using the RF pickup probe as shown in Figure V-6d. This probe consists of a shielded probe shaft with a small ceramic insulator extending from the end. A small wire (5 mil. tantalum, 0.5 cm long) extends from ther ceramic insulator. Its signal is amplified and mixed with a reference signal to give the interferometry trace as the probe is moved along the axis, the direction of the wave propagation.

When the absolute magnitude of the wave electric field is desired, a daignostic electron beam may be used. A small electron beam (8-10 kv, 2 mm diam., I < 1 μA, see Figure V-6c) is directed perpendicularly to the direction of wave propagation in the region of interest. The beam passes from the electron gun through the EPW electric field and is allowed to impinge on a phosphor-coated (on vacuum side) glass window to produce an illuminated image which can be viewed from outside. In the absence of EPW the image produced is a small, bright spot. When EPW are present the spot is elongated along the direction of the detected wave electric field, (see Figure V-6c). With the knowledge of the diagnostic beam voltage, the wave frequency and relative spatial profile of the wave intensity along the beam, one can deduce the magnitude of the EPW electric field by measurement of the extent of elongation of the beam image spot. By moving the diagnostic beam along $\hat{k}$ one can determine the spatial growth rate of the EPW electric field. This method provides absolute field measurements and has the least perturbation on the plasma. It is superior to metal disc or wire probes which can cause zeroth order changes in plasma density. Since the propagation characteristics of EPW are sensitively dependent on the background density, the usual probe diagnostics introduce errors in the measurements which become significant when information about the absolute magnitude of the wave electric field is desired.

Appendix A: Approximate Solution to the Beam Plasma Dispersion Equation near (ω_o, k_o).

Equation (2) can be cast into a convenient form by following the procedure of Malmberg and O'Neil. Since $\omega - kv_D + ik\bar{v}_b \approx \varepsilon_p \approx 0$, we taylor expand each factor on the LHS of equation (2) about the intersection (ω_o, k_o). Writing $\delta\omega \equiv \omega - \omega_o$, $\delta k \equiv k - k_o$ equation (2) becomes

$$\left[k_o\left(\frac{\partial \varepsilon_p}{\partial k}\right)_{\omega_o k_o}\frac{\delta k}{k_o} + \omega_o\left(\frac{\partial \varepsilon_p}{\partial \omega}\right)_{\omega_o k_o}\frac{\delta\omega}{\omega_o}\right]\left[\frac{\delta\omega}{\omega_o} - \frac{\delta k}{k_o} + i\left(\frac{\bar{v}_b}{v_D}\right)\frac{\delta k}{k_o}\right]^2 = \left(\frac{\omega_p}{\omega_o}\right)^2\frac{n_b}{n}$$

where use has been made of the fact that, since ω_o is real, $\omega_o = k_o v_D$. We can write this as

$$\left[P\frac{\delta\omega}{\omega_o} + Q\frac{\delta k}{k_o}\right]\left[\frac{\delta\omega}{\omega_o} - \frac{\delta k}{k_o} + \frac{i\bar{v}_b}{v_D}\right]^2 = \left(\frac{\omega_p}{\omega_o}\right)^2\frac{n_b}{n}, \qquad \text{(A-1)}$$

where, for a Maxwellian plasma, $f_e = \frac{1}{\sqrt{\pi}\bar{v}_e}\exp\left[-\left(v/\bar{v}_e\right)^2\right]$

$$P \equiv \omega_o\left(\frac{\partial \varepsilon_p(k,\omega)}{\partial \omega}\right)_{\omega_o, k_o} = 2\left[1 + 3\left(\frac{\bar{v}_e}{v_D}\right)^2\right],$$

$$Q \equiv k_o\left(\frac{\partial \varepsilon_p(k,\omega)}{\partial k}\right)_{\omega_o, k_o} = -6\left(\frac{\bar{v}_e}{v_D}\right)^2\left[1 - 7\left(\frac{\bar{v}_e}{v_D}\right)^2\right]$$

and

$$\omega_o \cong \omega_p\left[1 + \frac{3}{2}\left(\frac{\bar{v}_e}{v_D}\right)^2\right], \qquad \omega_o = k_o v_o.$$

By introducing the transformation

$$\frac{\delta\omega}{\omega_o} = -\left(\frac{RQ}{P+Q}\right)\quad x, \qquad R \equiv \left[\frac{-n_b}{n}\left(\frac{\omega_p}{\omega_o}\right)^2\frac{1}{Q}\right]^{1/3}$$

$$\frac{\delta k}{k} = -Ry + \left(\frac{RP}{P+Q}\right)\quad x, \qquad s \equiv \left(\frac{\bar{v}_b}{v_D}\right)\left(6\frac{n_o}{n_b}\frac{\bar{v}_e{}^2}{v_D{}^2}\right)^{1/3}$$

We obtain a simplified form of equation (2) in terms of dimensionless variables

$$y(y - x + is)^2 = 1.$$

This cubic equation has an exact analytic solution as shown in Appendix B. For comparison with experiment which measures spatial growth or damping rates, the above cubic equation is solved for complex y and real x, from which complex k and real ω are inferred.

Appendix B: Solutions of the dimensionless dispersion relation equaiton (3).

To solve equation (3) numerically, one has at least two options:

A) Using a comples root finding computer code, one can obtain values of Im (y), Re (y) for a desired range of values of x and s.

B) Write equation (3) in the form

$$y^3 + ay^2 + by + c = 0$$

where

$$a = 2(is - x),\ b = (is - x)^2,\ c = 0$$

One then may use the cubic format formula: (See Mathematical Handbok, M. R. Spiegel)

with $V \equiv \dfrac{3b - a^2}{9}$ $W \equiv \dfrac{9ab - 2a^3}{54}$

$$U \equiv \left(W + \sqrt{V^3 + W^2}\right)^{1/3} \quad T \equiv \left(R - \sqrt{V^3 + W^2}\right)^{1/3}$$

The three solutions to the cubic equation, for given a, b, c are:

$$y_1 = U + T - \frac{1}{3}a$$

$$y_2 = -\frac{1}{2}(U + T) - \frac{1}{3}a + \frac{i}{2}\sqrt{3}(U - T)$$

$$y_3 = -\frac{1}{2}(U + T) - \frac{1}{3}a - \frac{i}{2}\sqrt{3}(U - T)$$

With these formulas one can find the roots (y-values) for a given range of values of *x* and *s*, a procedure best carried out by straight forward computer calculation.

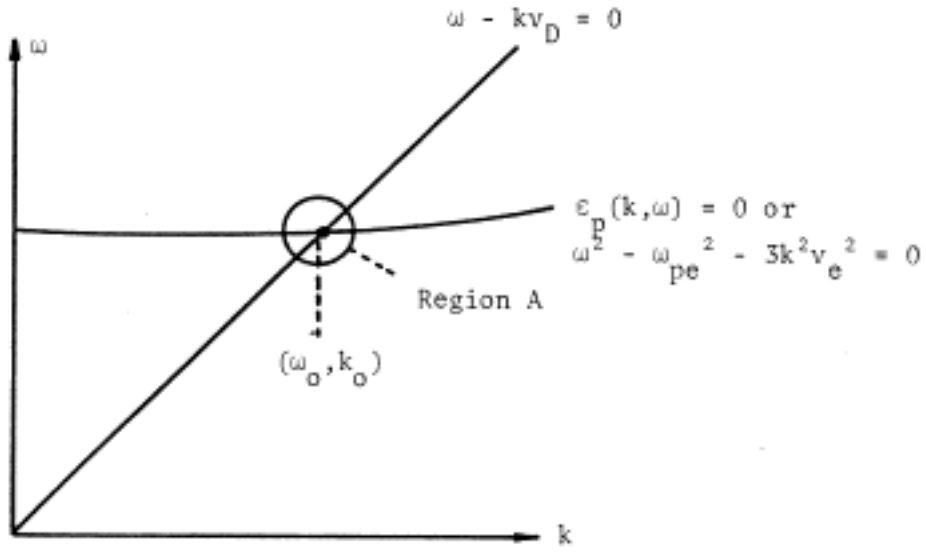

Figure V-1 Dispersion curves for uniform plasmas $\omega^2 = \omega_{pe}^2 + 3k^2v_e^2$ and beams $\omega - kv_D = 0$. The intersection region A is where strong interactions between beams and plasma occur.

(a) Warm beam

(s = 2)

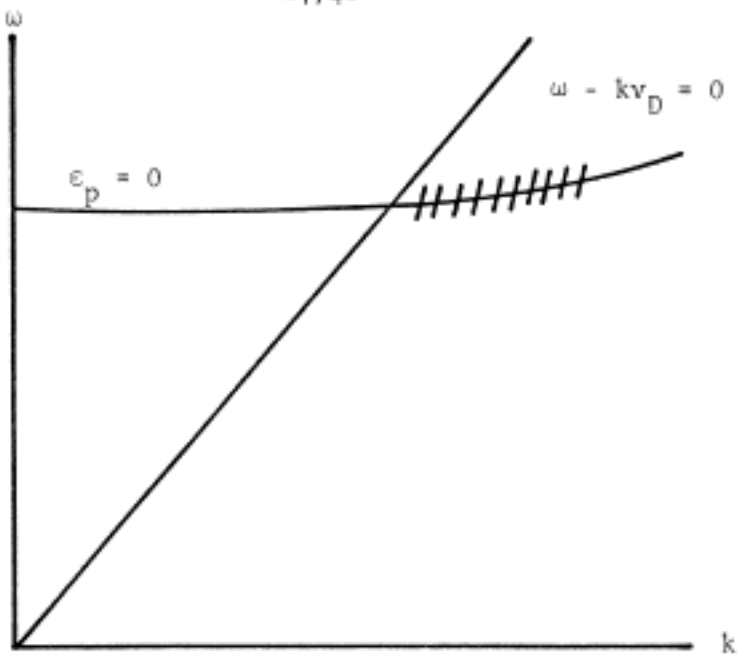

(b) Cold beam

(s = 0)

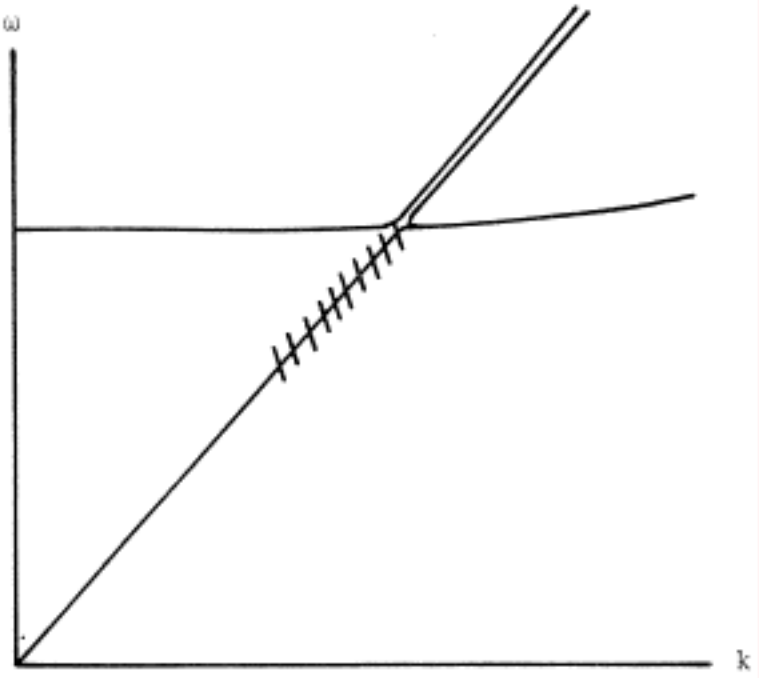

Figure V-2 Graphical Summary of the numerical solution of Equation (3) for a (a) Warm beam

(b) Cold beam

Cross hatched areas are the growth regions

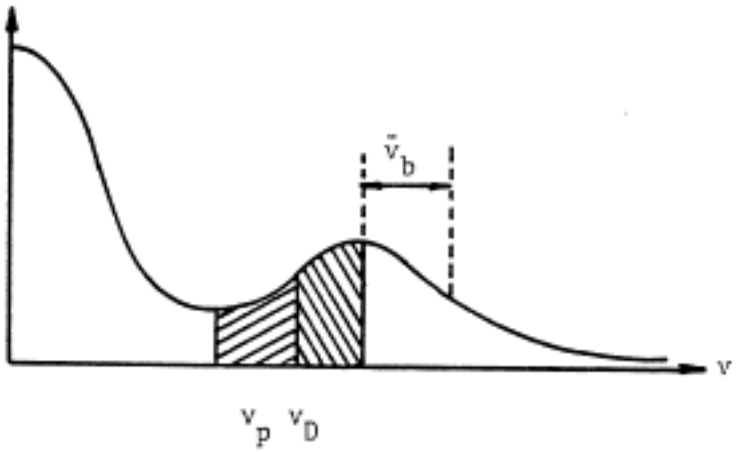

Figure V-3 Velocity distribution function for a beam-plasma. When $v_p < v_D$, there are more resonant particles with velocities greater than v_p than resonant particles with velocities less than v_p.

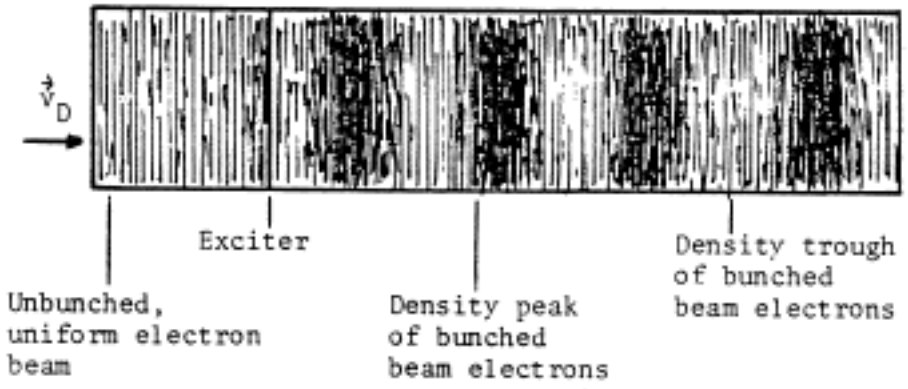

Figure V-4 Initial bunching of beam electrons by excitation grid. At the exciter, a certain fraction of the beam electrons will be bunched by the oscillating electric field there. Several λ_D away from the exciter the beam will have a periodic density variation which travels at the beam drift velocity, v_D.

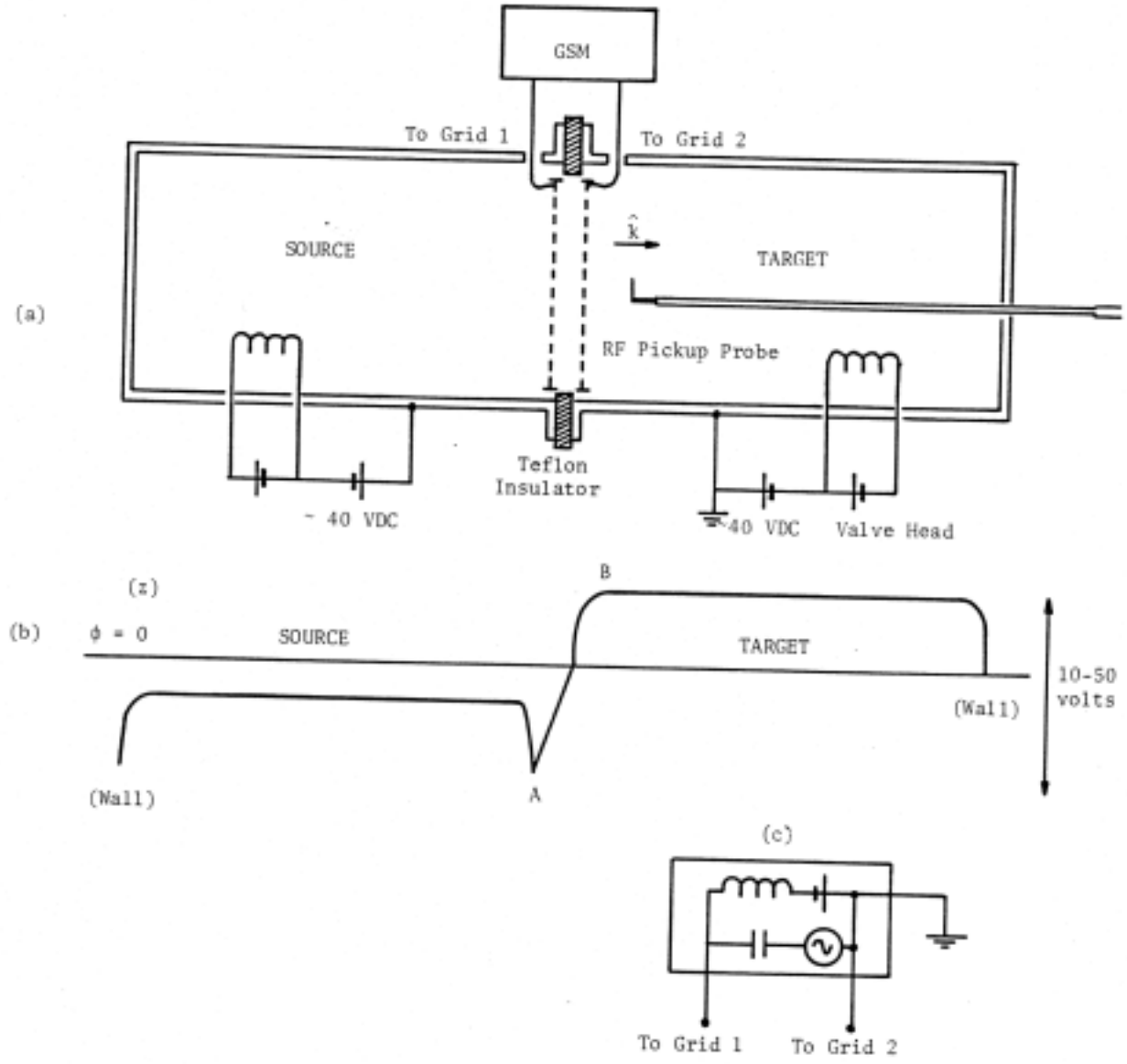

Figure V-5 Experimental Apparatur for EPW

(a) Vacuum Chamber showing arrangement of the Grids and Detection Probe.

(b) Potential along chamber axis, $\phi(z)$

(c) Grid Signal Mixer (GSM)

(A) Construction of and differentiated signals from the two sided Langmuir Probe

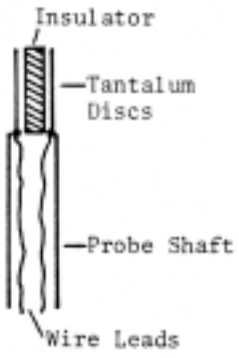

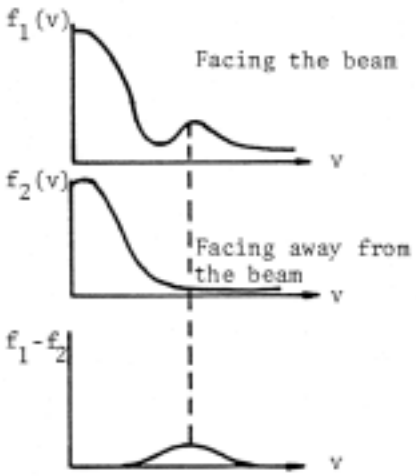

Two sided Langmuir probes

distribution functions measured by sides #1 and #2 and their differences.

(B) Construction of wire, RF pickup probe

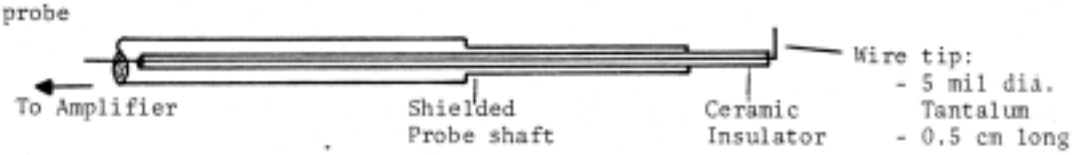

(C) Schematic representation of diagnostic electron beam

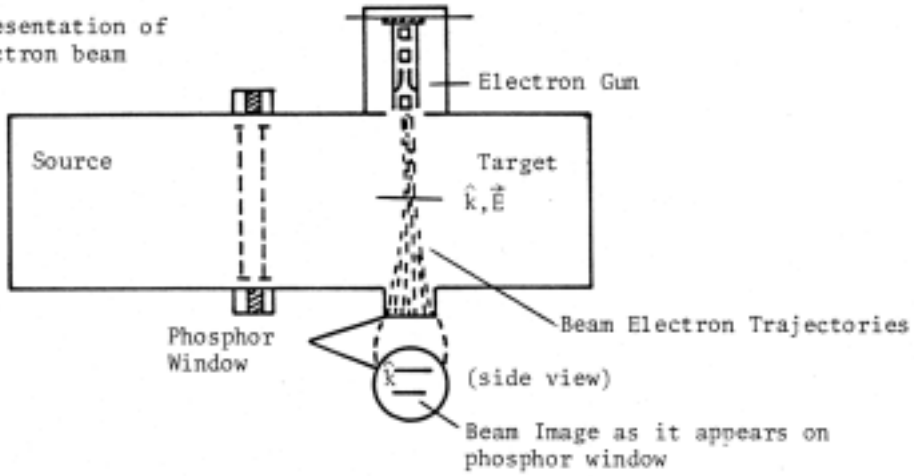

Figure V-6